AD-A047 487 CORNELL UNIV ITHACA N Y DEPT OF THEORETICAL AND APP--ETC F/G 11/4
ULTRASONIC NONDESTRUCTIVE TESTING OF COMPOSITE MATERIALS.(U)
SEP 77 W SACHSE, Y PAO AFOSR-76-2992

UNCLASSIFIED AFOSR-TR-77-1288 NL

1 OF 2
ADA047487

12 P.S.

AFOSR-TR- 77-1288

Department of
Theoretical and Applied Mechanics
CORNELL UNIVERSITY
ITHACA, NEW YORK

SECURITY CLASSIFICATION OF THIS PAGE (When Data Entered)

REPORT DOCUMENTATION PAGE

READ INSTRUCTIONS BEFORE COMPLETING FORM

1. REPORT NUMBER: AFOSR-TR- 77-1288
2. GOVT ACCESSION NO.
3. RECIPIENT'S CATALOG NUMBER

4. TITLE (and Subtitle): ULTRASONIC NONDESTRUCTIVE TESTING OF COMPOSITE MATERIALS.

5. TYPE OF REPORT & PERIOD COVERED: FINAL report
1 Apr [redacted]76 - 31 Mar [redacted]77
6. PERFORMING ORG. REPORT NUMBER

7. AUTHOR(s): WOLFGANG SACHSE
YIH-HSING PAO

8. CONTRACT OR GRANT NUMBER(s): AFOSR-76-2992

9. PERFORMING ORGANIZATION NAME AND ADDRESS
CORNELL UNIVERSITY
DEPARTMENT OF THEORETICAL AND APPLIED MECHANICS
ITHACA , N Y 14843

10. PROGRAM ELEMENT, PROJECT, TASK AREA & WORK UNIT NUMBERS
9782-05
61102F

11. CONTROLLING OFFICE NAME AND ADDRESS
AIR FORCE OFFICE OF SCIENTIFIC RESEARCH/NA
BLDG 410
BOLLING AIR FORCE BASE, D C 20332

12. REPORT DATE: Sep 77
13. NUMBER OF PAGES: 120 (119p.)

14. MONITORING AGENCY NAME & ADDRESS (if different from Controlling Office)

15. SECURITY CLASS. (of this report): UNCLASSIFIED
15a. DECLASSIFICATION/DOWNGRADING SCHEDULE

16. DISTRIBUTION STATEMENT (of this Report)

Approved for public release; distribution unlimited.

17. DISTRIBUTION STATEMENT (of the abstract entered in Block 20, if different from Report)

404 620

18. SUPPLEMENTARY NOTES

19. KEY WORDS (Continue on reverse side if necessary and identify by block number)
NONDESTRUCTIVE TESTING
COMPOSITE MATERIALS

20. ABSTRACT (Continue on reverse side if necessary and identify by block number)
The dispersion of elastic waves (ultrasonic waves) in fiber-reinforced materials is investigated by experimental and theoretical methods. A dependable continuous-wave-phase-comparison technique is developed along with the method of phase spectrum to determine the dispersion characteristics, and phase and group velocities in composites. Theoretically, the dispersion relation is determined from the analysis of multiple scattering of elastic waves with parallel cylinders.

FORM 1473 JAN 73 EDITION OF 1 NOV 65 IS OBSOLETE

UNCLASSIFIED

SECURITY CLASSIFICATION OF THIS PAGE (When Data Entered)

ULTRASONIC NON-DESTRUCTIVE TESTING
OF
COMPOSITE MATERIALS

Final Report
for the
Air Force Office of Scientific Research

~~Grant AF726992~~
AFOSR-76-2992

Wolfgang Sachse, Principal Investigator

and

Yih-Hsing Pao, Co-Principal Investigator

Department of Theoretical and Applied Mechanics
Cornell University, Ithaca, New York - 14853

September 1977

Contents

I. Program Overview

This final report contains the first year's results of a project originally proposed as a three-year research program. The main objective was the theoretical and experimental investigation of the propagation and scattering of ultrasonic waves in fiber-reinforced composite materials, both with and without flaws. The program was supported by AFSOR from April 1, 1976 to March 31, 1977.

It was recognized at the outset that composite materials present unique ultrasonic inspection problems. First, there is their inherent inhomogeneity. For unidirectional fibers the propagation of elastic waves will be similar to that in anisotropic materials such as single crystals. Second, there is a characteristic dimension, the filament diameter or its ply spacing, associated with the microstructural aspects of the composite. For a boron-epoxy composite these are 0.08 mm and 0.20 mm, respectively. Since ultrasonic polses used in most NDT situations contain frequency components in the megahertz range, interrogation pulses will contain wavelengths on the order of the material dimension, and the propagation of ultrasonic pulses through the composite will be greatly affected by the multiple scattering of waves. The observed dispersion and attenuation of ultrasonic waves in composites is a result of the multiple scattering. Finally, in many cases, particularly when the composite consists of an epoxy matrix, the ultrasonic signals are highly damped.

The research program completed has focused on each of the above areas, and we believe that significant progress has been made. The research program has benefitted from close interaction between the experimental and the theoretical work, and from support received from other sources prior

to the initiation of this program. Experimental techniques utilizing continuous waves and broadband pulse measurements were developed. Analyses of the multiple scattering of elastic waves by fibers imebdded in otherwise homogeneous matrix materials were made. Details are described in the next section.

During the year, two faculty members (W. Sachse and Y.H. Pao), two post-doctoral research associates (V.V. Varadan and C.S. Ting) and several graduate students worked either part- or full-time on this project.

II. ACCOMPLISHMENTS

(A) The frequency-dependent propagational characteristics of ultrasonic waves in various directions of boron-spoxy specimens have been investigated. Two ultrasonic techniques were developed for the accurate determination of ultrasonic phase and group velocities in highly absorbtive composite materials. Either technique can also be used for the determination of the dispersion relation for material. Both techniques have been demonstrated with longitudinal and shear waves of frequencies ranging from 0.5 to about 10 MHz propagating in various directions to the fiber axis.

The continuous-waves technique is an improvement on the existing method of phase comparison. By transmitting with variable frequency, one can determine the phase velocity of waves in a composite if the number of complete sinusoidal waves is known. In this method, a constraint equation is found which permits the determination of the absolute number of wave lengths of a wave in a specimen.

This work was presented at the 89th Meeting of the Acoustical Society of America at the Pennsylvania State University in June 1977 and a paper (copy appended) has been submitted for publication to the Journal of the

Acoustical Society of America.

(B) The second technique, ultrasonic phase spectroscopy, measures the phase spectrum of a broadband ultrasonic pulse. We have shown that the phase spectrum of a propagating pulse is related to the dispersion relation of the medium from which the phase and group velocities of the medium can be calculated as a function of fequency. A digital phase spectrum analyzer has been set in operation to determine the propagational characteristics of longitudinal and shear broadband ultrasonic pulses propagating in boron-epoxy specimens and in other dispersive materials.

This portion of the program was supported in part by the National Science Foundation through grants to the College of Engineering and the Materials Science Center at Cornell University. The phase spectroscopy technique was described in a presentation at the ARPA/AFML Review of Quantitative NDE in June 1977. A paper (copy appended) has been accepted for publication in the Journal of Applied Physics.

(C) In the theoretical study of the multiple scattering of waves by fibers in a composite, the newly-developed method of the transition matrix was extended to the case of multiple scattering of SH waves (scalar waves) normally incident on cylinders of arbitrary cross section. Using the transition matrix of a single obstacle, statistical averaging, and Lax's "quasi-crysstalline" approximation, we developed equations for the average amplitudes of scattered and excitation fields, from which the dispersion relation and hence the phase and group velocities for the material are obtained. In the Rayleigh (low frequency) limit, the effective elastic properties of the composite agree with the existing results in the literature.

These results were reported in the Compoiste Materials Review, held at Wright-Patterson AFB in October 1976; and they have been submitted for

publication to the Journal of the Acoustical Society of America (copy appended).

Extensions of the above to the scattering situation of either P or SV waves normally incident on the fibers have also been made. The results were reported at the "IUTAM Sumposium on Modern Problems in Elastic Wave Propagation" (Northwester University, Evanstion, Ill., Sept. 1977). Copies of a manuscript containing these results will be sent to AFOSR when completed.

III. CONCLUSIONS

The propagation and scattering of ultrasonic waves and pulses in composite materials have been studied. Two experimental techniques have been developed for accurately determining the dispersive nature of the propagation of ultrasonic waves in such materials. A theory for the multiple scattering of elastic waves by thin fibers of arbitrary shape was formulated. Based on the theory, dispersion relations are found for the ultrasonic longitudinal and shear waves propagating normal to the fiber directions.

APPENDIX A.

MEASUREMENT OF ULTRASONIC DISPERSION BY PHASE COMPARISON OF CONTINUOUS HARMONIC WAVES

C. S. Ting and Wolfgang Sachse

Department of Theoretical and Applied Mechanics
Cornell University, Ithaca, New York - 14853

MEASUREMENT OF ULTRASONIC DISPERSION BY PHASE COMPARISON OF CONTINUOUS HARMONIC WAVES

C. S. Ting and Wolfgang Sachse

Department of Theoretical and Applied Mechanics
Cornell University, Ithaca, New York - 14853

Abstract

The method of phase comparison of continuous waves is applied to determine the dispersion relation, phase and group velocities as a function of frequency of dispersive materials. A combination of the variable frequency method and the variable path-length method is found necessary to eliminate any uncertainty in the dispersion relation determination. Experiments are performed on specimens of various thicknesses. A constraint equation can be derived since the dispersion relation is unique and independent of the specimen thickness. This equation provides a procedure for determining the absolute number of wavelengths in the specimen. A transducer and electronics compensation procedure is also used. Measurements in uni-directional, fiber-reinforced Boron-Epoxy specimens show good agreement with results reported previously.

We describe in this paper a continuous-wave, through-transmission, phase comparison method for measuring the phase and group velocities of ultrasonic waves in dispersive materials. The method is an adaptation of the phase-comparison methods described by Lynnworth, et al [1] which have been reviewed by Papadakis [2]. The procedure we shall describe provides an unambiguous means for determining the exact wavelength of an ultrasonic wave in a solid specimen. This is then used to find the dispersion relation, phase and group velocities as a function of frequency for the material.

I. Introduction

The speed of propagation of a monochromatic wave can be defined as the speed with which the phase of the wave is propagated [3]. A plane wave, propagating undamped in the x-direction, can be described at (x,t) as

$$u(x,t) = u_o e^{i(\omega t \pm kx)} \tag{1}$$

where the quantity $(\omega t \pm kx)$ is known as the phase function, $\omega (=2\pi f)$ is the circular frequency and $k\ (=2\pi/\lambda)$ is the wavenumber. Surfaces of constant phase propagate at speed v where

$$v = dx/dt = \omega/k = f\lambda \tag{2}$$

v is the phase velocity.

It can be shown [4] that a pulse, being a superposition of waves, has its mean amplitude propagate with a group velocity given by

$$U = d\omega/dk = df/d(1/\lambda) \tag{3}$$

When a wave is subjected to frequency-dependent damping, complications arise in defining its phase and group velocity. These are discussed by Sachse and Pao [5].

From Equations (2) and (3) one obtains

$$U = \frac{d(vk)}{dk} = v + k\frac{dv}{dk} \tag{4}$$

an equation relating the phase and group velocities. Thus, only when $v \neq v(k)$ will the group velocity equal the phase velocity. When the propagating medium is dispersive, the phase and group velocities are unequal and both depend on the frequency (wavelength) of the wave. Furthermore, pulses change their shape while propagating through such media.

The measurement of phase and group velocities with continuous waves and pulse techniques in dispersive materials has been reviewed by Young [6], Papadakis [2] and recently by Sachse and Pao [5]. This paper is restricted to a discussion of measurements made with continuous harmonic waves in dispersive solids.

The phase velocity-frequency behavior and hence the dispersion relation can be determined from continuous wave measurements only if the wavelength of the wave is known unambiguously. This is usually impossible in solids unless they are transparent so that the wavelength of a wave can be directly measured as a function of frequency with optical techniques [7].

In an attempt to measure the wavelength of the wave, Lynnworth, et al [1] used specimens consisting of two wedges such that the propagation path length between source and receiving transducer could be varied. The length

changes corresponding to a 2π phase change in the received signal relative to the input signal, should correspond to the wavelength in the specimen. The difficulty with the technique appears to be associated with anomalous effects arising from the interface and microstructure of the materials used.

The group velocity can be determined once the dispersion relation $k = \hat{k}(\omega)$ (or $\omega = \hat{\omega}(k)$) or the frequency dependence of the phase velocity is known for the material. If, however, only the group velocity is known as a function of frequency, it is impossible to determine v uniquely by integration of Eqn. (4). Missing is the precise value of k at the lower limit of integration.

Because a wavelength determination solids is difficult, in a continuous wave experiment the frequency of excitation is varied and the resonance frequencies of the specimen determined. Even though the technique has been in existence for a long time, few measurements in dispersive media can be found in the literature. One example previously cited, is the work of Lynnworth, et al [1] who measured the group velocity this way in 3-dimensional carbon-phenolic specimens.

The measurement technique is sometimes called the π-phase comparison technique. In it, a continuous wave of freqnency f is transmitted through a specimen of length L. Data are obtained by determining the lowest frequency at which the signal received at L is out-of-phase with the input signal. This corresponds to a half-wavelength in the specimen, hence $\lambda/2 = L$. Increasing the frequency of excitation, the received signal is successively brought in-phase and π-radians out-of-phase with the input signal. At each condition the number of cycles of the wave is increased by one-half and so the number of cycles in the specimen, N, is known at

every frequency. The process is continued until no signal is detected at the transducer, being the result of specimen attenuation effects or transducer bandwidth limitations.

The dispersion relation and the phase velocity are determined at each frequency f, for which N is known. Since

$$\lambda = L/N \tag{5}$$

the dispersion relation k or ω is specified. The phase velocity is

$$v = f\lambda = \frac{fL}{N} \tag{6}$$

In addition, the group velocity, U, is known, since

$$U = df/d(\frac{1}{\lambda}) = L\ df/dN \tag{7}$$

The crucial point in the wavelength determination is that N is known unambiguously over the entire frequency range. If this is not the case, the group velocity U can still be determined as follows. If at frequency f_1 an in-phase or an out-of-phase condition exists such that $N = N_1$ and if the frequency is then adjusted to f_2 where $f_2 = f_1 + \Delta f$, and at which another in-phase or out-of-phase condition exists such that $N_2 = N_1 + \Delta N$, then we find

$$\frac{\Delta\omega}{\Delta k} = \frac{\omega_2 - \omega_1}{k_2 - k_1} = L\,\frac{2\pi\Delta f}{2\pi\Delta N} \tag{8}$$

In the limit, as $k \to 0$, this equals the group velocity U. Thus,

$$U = L\ df/dN \tag{9}$$

It was pointed out in Ref (5) that it would be possible to determine

the phase velocity from Eqn. (4) by integration, provided that the value for $k_1 (= \frac{2\pi N_1}{L})$ which appears in the integration constant is known. This is in agreement with the discussion earlier.

A unique determination of N, the number of wavelengths in a specimen, is experimentally quite difficult if not impossible in non-transparent solids. As Papadakis has pointed out [2], at low frequencies spurious interferences, sidewall reflections and complex modes in a specimen make it difficult to identify the first out-of-phase condition as well as subsequent in- and out-of-phase conditions. With composite material specimens, we have observed the multimode phenomena to occur below about 0.3 MHz which appears to be inherent to such materials. The presence of the phenomena is indicated by several successive in-phase (or out-of-phase) conditions being observed at irregular frequency intervals.

If the material is non-dispersive in some frequency range, then v = U and a group velocity measurement can be used to determine the wavelength and hence N at a frequency in that range. If, however, the medium possesses stop-bands [8], the wavelength becomes indeterminate. In the next section we describe a method which combines the variable frequency method and the variable path-length method to determine the exact number of cycles, N, in a specimen as a function of frequency.

II. Basis of the Method

The measurements on a specimen are begun at any frequency f at which the input and output signals are in-phase. This condition is assigned any arbitrary integer value. The excitation frequency is then increased and the number of cylces of phase, N^*, relative to the initial point, recorded as a function of frequency. It is clear, that in order to obtain the absolute value of cycles of phase, an integer value of variation, δN, must

be added to each point.

The number of relative cycles of phase, however, also contains the effects of frequency-dependent phase shifts caused by the transducers and amplifiers. This is denoted by $n(f)$ and it must be subtracted from the $N^* + \delta N$ cycles of relative phase to obtain the absolute number of cycles of phase in the specimen. Hence

$$N = N^* + \delta N - n(f) \tag{10}$$

A. $n(f)$ Determination

If the delay time t_o resulting from the transducers and amplifiers is a constant as a function of frequency, then the cycles of phase shift resulting from these is

$$n = \frac{\phi_o}{2\pi} = \frac{\omega t_o}{2\pi} = f t_o \tag{11}$$

More generally, however, the cycles of phase shift caused by these elements is also frequency-dependent, hence $n(f)$ must be determined experimentally. Experience has shown that determination of $n(f)$ is to be preferred over the use of a second set of transducers which are in intimate contact and coupled to an amplifier. It is generally very difficult to obtain two sets of ultrasonic transducers whose frequency-dependent phase shifts are identical.

The determination of $n(f)$ can be accomplished in two ways. In one, the transducers are placed in intimate contact and the function $n(f)$ is determined directly from the cycles of phase shift, n^*, measured between input and output transducers as a function of frequency. Alternately, a non-dispersive highly-attenuating specimen is used in the phase-comparison system. This facilitates measurements to be reliably made to the

lowest out-of-phase frequency. From Eqn. (5)

$$N = L/\lambda = \frac{Lk}{2\pi}$$

If the phase velocity of the non-dispersive material is v_o, then the dispersion relation is

$$k = (\frac{1}{v_o})\omega = \frac{2\pi}{v_o} f \qquad (12)$$

Combining these equations, one finds

$$N = \frac{L}{v_o} f \qquad (13)$$

Therefore, the non-specimen phase shift is determined from

$$n(f) = n^*(f) - \frac{L}{v_o} f \qquad (14)$$

and this must be subtracted from the measured cycles of relative phase shift.

B. δN Determination

The value of δN can be determined by performing phase-comparison measurements on specimens of various lengths. Since the wavenumber is directly related to the number of cycles of phase in a specimen according to Eqn. (5), then, if a set of m specimens of length L_i is tested and for each, $N_i^*(f)$ is measured, the following set of m equations result

$$k_i(f) = \frac{2\pi}{L_i}[N_i^*(f)+\delta N_i-n(f)] \qquad (15)$$

The dispersion relation, $\omega = \hat{\omega}(k)$, is unique for the material and independent

of specimen length. It follows, therefore, that at any frequency f

$$k_1(f) = k_2(f) = k_3(f) = \ldots = k_m(f) \quad (16)$$

or

$$\frac{2\pi}{L_1}[N_1^*(f)+\delta N_1-n(f)] = \frac{2\pi}{L_2}[N_2^*(f)+\delta N_2-n(f)] = \ldots = \frac{2\pi}{L_m}[N_m^*(f)+\delta N_m-n(f)] \quad (17)$$

Equations (17) are quivalent to a set of $(m-1)$ linearly independent equations for the m unknowns, δN_1, δN_2, δN_3, ... δN_m. An additional condition is that the δN_i are to be integer values. Hence, the δN_m can all be uniquely determined.

Eqns. (17) can be rewritten in the form

$$\delta N_i = \frac{L_i}{L_1}\delta N_1 + B_i \qquad i = 2, 3, 4, \ldots, m \quad (18)$$

where

$$B_i = \{L_i N_1^*(f)-L_1 N_i^*(f)-(L_i-L_1)n(f)\}$$

For δN_i to be independent of frequency, requires that B_i be also. The requirement that the δN_i values be exact integers is generally not attainable from experimental measurements. The requirement is therefore relaxed such that the δN_i be close to integer values. Thus, in practice, one finds the set of δN_i which satisfy Eqn. (18) and whose summed deviation of each δN_i to its nearest integer is a minimum.

The solutions obtained, depend clearly on the various specimen lengths chosen. In order to obtain a solution without ambiguity, one must chose specimen lengths which preclude multiple solutions.

An extreme case is that in which all the specimens are of equal length. In that case, $B_i = 0$ and δN_i cannot be determined uniquely. The optimal

choice of specimen lengths to be used in a series of experiments is not immediately apparent. If the thickness ratios between specimens is $1:\frac{1}{2}:\frac{1}{3}:\frac{1}{4}:\ \ldots$, the common denominator is as large as possible. If five specimens are considered, with $L_i = 1$, and if at a value of δN_1 the other δN_i are all integer values, only when δN_1 is equal to 60 will all the other δN_i equal integer values again. It is clear that a judicious choice of specimen thickness ratios should be used if the dispersion relation for the material is to be determined unambiguously.

Although the number of specimens is at minimum two, a larger number of specimens greatly simplifies the δN_1 determination.

III. Experiments

The electronic system for making ultrasonic phase-comparison measurements is shown in Figure 1. It is similar to that described by Papadakis [2] and consists essentially of a continuous radio-frequency oscillator (HP 606A), a frequency counter (HP5326B), transducers (Panametrics VIP-Series), specimen holder, amplifiers and display oscilloscope (Tektronix 7A18, 7704A). Both input and received signals are displayed on the oscilloscope. The signals were amplified to the same level and added. A null signal was used to indicate an out-of-phase condition. The in-phase condition was determined similarly with one of the signals inverted. A vector voltmeter can also be connected to input and receiving transducers and the phase measured directly.

The determination of the tranducer and electronic phase delay, n(f), was determined by the two methods described in Section II. The results are shown in Figure 2. The data points indicated by Method (I) are the results obtained when the two transducers were in intimate contact and the phase

of the received signal was measured relative to the excitation signal as a function of frequency. The line indicated on Figure 2 passes through the points determined from the data of a 1.27 cm thick specimen of plexiglass placed between the transducers with the data being reduced according to the procedure described in Section II. The measurements were repeated with a 1.27 cm thick specimen of brass. The results were identical.

To demonstrate the applicability of the data analysis procedure, phase-comparison measurements were made on specimens cut form a 96-ply "Scotchply" uni-directional, boron-epoxy composite panel. The specimen material is the same as that used in some earlier elastic moduli experiments and the characteristics of the material have been reported previously [9]. Shear waves were used in the experiments to be described. The wave propagation direction was coincident with the fiber direction and the particle polarization direction was perpendicular to the ply layers of the composite.

Five specimens of the same orientation, but possessing different thicknesses were used. The original data obtained from phase-comparison measurements is shown in Figure 3. The number of cycles of phase, N^*, indicated on the ordinate is measured relative to a particular in-phase, out-of-phase condition. The values of B_i in Eqn. (18) were evaluated at five frequencies: 2, 3, 4, 5, and 6 MHz. The values of N_i at each frequency were obtained by a linear interpolation of the two adjacent data points. With the values of $n(f)$, it was found that the variation of B_i at these five frequencies is less than 0.07 cycle of phase delay. Using the averaged values of B_i and the length ratios, L_i/L_1, Eqn. (18) is used to evaluate the various δN_i $(i > 1)$ in terms of the δN_1. One

finds

$$\begin{aligned} \delta N_2 &= 0.911\ \delta N_1 + 0.563\ (\pm 0.035) \\ \delta N_3 &= 0.310\ \delta N_1 + 0.398\ (\pm 0.021) \\ \delta N_4 &= 0.501\ \delta N_1 + 0.955\ (\pm 0.023) \\ \delta N_5 &= 1.466\ \delta N_1 + 0.820\ (\pm 0.034) \end{aligned} \tag{19}$$

This set of equations is plotted in Figure 4.

As stated in Section II, in order to determine the appropriate value for the δN_1, the sum of the deviation of each $\delta N_i (i > 1)$ from its nearest integer value must be a minimum. This can be done numerically using Eqns. (19) or it can be determined directly from Figure 4 with a calibrated scale. The deviations of each δN_i $(i > 1)$ from its nearest integer value are summed for every integer value of δN_1 and this total deviation is plotted versus δN_1 as shown in Figure 5. It is clear that for $\delta N_1 = 2$ the total deviation is a minimum. It follows then that $\delta N_2 = \delta N_3 = 1$, $\delta N_4 = 2$ and $\delta N_5 = 4$ for the example considered.

Once the δN_i have been determined, the dispersion relation for the material is established according to Eqn. (15). This is shown in Figure 6 with all the original data (Fig. 2) now fitting onto one continuous curve.

The phase velocity, $v(=2\pi f/k)$ is determined directly from the dispersion curve. The result for the 0.543 cm thick specimen is shown in Figure 7. The group velocity is determined by differentiating the dispersion curve. In order that artificats arising from numerical differentiation of the discrete points of the dispersion curve be minimized, a polynomial is fit to the dispersion data. In the present experiments, a cubic polynomial of f as a function of k was used with the resulting polynomial

coefficients given in Table I. The group velocity is then determined as a function of frequency in closed form from the dispersion curve polynomial. As a check of this procedure, the data points comprising the dispersion relation were analyzed point-by-point with a four-point Lagrangian interpolation technique [10] to determine the group velocity. The results of both group velocity determinations for the 0.543 cm thick specimen are also shown in Figure 7.

The phase and group velocity determinations made on all five specimens is compared in Figure 8. The phase velocity results are nearly identical while the group velocity results show a slightly large scatter. For comparison, the results of Tauchert and Guzelsu [11] who used an r.f. burst measurement technique to determine the time delay of the burst and so its group velocity through specimens of similar material. Although their measurements were made with different transucers at frequencies of 0.5, 2.25, 5.0 and 10 MHz, the line shown on Figure 8 is drawn through all their data points. The agreement with the results of continuous wave measurements is within 8%.

IV. Conclusions

By combining the variable frequency and the variable path length continuous wave techniques, we have shown that the dispersion relation for a material can be determined from π-phase comparison measurements.

The procedure utilizes phase data relative to an arbitrary starting frequency which has been modified to take into account the phase delays associated with the transducers and electronics. Since the dispersion relation for a material is unique and the number of cycles must be an integer number, it is shown that the number of cycles at the test start

can be established and so the dispersion relation for the material is found to which a polynomial can be fitted. Both phase and group velocities can then be determined from the dispersion relation point-by-point numerically or in closed form by differentiation of the polynomial.

The results obtained are consistent from specimen to specimen, regardless of length. Furthermore, the group velocity determination is in agreement with that obtained with a r.f. burst technique.

Acknowledgments

This work was supported in part by the Air Force Office of Scientific Research and by the National Science Foundation through the Materials Science Center at Cornell University.

References:

1. L. Lynnworth, E. P. Papadakis and W. Rea, "Ultrasonic Measurement of Phase and Group Velocity Using Continuous Wave Transmission Techniques," AMMRC Report CTR 73-2, January 1973.

2. E. P. Papadakis, Chapt. 5 in Physical Acoustics, Vol. XII, W. P. Mason and R. N. Thurston, Eds., Academic Press, New York, 1976, pp. 277-374.

3. R. B. Lindsay, Mechanical Radiation, McGraw-Hill Book Co., New York (1960), p. 27.

4. L. Brillouin, Wave Propagation and Group Velocity, Academic Press, New York, 1960.

5. W. Sachse and Y. H. Pao, Report #2773, Materials Science Center, Cornell University, Ithaca, NY (July 1977). To appear in J. Appl. Phys.

6. E. H. Young, Jr., IRE Trans. UE-9, 13-21 (1962).

7. C. H. Palmer, R. O. Glaus and S. E. Fick, Applied Optics, 16, 1849-1856 (1977).

8. H. J. Sutherland and R. Lingle, J. Composite Matls., 6, 490-502 (1972).

9. W. Sachse, J. Comp. Matls., 8, 378-390 (1974).

10. R. W. Hamming, Numerical Methods for Scientists and Engineers, McGraw-Hill Book Co., New York, 1962, pp. 94-97.

11. T. Tauchert and A. N. Guzelsu, Trans. ASME-J. Appl. Mech., 39, 98-102, (1972).

Table I - Dispersion relation polynomial coefficients

$$f = a_o + a_1 k + a_2 k^2 + a_3 k^3$$

Specimen	a_o	a_1 ($\times 10^{-1}$)	a_2 ($\times 10^{-3}$)	a_3 ($\times 10^{-6}$)
i = 1 (0.335 cm)	0.2819	0.1301	0.3632	-0.6759
i = 2 (0.543 cm)	0.2084	0.1527	0.3522	-0.6160
i = 3 (0.878 cm)	0.2567	0.1270	0.3788	-0.7136
i = 4 (1.753 cm)	0.2115	0.1530	0.3438	-0.5604
i = 5 (2.569 cm)	0.1935	0.1569	0.3362	-0.5509

Figure Captions

Figure 1 - Schematic of the experimental setup.

Figure 2 - Measured transducer and electronics phase delay. Method I: Transducers in contact; Method II: Measured using a plexiglass sample.

Figure 3. Original phase delay data obtained from shear waves in Boron-Epoxy, propagating along the fiber direction, with polarization normal to the ply layers. N* is the cycles of phase relative to any first in-phase, out-of-phase condition.

Figure 4 - Phase shift of the specimens i = 2,3,4,5 for various phase shift values of specimen i = 1, based on the data shown in Figure 3.

Figure 5 - Summed phase shift obtained from Fig. 4 for various values of the phase shift for the data of specimen i = 1.

Figure 6 - The dispersion relation derived from the data shown in Figure 3.

Figure 7 - The corrected dispersion relation data for the 0.543 cm thick specimen. Also shown is the polynomial curve fit and the derived phase and group velocity. Open circles represent the group velocity determined with the four-point Lagrangian interpolation technique.

Figure 8 - Phase and group velocities obtained from all the data shown in Figure 3. Comparison is made with the results obtained from r.f. burst measurements by Tauchert and Guzelsu (Ref. 11).

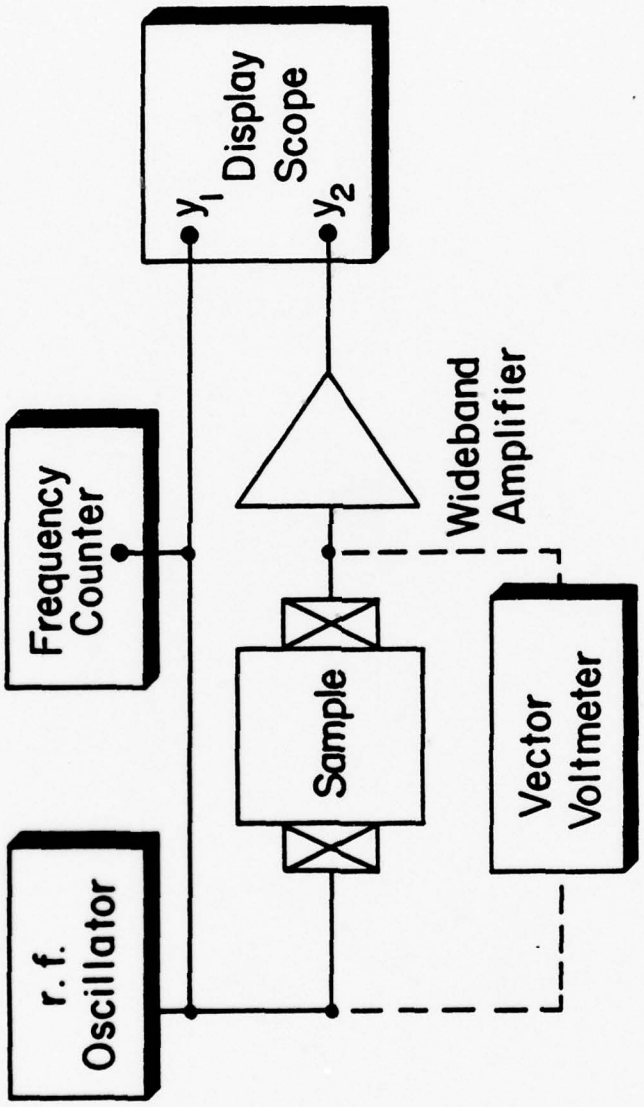
Display Scope
y_1
y_2
Wideband Amplifier
Frequency Counter
Sample
Vector Voltmeter
r. f. Oscillator

Figure 1

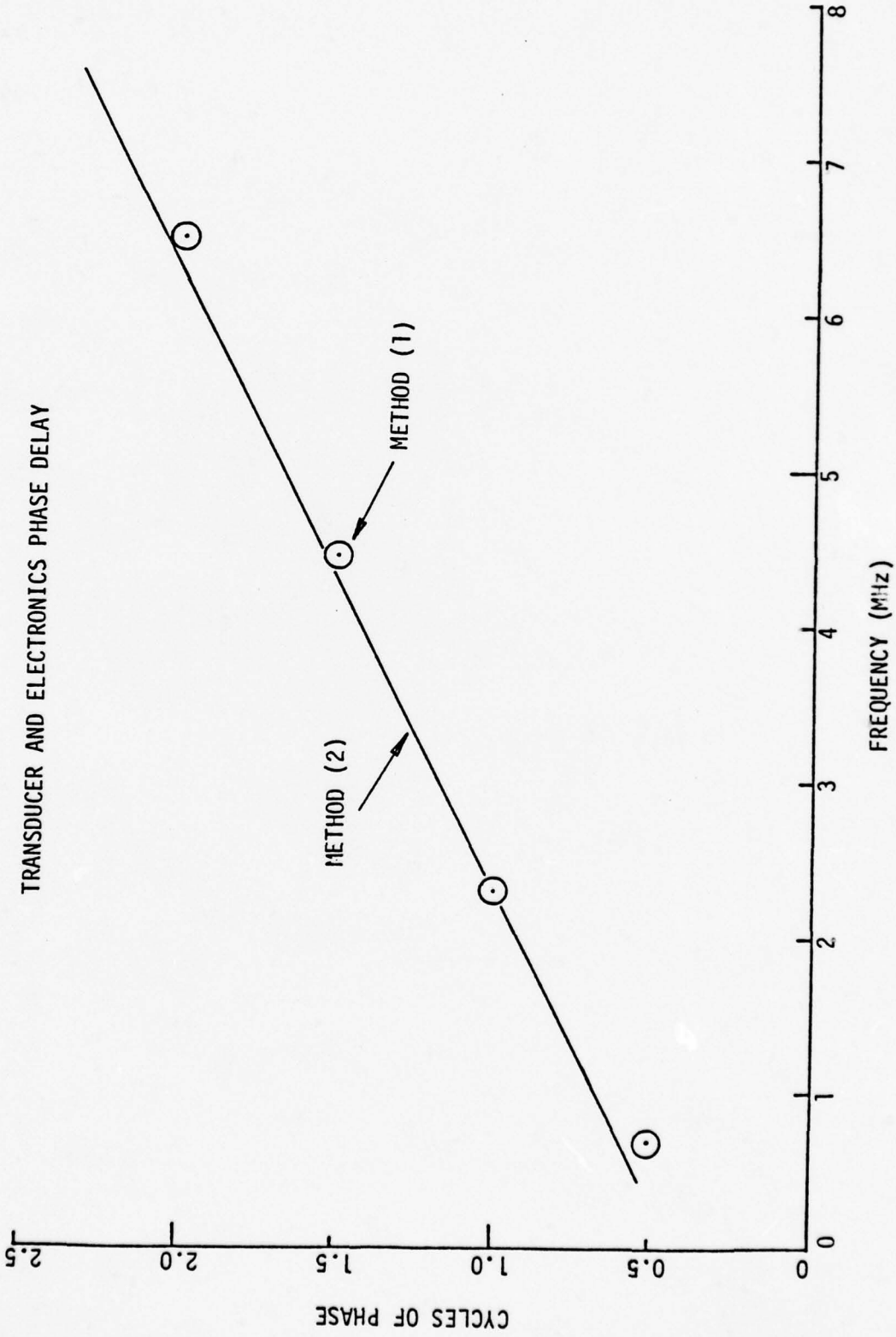
TRANSDUCER AND ELECTRONICS PHASE DELAY
METHOD (1)
METHOD (2)
CYCLES OF PHASE
0
0.5
1.0
1.5
2.0
2.5
FREQUENCY (MHz)
0
1
2
3
4
5
6
7
8

Figure 2

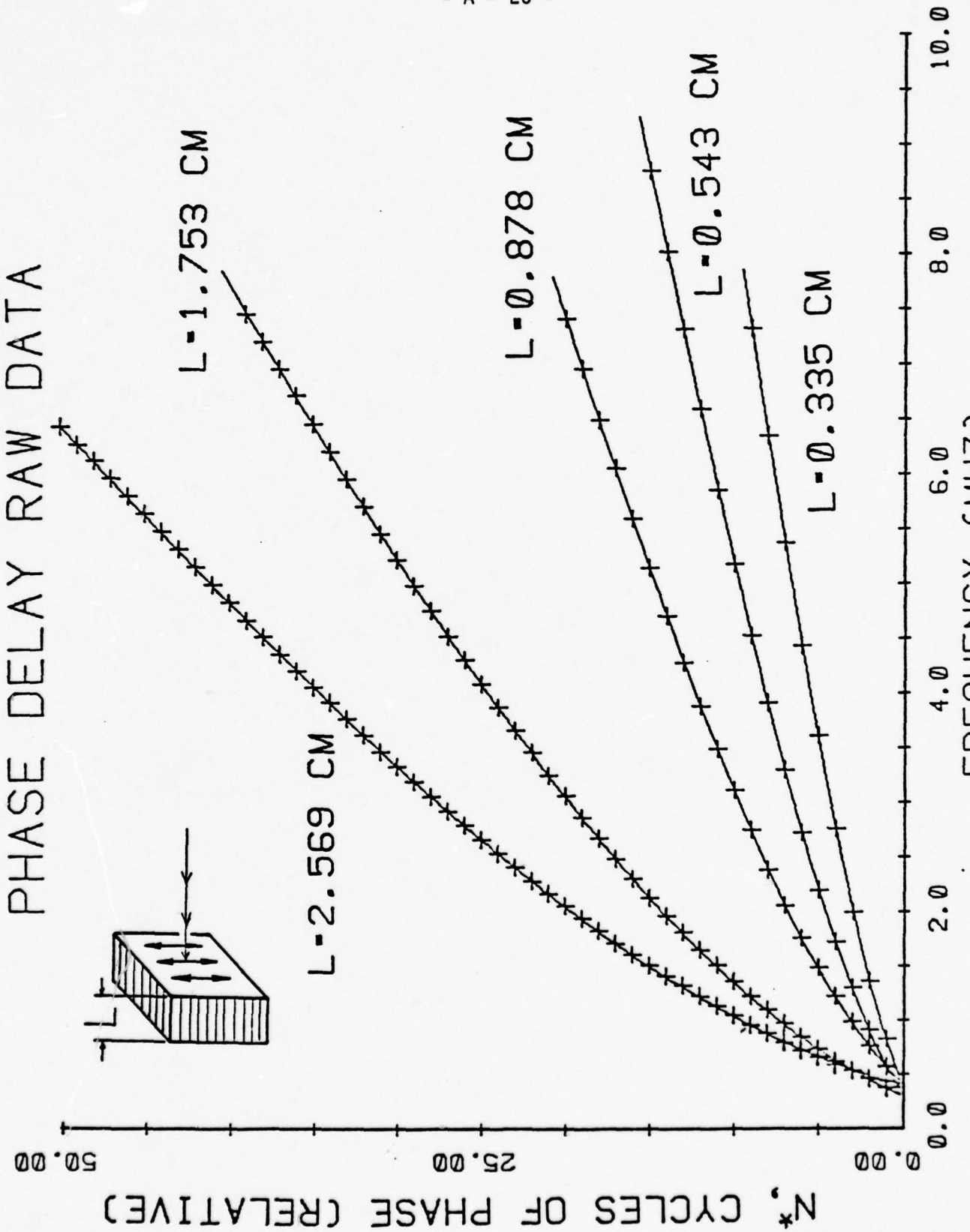
PHASE DELAY RAW DATA
L-1.753 CM
L-0.878 CM
L-0.543 CM
L-0.335 CM
L-2.569 CM
L
N*, CYCLES OF PHASE (RELATIVE)
0.00
25.00
50.00
0.0
2.0
4.0
6.0
8.0
10.0
FREQUENCY (MHZ)

Figure 3

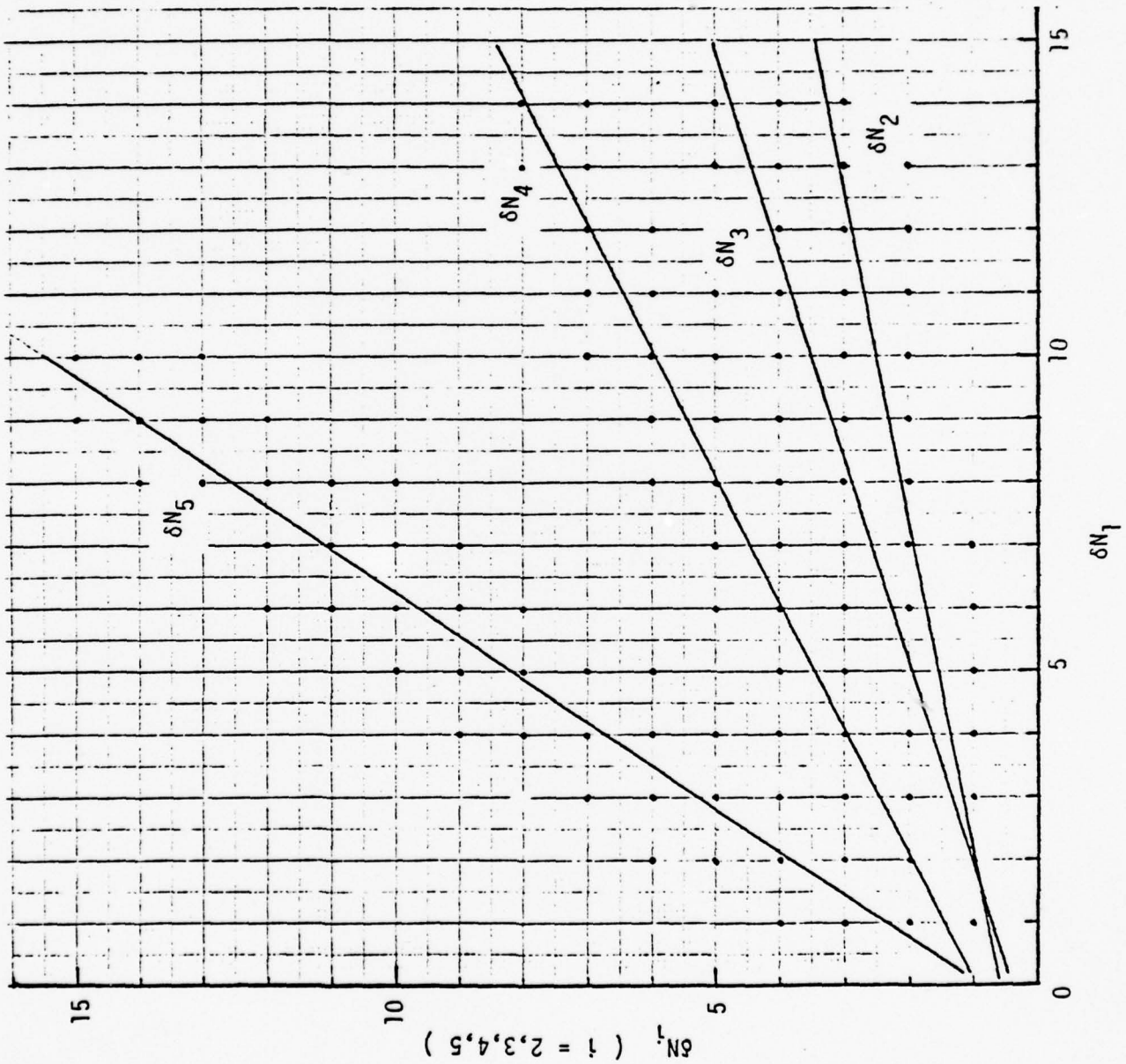

Figure 4

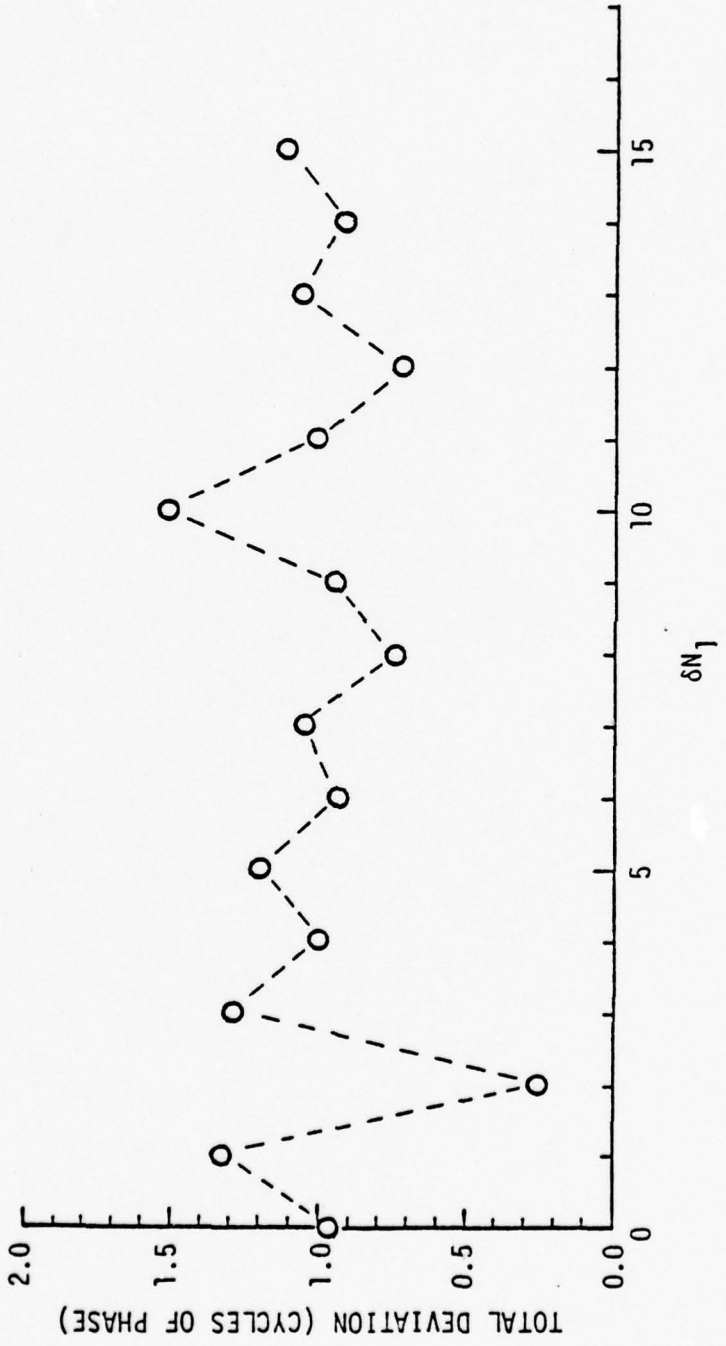
TOTAL DEVIATION (CYCLES OF PHASE)
2.0
1.5
1.0
0.5
0.0
0
5
10
15
δN_1

Figure 5

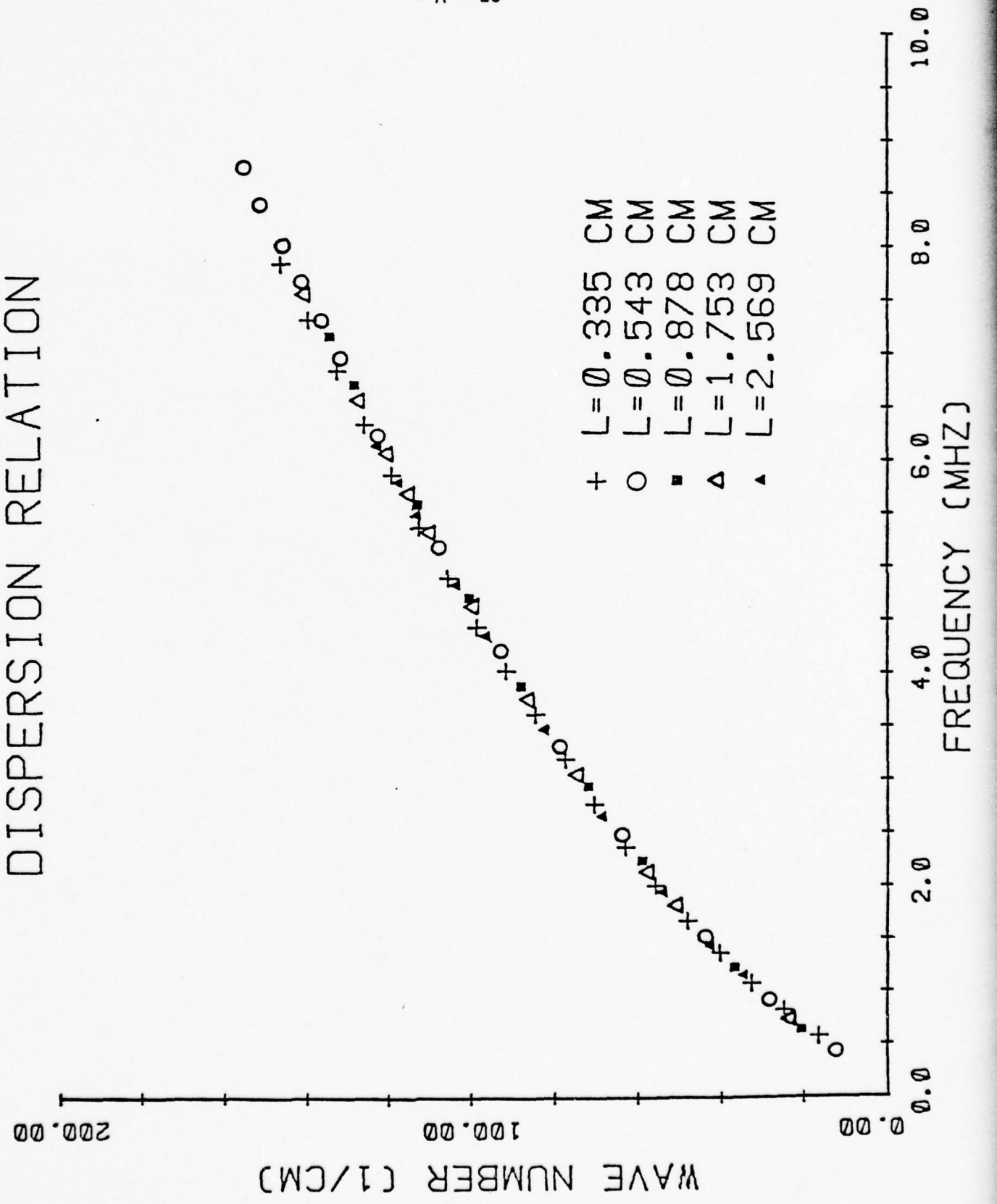
DISPERSION RELATION
+ L=0.335 CM
○ L=0.543 CM
■ L=0.878 CM
△ L=1.753 CM
▲ L=2.569 CM
WAVE NUMBER (1/CM)
0.00
100.00
200.00
0.0
2.0
4.0
6.0
8.0
10.0
FREQUENCY (MHZ)

Figure 6

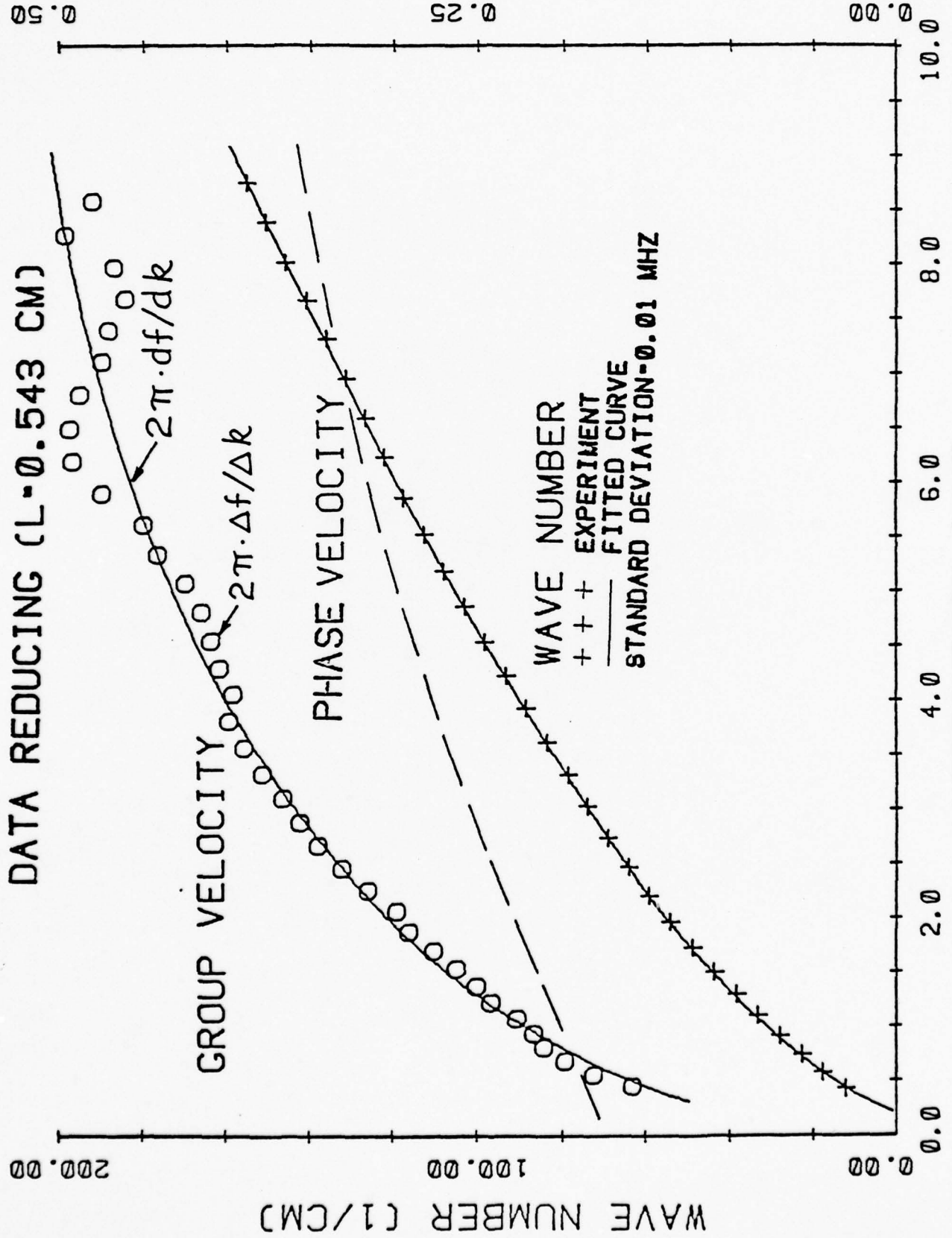
DATA REDUCING (L=0.543 CM)
GROUP VELOCITY
PHASE VELOCITY
WAVE NUMBER
+++ EXPERIMENT
FITTED CURVE
STANDARD DEVIATION=0.01 MHZ
2π·df/dk
2π·Δf/Δk
WAVE NUMBER (1/CM)
VELOCITY (CM/USEC)
FREQUENCY (MHZ)
0.00
100.00
200.00
0.00
0.25
0.50
0.0
2.0
4.0
6.0
8.0
10.0

Figure 7

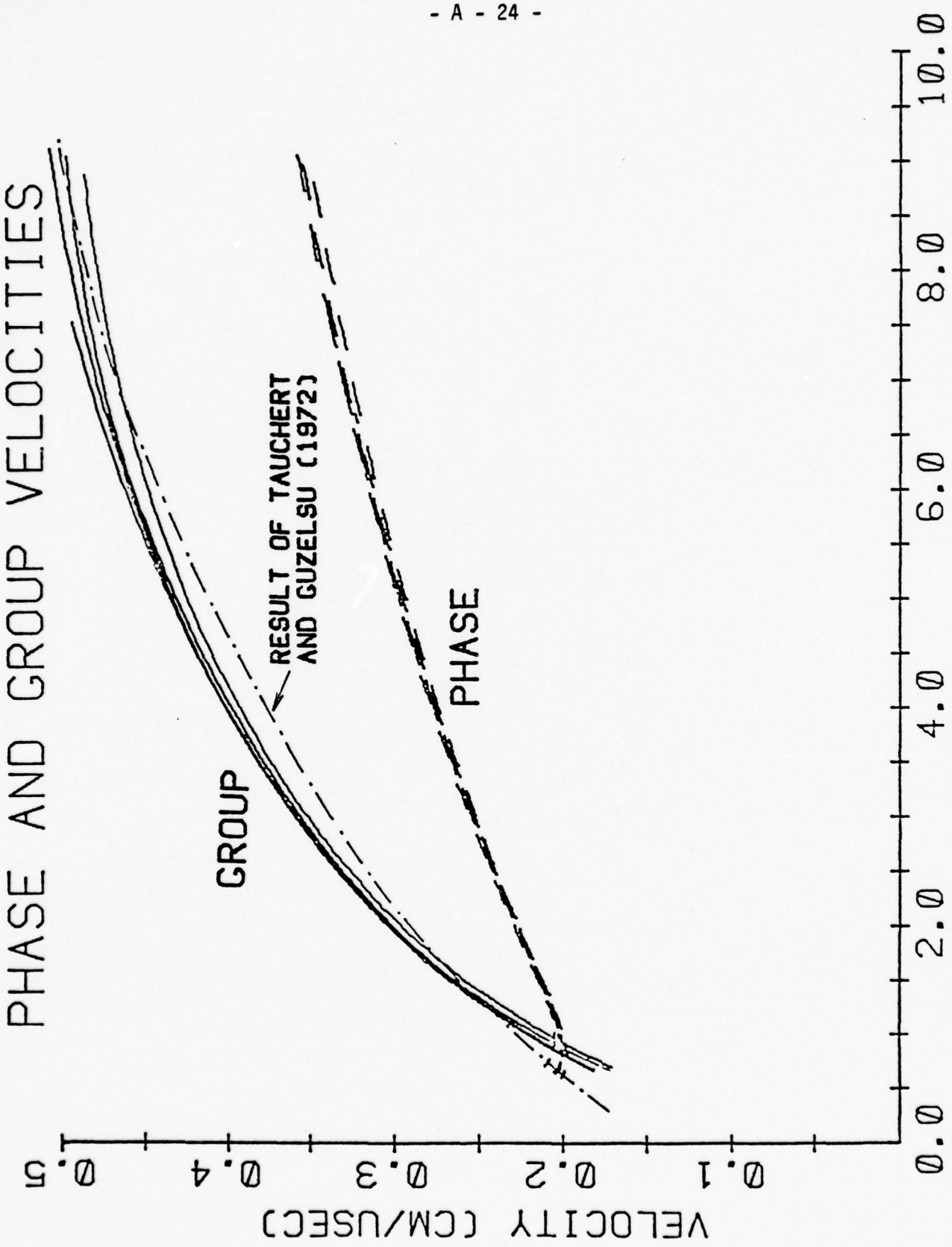
PHASE AND GROUP VELOCITIES
GROUP
RESULT OF TAUCHERT AND GUZELSU (1972)
PHASE
VELOCITY (CM/USEC)
0.1
0.2
0.3
0.4
0.5
0.0
2.0
4.0
6.0
8.0
10.0
FREQUENCY (MHZ)

Figure 8

APPENDIX B.

ON THE DETERMINATION OF PHASE AND GROUP VELOCITIES OF DISPERSIVE WAVES IN SOLIDS

Wolfgang Sachse and Yih-Hsing Pao

Department of Theoretical and Applied Mechanics
Cornell University, Ithaca, N. Y. - 14853

January 1977
(Revised July 1977)

Report #2773

Issued by

The Materials Science Center

ON THE DETERMINATION OF PHASE AND GROUP VELOCITIES OF DISPERSIVE WAVES IN SOLIDS

Wolfgang Sachse and Yih-Hsing Pao
Department of Theoretical and Applied Mechanics
Cornell University, Ithaca, N.Y. 14853

ABSTRACT

A new technique is developed to determine the dispersion relation and the propagational speeds of waves in dispersive solids. The phase spectrum of a broadband pulse is linearly related to the dispersion relation of the dispersive medium. The method is simpler than the continuous wave-phase comparison technique. Application is made to measure the phase and group velocities of waves in fiber-reinforced composite materials and in thin wires. This technique is expected to be applicable to measurements of acoustic or electromagnetic wave speeds in other dispersive media.

I. INTRODUCTION

The velocity of a wave is usually associated with the phase difference between the vibrations observed at two different points during the passage of the wave. A plane harmonic wave of amplitude A, angular frequency ω $(= 2\pi f)$ and wavelength $\lambda(= 2\pi/k)$, propagating in a non-attenuating medium may be represented by $A\cos(\omega t - kx+\xi) = A\cos\omega(t - kx/\omega+\varepsilon)$ where $\xi=\omega\varepsilon$ is a constant. The phase of the wave is then defined by the argument of the cosine function and the wave velocity is $v = \omega/k$, which is usually called the phase velocity.

When the phase velocity v of a plane harmonic wave is a function of its frequency or wavelength, then the propagating medium, according to Havelock [1], is dispersive. Such dispersion may be caused by: (i) the presence of specimen boundaries (geometric dispersion), (ii) the frequency dependence of material constants, such as mass density, elastic moduli, dielectric constants, etc. (material dispersion), (iii) the scattering of waves by densely distributed, fine inhomogeneities in a material (scattering dispersion), (iv) the absorption or dissipation of wave energy into heat, or other forms of energy in an irreversible process (dissipative dispersion), and (v) the dependence of the wave speed on the wave amplitude (non-linear dispersion). We shall omit the last-mentioned source of dispersion in the analysis to be presented. The theory of the propagation of pulses in dispersive media is well known [1-3]. The principal feature is that the pulse does not retain its initial shape as it propagates through the dispersive medium. Thus, a short duration pulse may be dispersed into wave trains in time.

Measurements of the phase versus frequency of continuous waves in dispersive media determines the group velocity of the wave. By definition, the group velocity U equals $d\omega/dk = v + k\, dv/dk$. From the data of U versus ω, it seems that one could evaluate v as a function of k by integrating the preceeding equation. However, in order to complete the integration, it would require precise values of ω and k at the lower limit of integrations and these could not be easily obtained experimentally.

For unidirectional waves in a solid, the dispersion characteristics are similar to those of the propagation of electromagnetic signals in transmission lines, or those of ultrasonic signals in delay lines. The former is disscussed in many standard texts [4] and the latter was addressed by Young [5]. Young clearly defined the concept of "phase delay" of continuous waves, and "group delay" of a narrow bandwidth pulse, and he showed that the latter is related to the derivatives of the phase characteristics of the pulse with respect to frequency. From the "group delay," the group velocity of a pulse can be determined. However, Young [5] considered only waves without attenuation, and pulses with narrow bandwidth.

Previous experimental work in solids has dealt with both continuous-waves and pulses. As mentioned above, the phase velocity may be frequency-dependent. Thus errors in its determination are minimized by using monochromatic waves. In the so-called π-point phase comparison technique, which appears to have been first used by Balamuth [6] and is recently reviewed by Papadakis [7], the half-wavelength of the wave is determined directly by varying the propagation distance between source and receiver and observing the corresponding π-phase change of the received signal. Although such measurements are easily carried out in gaseous and fluid media, this is not the case in solids.

The main difficulty of the π-point phase technique is that the phase must be measured to a frequency low enough so that the phases between the transmitted and received signals differ exactly by π, or a known multiple of π [7]. To overcome this difficulty, Lynnworth et al. [8] used a sliding wedge technique to vary the propagation length in 3-dimensional carbon-phenolic composite specimens to determine the wavelength and hence the phase velocity directly. Unfortunately, the wedge interface and the pronounced material microstructure can give rise to anomalous effects. Other researchers used specimens of fixed thickness and varied the frequency of excitation. The group velocity is thus determined as a function of frequency, as will be discussed in more detail in Section II. Recently, however, Ting and Sachse [9] have combined the variable frequency method and the variable path-length method. They developed a constraint equation from which the number of wavelengths in a specimen can be established unambiguously.

Pulse measurements of the dispersion have been made with broadband pulses as well as narrowband bursts. In a broadband pulse technique, the frequency dependent reflection coefficient of a pulse from a buffer-specimen interface is measured, from this, the frequency-dependent phase velocity of the specimen inferred. The technique has been applied to phase velocity measurements in teflon [8] and boron-epoxy specimens [10]. There is serious question, however, whether the measured phase velocity is that which characterizes the bulk material, rather than the interfacial layer at the buffer and specimen interface.

In burst measurements, one measures the delay of a burst with a certain center frequency through the thickness of a specimen. Tauchert [11], utilizing pairs of transducers with differing center frequencies, measured the

group velocity in this way in boron-epoxy composite materials. Using a single pair of broadband transducers and varying the frequency of the electrical excitation burst, Sutherland and Lingle [12] measured dispersive effects in boron-aluminum specimens. With burst delay measurements in very dispersive materials, it is possible to unambiguously identify equivalent points in the undelayed burst and the specimen-delayed burst therefore, it is not clear what wavespeed is actually measured [7]. Furthermore, as emphasized by Young [5], the envelope of a received signal may differ considerably from the input signal and this makes it difficult to determine its delay-time through a specimen. This problem can be minimized by amplitude modulating the r.f. carrier with a particular, smooth envelope such as a Gaussian contour [5].

Other examples of elastic wave dispersion measurements are those with a shock tube technique by Whittier and Peck [13], in carbon-phenolic composites; by Yew and Yogi [14], in steel-epoxy specimens with an optical interferometry technique; and by Kaarsberg [15] in geological materials with ultrasonic techniques.

Our investigation was motivated primarily by the determination of wave speeds in eutectic and fiber-reinforced composite materials, and porous solids. In Section III of this paper we review the principles of the π-point phase comparison method and its limitations in uniquely determining the dispersion relation of a material.

In Section IV, we propose a different technique - based on the phase spectral analysis of a broadband pulse - for the determination of phase and group velocities of waves in dispersive media. In this technique, the phase function of a Fourier-analyzed pulse is evaluated. It is shown how

the phase and group velocities as well as the dispersion relation for the material can be determined directly from it. The experimental technique and its implementation are described in Section V. In Section VI we show the results obtained with this technique to characterize dispersive and non-dispersive materials and to compare them with the results obtained with the continuous wave, π-point phase comparison technique.

Although the examples we cite in this paper are limited to ultrasonic stress waves and pulses propagating in dispersive solids, the principle and the experimental technique described in Sections III and IV are perfectly general, such that similar observations can be made with linear acoustic, electro-magnetic, or optical waves propagating in dispersive media. A general discussion of the dispersion of waves and the concept of group velocity can be found in Refs. [16] and [17].

II. DISPERSION OF A LINEAR, CAUSAL SYSTEM

A solid specimen sustaining the propagation of a plane wave along a length or thickness dimension, comprises a one-dimensional, linear system. Such systems admit plane wave solutions of the form:

$$u(x,t) = Ae^{i\omega(t\pm x/v-\xi)} = Ae^{i(\omega t\pm kx-\varepsilon)} \qquad (1)$$

As noted earlier, the phase velocity $v(=\omega/k)$ is a constant for non-dispersive media. More generally, v is a function of ω. Also, in real systems, the wave amplitude gradually attenuates through beam spreading, scattering, mode conversion, coupling losses between transducer

and specimen and the absorption and dissipation of energy in the specimen material. As long as the total energy is conserved, ω must be real and the attenuation of the wave amplitude can be accounted for by letting k be complex. That is

$$k = \beta + i\alpha \tag{2}$$

For waves propagating in the direction of $+x$, Eq. (1) is then written as

$$u(x,t) = Ae^{-\alpha x}e^{i(\omega t \pm \beta x - \omega \xi)} \tag{3}$$

In general, both α and β in Eqs. (2) and (3) are functions of ω.

Although the function in (3) is not periodic, we can still define a phase velocity v, and group velocity U of the wave as

$$v = \frac{\omega}{Re(k)} = \frac{\omega}{\beta}, \quad U = \frac{d\omega}{d\beta} \tag{4}$$

The wave length of the decaying sinusoidal wave is $2\pi/\beta$, and α is the attenuation factors. We caution that the group velocity U as customarily defined only has physical significance when $\alpha(\omega)$ is small [16]. By small $\alpha(\omega)$ we mean that the attenuation in nepers for one wave length is small.

The dispersive property of a physical system is characterized by specifying the α and β as functions of ω. For a causal system, in which the response of the system to a driving force cannot precede the first arrival of the signal generated by the driving force, the $\alpha(\omega)$ and $\beta(\omega)$ are related by Kramers-Kronig relation. Mathematically, for a causal system, the $\alpha(\omega)$ is related to the Hilbert transform of $\beta(\omega)$, and vice versa [3]. Thus we shall regard that $\alpha(\omega)$ can be calculated from $\beta(\omega)$, and the dispersion property of the linear causal system is defined by the relation

$$\beta = \hat{\beta}(\omega), \quad \text{or} \quad \omega = \hat{\omega}(\beta) \tag{5}$$

In Eq. (5), $\hat{\beta}(\omega)$ is a real function of the real variable ω, and $\hat{\omega}(\beta)$ is the inverse function of $\hat{\beta}(\omega)$. The objective of the experiments is to determine the dispersion relation, Eq. (5), for a solid medium, and then to calculate $v(\omega)$ and $U(\omega)$ from Eq. (4); or to measure either v or U and then determine the dispersion relation, Eq. (5).

If there exists a dissipative mechanism in the system, the frequency ω may also be complex valued. One example is the thermoelastic wave in solids [18, 19]. In such a case, there are two choices: one is to restrict the answer to real ω but complex k, the other is to limit the answer to real k but complex ω. The corresponding phase velocities are defined respectively as $v = \omega/\mathrm{Re}(k)$ and $v = \mathrm{Re}(\omega)/k$, and the two results do not always agree. The meaning of group velocity also becomes uncertain. The situation is further complicated by possible anisotropy in the material. The concept of phase and group velocity for waves in a dissipative and anisotropic medium has been discussed in Ref. [19].

III. THE METHOD OF π-POINT PHASE COMPARISON

By transmitting continuous waves of varying frequencies through a specimen of length L, a phase versus frequency relation can be measured for the specimen. By adjusting the frequency to, say, f_1, the signal at the receiver is first brought into in-phase or π-radians out-of-phase with that from the transmitter. At this frequency, let the wavelength be λ_1, and the number of complete sine waves by N_1 thus $f_1 = v_1 N_1/L$ where v_1 is the phase velocity. An increment of the phase by a known multiple of π radians is made by changing the frequency to f_2 with N_2 number of sine waves of length λ_2, and $f_2 = v_2 N_2/L$.

For nondispersive waves, $v_1 = v_2 = v$. By setting $N_2 = N_1 + 1$ in the experiment [7], we find

$$v = L(f_2 - f_1) \tag{6}$$

In this situation, it is not necessary to know the exact value of N_1 at the starting point.

For dispersive media, v_1 differs from v_2 because of the change of frequency, and so one cannot determine either, unless N_1 is known exactly. However, as illustrated by the hypothetical experimental data shown in Fig. 1, it is still possible to determine the group velocity U by measureing $f_j (j = 1,2,3,\ldots)$ and N_j where $N_{j+1} = N_j + 1$. This follows from the *following relations:*

$$U = \lim_{\Delta N \to 0} \left(L \frac{\Delta f}{\Delta N}\right) = L \frac{df}{dN} = \frac{L}{dN/df} \tag{7}$$

In this case, U is only determined in a range of frequencies higher than f_1.

Once $U(N)$ is determined for a range of $N \geq N_1$, the phase velocity can be calculated by the following integration

$$v = \frac{1}{N} \int^{N} U(N)dN + v_1 \frac{N_1}{N} \tag{8}$$

Thus, we are facing an uncertainty unless the value for N_1 is known. This can easily be seen from Fig. 1, in which the location of N_1 is uncertain. The slope of the tangent to the curve f vs. N which is related to the group velocity can be calculated for $N > N_1$ but the slope of the secant (a line from the origin to a point on the curve) cannot be determined. The slope of the secant is precisely v/L.

IV. THE METHOD OF PHASE SPECTRAL ANALYSIS

Fourier Synthesis of the Transmitted Pulse

It was mentioned that a linear system admits plane harmonic waves described by Eq. (1), and if attenuation exists, by Eq. (3). Based on the principle of superposition, a pulse $u(x,t)$ propagating in the linear medium $x \geq 0$ may be expressed as an addition of all plane harmonic waves,

$$u(x,t) = \frac{1}{2\pi} \int_{-\infty}^{\infty} d\omega \int_{-\infty}^{\infty} A(\xi) e^{-\alpha x} e^{i\omega(t-x/v-\xi)} d\xi \qquad (9)$$

where $A(\xi)$ is an unspecified amplitude function, and both v and α are functions of ω.

Assuming that the medium is at rest initially, and a disturbance $F(t)$ is generated at the location $x = 0$, for $t \geq 0$, that is

$$u(0,t) = F(t) \qquad (10)$$

Then, from Eq. (9), we find

$$F(t) = \frac{1}{2\pi} \int_{-\infty}^{\infty} d\omega \int_{-\infty}^{\infty} A(\xi) e^{i\omega(t-\xi)} d\xi \qquad (11)$$

This expression is exactly the Fourier integral representation of the input time function $F(t)$. Hence $A(\xi) = F(\xi)$, and the amplitudes of the superposed plane waves are fixed by the end condition at $x = 0$. We thus write Eq. (9) as

$$u(x,t) = \frac{1}{2\pi} \int_{-\infty}^{\infty} d\omega \int_{-\infty}^{\infty} F(\xi) e^{-\alpha x} e^{i\omega(t-x/v-\xi)} d\xi \ . \qquad (12)$$

If α and v are constant, we find from Eq. (12) and the theorem of Fourier integral the well-known result

$$u(x,t) = F(t-x/v) e^{-\alpha x} \qquad (13)$$

The input pulse $F(t)$ at $x = 0$ propagates through the non-dispersive medium without a change of shape, except for an exponential decrease in amplitude.

When both α and v are functions of ω, the double integral in Eq. (12) gives rise to the dispersed pulse at any location. To determine the signal at $x = L$ in a specimen, we evaluate first the integration with respect to ξ,

$$u(L,t) = \frac{1}{2\pi} \int_{-\infty}^{\infty} \bar{F}(\omega) e^{-\alpha L} e^{i\omega(t-L/v)} d\omega \tag{14}$$

where

$$\bar{F}(\omega) = \int_{-\infty}^{\infty} F(\xi) e^{-i\omega\xi} d\xi \tag{15}$$

Note that $\bar{F}(\omega)$ is the Fourier transform of the input $F(t)$ which is supposed to be known. Since $\beta = \omega/v$, Eq. (14) can be rewritten as

$$u(L,t) = \frac{1}{2\pi} \int_{-\infty}^{\infty} [\bar{F}(\omega) e^{-\alpha L} e^{-i\beta L}] e^{i\omega t} d\omega \tag{16}$$

The exact shape $u(L,t)$ can be calculated from the above integral if the dispersion relation (Eq. 5) is known, but the calculation will be in general be very difficult. However, the spectrum of the transmitted pulse at $x = L$ is given by the Fourier transform of $u(L,t)$, which is precisely the quantity inside the brackets of Eq. (16),

$$\bar{u}(L,\omega) = \bar{F}(\omega) e^{-\alpha L} e^{-i\beta L} \tag{17}$$

In general, the Fourier transform of a causal time function $F(t)$ may be complex. Thus

$$\bar{F}(\omega) = |\bar{F}(\omega)| e^{-i\omega\xi} = |\bar{F}(\omega)| e^{-i\phi_o} \tag{18}$$

where $\phi_o = \omega\xi$. Eq. (17) can then be written as

$$\bar{u}(L,\omega) = |\bar{F}(\omega) e^{-\alpha L}| e^{-i(\beta L + \omega\xi)} \tag{19}$$

This means that the phase spectrum of $u(L,t)$ is given by

$$\phi(\omega) = \beta L + \phi_o = L\hat{\beta}(\omega) + \omega\xi \qquad (20)$$

It is seen from Eq. (20) that the phase spectrum of the transmitted pulse is linearly related to the dispersion relation $\hat{\beta}(\omega)$ of the meidum.

Phase Spectra and Dispersion Relations

In the next section, we show experimentally that an accurate spectrum of the transmitted pulse $u(L,t)$ can be determined by digital analysis. The spectrum is composed of two parts: the amplitude spectrum and the phase spectrum. The latter is precisely the $\phi(\omega)$ of Eq. (20). Thus, the dispersion relation of a medium is determined uniquely by the phase spectrum of a propagating pulse,

$$\hat{\beta}(\omega) = \frac{1}{L}[\phi(\omega)-\phi_o] \qquad (21)$$

The phase velocity is obtainable from the experimental data,

$$v(\omega) = \frac{\omega}{\beta} = \frac{\omega L}{\phi(\omega)-\phi_o} \qquad (22)$$

By differentiating the phase function, we obtain

$$\frac{d\phi(\omega)}{d\omega} = L\frac{d\hat{\beta}}{d\omega} + \xi = \frac{L}{d\omega/d\beta} + \xi = \frac{L}{U} + \xi \qquad (23)$$

The group velocity U can then be calculated from the derivatives of the phase spectrum

$$U = L\left(\frac{d\phi}{d\omega} - \xi\right)^{-1} \qquad (24)$$

When ω is complex-valued, as in a dissipative medium, the Fourier synthesis in Eq. (9) is meaningless unless the path of integration for the complex variable ω is specified. An alternative would be to assume k real valued and to write

$$u(x,t) = \frac{1}{2\pi}\int_{-\infty}^{\infty} dk \int_{-\infty}^{\infty} A(\zeta)e^{ik(vt-x-\zeta)}d\zeta \qquad (25)$$

The ζ is a phase constant in the space-axis, and $v = \omega/k$ must be complex valued for a medium with damping. As shown by Havelock [1], an integral representation such as Eq. (25) is suitable for analyzing initial value problems (u is given at $t = 0$). For waves in a medium without dissipation, these two representations (Eqs. 9 and 25) are equivalent.

A Simple Example

That the phase spectrum of a propagating pulse is related to the group velocity may be illustrated by the following simple example. Consider a square pulse of duration $2T_o$ generated at $x = 0$,

$$u(0,t) = u_o \qquad 0 < t < 2T_o \tag{26}$$

and $u(0,t) = 0$ for $t < 0$, and for $t > 2T_o$. At time $t = T$, the pulse travels through a non-dispersive and non-attenuating medium a distance L. Since the pulse shape is preserved (Eq. 13), the disturbance at $x = L$ is

$$u(L,t) = u_o \qquad T < t < T+2T_o \tag{27}$$

and $u(L,t) = 0$ for $t < T$ and $t > T+2T_o$. The Fourier transform of $u(0,t)$ and $u(L,t)$ are respectively

$$\bar{u}(0,\omega) = 2T_o \frac{\sin\omega T_o}{\omega T_o} e^{-i\omega T_o} \tag{28}$$

$$\bar{u}(L,\omega) = 2T_o \frac{\sin\omega T_o}{\omega T_o} e^{-i\omega(T+T_o)} \tag{29}$$

The phase spectrum of $\bar{u}(L,\omega)$ and its derivative are

$$\phi(\omega) = \omega(T+T_o), \qquad d\phi/d\omega = T+T_o \tag{30}$$

Comparing Eq. (29) with Eq. (19) with $\alpha = 0$, Eq. (30) with Eq. (23), we identify $\xi = T_o$ and find $T = L/U$. This last result states that the square pulse traverses the distance L with the group velocity U which, in this case, is also equal to the phase velocity.

V. EXPERIMENTS AND DIGITAL SPECTRAL ANALYSIS

The two methods described in the previous sections were implemented to measure the dispersion relation and phase and group velocities for non-dispersive and dispersive materials. The experimental set-up for the continuous wave π-point phase difference measurements is similar to that in Ref. 7 (Fig. 22). The block diagram for the equipment used in the pulse transmission experiments is shown in Fig. 2. Two nearly identical broadband transducers were used in both experiments.

In the continuous wave experiments, the source transducer was excited with a 10 volt peak-to-peak harmonic wave ranging in frequency from 50 kHz to 20 MHz. The signals from the receiver transducer were amplified and displayed on an oscilloscope. The amplitude and phase measurements of the continuous waves were made directly from the oscilloscope, and with a vector voltmeter for frequencies above 1 MHz.

In the pulse experiments, the source transducer was excited with a -250 volt pulse of 35 nsec duration. A sampling oscilloscope was used to overcome the bandwidth limitation of the A/D converter attached to a mini-computer. Any selected portion of a time record could be sampled by means of a digital delay unit used in conjunction with the sampling plug-in unit of the oscilloscope.

A Fast-Fourier transform algorithm was used to compute the Fourier amplitudes of the input time function $F(t)$. The actual time record is associated with 1024 time domain data points which were padded with 1024 zeroes. The real and imaginary parts of the Fourier transform, $\bar{F}_1(\omega)$ and $\bar{F}_2(\omega)$, respetively, were first calculated. The absolute value of the transform is given by $|\bar{F}(\omega)| = [\bar{F}_1(\omega)\bar{F}_2(\omega)]^{1/2}$, and the phase function by $\phi(\omega) = \tan^{-1}[\bar{F}_2(\omega)/\bar{F}_1(\omega)]$.

The computer algorithm limits the values of ϕ in the reduced range from π to $-\pi$. Thus, discontinuities of π for the phase spectra were found whenever the magnitude of $\phi(\omega)$ becomes less than or greater than zero and 2π. This was corrected for by adding or subtracting the amount of jump to render the phase spectrum continuous. The resultant data was then used to compute the wavenumber, phase velocity and group velocity associated with the pulses $u(0,t)$ and $u(L,t)$ according to Eqs. (21), (22) and (24).

To initialize the pulse analysis system and thus set ϕ_o, the source transducer was placed in intimate contact with the receiving transducer and the maximum of the received excitation pulse was made to coincide with the start of the sampled time record by means of the vernier-controlled digital delay unit. In this way ϕ_o was set equal to 0. Alternatively, the phase spectrum of the received excitation pulse could be computed and stored in the data analysis system. This spectrum is exactly ϕ_o and it could be subtracted from all subsequent phase spectra calculations.

The sampled sweep was digitally delayed in steps of 100 nsec until the pulse to be analyzed was displayed on the sampling oscilloscope. The time shift, τ_s, in increments of 100 nsec, relative to $\tau_s = 0.0$ was read into the computer as was the propagation distance, L. Equations (21), (22) and (24) for the dispersion relation, phase and group velocity, respectively were modified to include the time shift factor. They are, in terms of frequency f,

$$\hat{\beta}(f) = L^{-1}[\phi_o - \phi(f)] + 2\pi f\tau_s \qquad (31)$$

$$v(f) = \frac{2\pi fL}{[\phi_o - \phi(f)] + 2\pi f\tau_s} \qquad (32)$$

$$U(f) = 2\pi L/(d\phi/df - \tau_s) \qquad (33)$$

The operation of the system was checked by entering a simulated square pulse, and the phase spectrum $\phi(\omega)$ was indeed a straight line as given by Eq. (30).

VI. EXPERIMENTAL RESULTS

To experiment with waves in a non-dispersive medium, a broadband longitudinal ultrasonic pulse, comprised mainly of frequency components from 3 to 12 MHz was propagated through a 1.900 cm thick specimen of 6061-T6 aluminum. In Figure 3(a) is shown the excitation pulse $u(0,t)$ and in Fig. 3(b) the first received pulse $u(L,t)$ at L = 1.900 cm. In Figures 3(c) and 3(d) are shown the Fourier amplitude spectrum and phase spectrum of $u(L,t)$. Fig. 3(d) also yields the dispersion relation as $\beta = \phi/L$ (Eq. 21). The calculated phase velocity and group velocity of this specimen

are shown in Figs. 3(e) and 3(f). It is clear from Fig. 3(d) that there is little dispersion in this material in the frequency range from 0 to 20 MHz.

The circular dots shown in Figure 3(f) represent the group velocity values determined from the data measured by the continuous-wave, π-phase technique (Eq. 7). For this specimen, no measurements were possible below 1.5 MHz because transducer near-field effects dominated the observations. At frequencies above 7 MHz, data were recorded only at integer frequency points. The average group velocity measured using the continuous-wave technique was 0.618 ± 0.009 cm/μsec.

The results for a dispersive medium such as composite materials are shown in Figure 4. A broadband shear pulse is propagated through a 0.546 cm thick specimen of 96-ply Boron-Epoxy. In this case, the wave propagates in the direction of the fiber and the particle displacement direction is perpendicular to the fiber and parallel to the ply layers. Figs. 4(a) and 4(b) show the initial pulse and the dispersed pulse, respectively, detected at the receiving transducer. It is apparent that the high frequency components of the pulse propagate faster than the low frequency components. The relative amplitudes of the various frequency components in the pulse are shown in Fig. 4(c). As expected, the high-frequency components are markedly lower in amplitude than the low-frequency components. The dispersion relation is shown in Fig. 4(d), which is no longer a linear function of ω. This curve is obtained from the experimental phase spectrum by scaling the

ordinate with the length L. Figures 4(e) and 4(f) show the results of the phase and group velocity computation for the frequency range 0 - 10.0 MHz. Results for the spectral amplitudes beyond 10.0 MHz are not dependable, as the amplitudes become negligibly small there.

The circular dots on the group velocity curve are obtained from the π-phase technique. The extent of the dispersion can be readily seen in the dispersion curve in Fig. 4(d).

As another demonstration of the application of the Fourier phase analysis technique, we show its use in the analysis of a broadband pulse propagating in a 76.4 cm length of 1.61 mm (OD) Remendur tubing. In this case, both source and receiving transducers consisted of 280 turn coils of #32 AWG wire wound on a section of glass tubing. The coils were slipped over the ends of the Remendur tubing and a -50 volt pulse having a width of about 1 μsec was used as excitation. The incident pulse contains frequency components from 150 to 500 KHz. The signal, received with a second coil placed over the other end of the tubing, is shown after 40 db amplification in Fig. 5(a). The pulse has been shifted by 135.7 μsec to bring it on scale. In contrast to the previous example, the low frequency components of the pulse in this case propagate faster than the high frequency components. The amplitude spectrum normalized to the maximum value is shown in Fig. 5(b), while in Fig. 5(c) are shown the derived dispersion relation, phase and group velocities for this material.

VII. CONCLUSIONS

In this paper, it has been shown that the pulse phase spectrum defines the dispersion relation of a linear causal medium, and a phase spectral analysis of a dispersed pulse yields results for both phase and group velocities of waves in dispersive media.

Most continuous-wave techniques require tedious frequency scanning and data reduction. In contrast, the pulse analysis technique is rapid. The technique appears not to be restricted to the analysis of elastic pulses propagating in solids. It could well find application to studies of the dispersion of acoustic or electro-magnetic waves in dispersive media.

ACKNOWLEDGMENTS

We acknowledge the financial support of the National Science Foundation and the Air Force Office of Scientific Research. The NSF support was through a grant to the Materials Science Center of Cornell University and a grant to the College of Engineering.

References:

[1] T. H. Havelock, The Propagation of Disturbances in Dispersive Media, Cambridge University Press, London, 1914.

[2] L. Brillouin, Wave Propagation and Group Velocity, Academic Press, New York, 1960.

[3] M. Elices and F. Garcia-Moliner, Chapt. 4 in Physical Acoustics, vol. V, W. P. Mason and R. N. Thurston, Eds., Academic Press, New York, 1968, pp. 163-219.

[4] R. B. Adler, L. J. Chu and R. M. Fano, Electromagnetic Energy Transmission and Radiation, John Wiley and Sons, Inc., New York, 1960.

[5] E. H. Young, Jr., IRE Trans. UE-9, 13-21 (1962).

[6] L. Balamuth, Phys. Rev., 45, 715-720 (1934).

[7] E. P. Papadakis, Chapt. 5 in Physical Acoustics, Vol. XII, W. P. Mason and R. B. Thurston, Eds., Academic Press, New York, 1976, pp. 277-374.

[8] L. Lynnworth, E. P. Papdakis and W. Rea, "Ultrasonic Measurement of Phase and Group Velocity Using Continuous Wave Transmission Techniques," AMMRC Report CTR 73-2 January 1973.

[9] C. S. Ting and W. Sachse, J. Acoust. Soc. Am., 61, S15 (1977).

[10] W. Sachse and Y. H. Pao, "Ultrasonic Non-destructive Testing of Composite Materials," AFML-AFOSR Mechanics of Composites Review, (AFML Dayton, Ohio, October 1976), pp. 199-207.

[11] T. Tauchert and A. N. Guzelsu, Trans. ASME-J. Appl. Mech., 39, 98-102 (1972).

[12] H. J. Sutherland and R. Lingle, J. Compoiste Matls., 6, 490-502 (1972).

[13] J. S. Whittier and J. C. Peck, J. Appl. Mechanics, 36, 485-490 (1969).

[14] C. H. Yew and P. N. Yogi, in 12th Annual Meeting of the Soc. of Eng. Sic., M. Stern, Ed., (Univ. Texas, Austin, 1975), pp. 497-508.

[15] E. A. Kaarlsberg, Geophysics, 40, 955-961 (1975).

[16] M. J. Lighthill, J. Inst. Maths. Applics., 1, 1-28 (1965).

[17] G. B. Whitham, Linear and Nonlinear Waves, John Wiley & Sons, New York, 1974.

[18] P. Chadwick, "Thermoelasticity, the Dynamic Theory," in Progress in Solid Mechanics, v. 1, Edited by I. N. Sneddon and R. Hill, North-Holland Publishing Co., Amsterdam, 1960.

[19] D. K. Banerjee and Y. H. Pao, J. Acoust. Soc. Am., 56, 1444-1454 (1974).

Figure Captions

Figure 1. Hypothetical dispersion curve-frequency (f) versus number of waves in a length L(N).

Figure 2. Block diagram of the apparatus for measuring the phase spectrum.

Figure 3. Pulse propagation, dispersion, phase and group velocities of waves in 6061-T6 Aluminum

(a) Input P- pulse in voltage (τ_s = 0.0 μsec).

(b) Received P-pulse at L in voltage (τ_s = 2.6 μsec).

(c) The amplitude spectrum of the received pulse (Relative amplitude versus frequency f in mega hertz).

(d) The phase spectrum of the received pulse and the dispersion relation (wave number β in 1/cm versus frequency f in mega hertz).

(e) Phase velocity v (cm/μsec) versus frequency f (mega hertz).

(f) Group velocity U (cm/μsec) versus frequency f (mega hertz).

Figure 4. Pulse propagation, dispersion, phase and group velocities of waves in 96-ply boron-epoxy composite materials. (Shear wave propagating in the direction of the fibers)

(a) Input S-pulse in voltage (τ_s = 0.0 μsec).

(b) Received S-pulse at L in voltage (τ_s = 0.0 μsec).

(c) The amplitude spectrum of the received pulse (Relative amplitude versus frequency f in mega hertz).

(d) The phase spectrum of the received pulse and the dispersion relation (wave number β in 1/cm versus frequency f in mega hertz).

(e) Phase velocity v (cm/μsec) versus frequency f (mega hertz).

(f) Group velocity U (cm/μsec) versus frequency f (mega hertz).

Figure 5. Dispersion of a pulse in a Remendur Tubing of 1.61 mm outer diameter

(a) Received extensional pulse at L in voltage (τ_s = 135.7 μsec).

(b) The amplitude spectrum of the received pulse (relative magnitude versus frequency f in mega hertz).

(c) Dispersion relation (wave number β in 1/cm versus frequency in mega hertz), phase velocity v in cm/μsec, and group velocity U in cm/μsec.

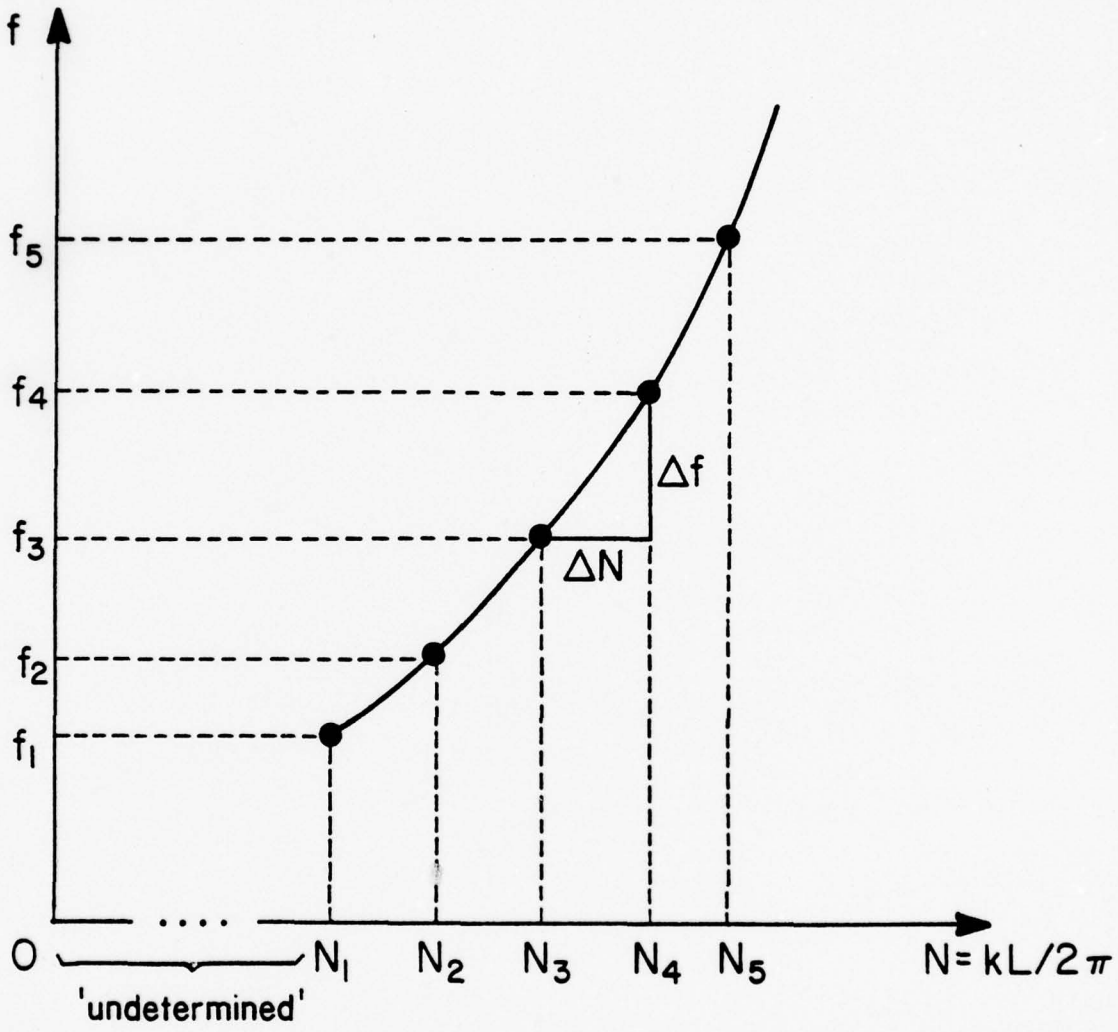

Figure 1

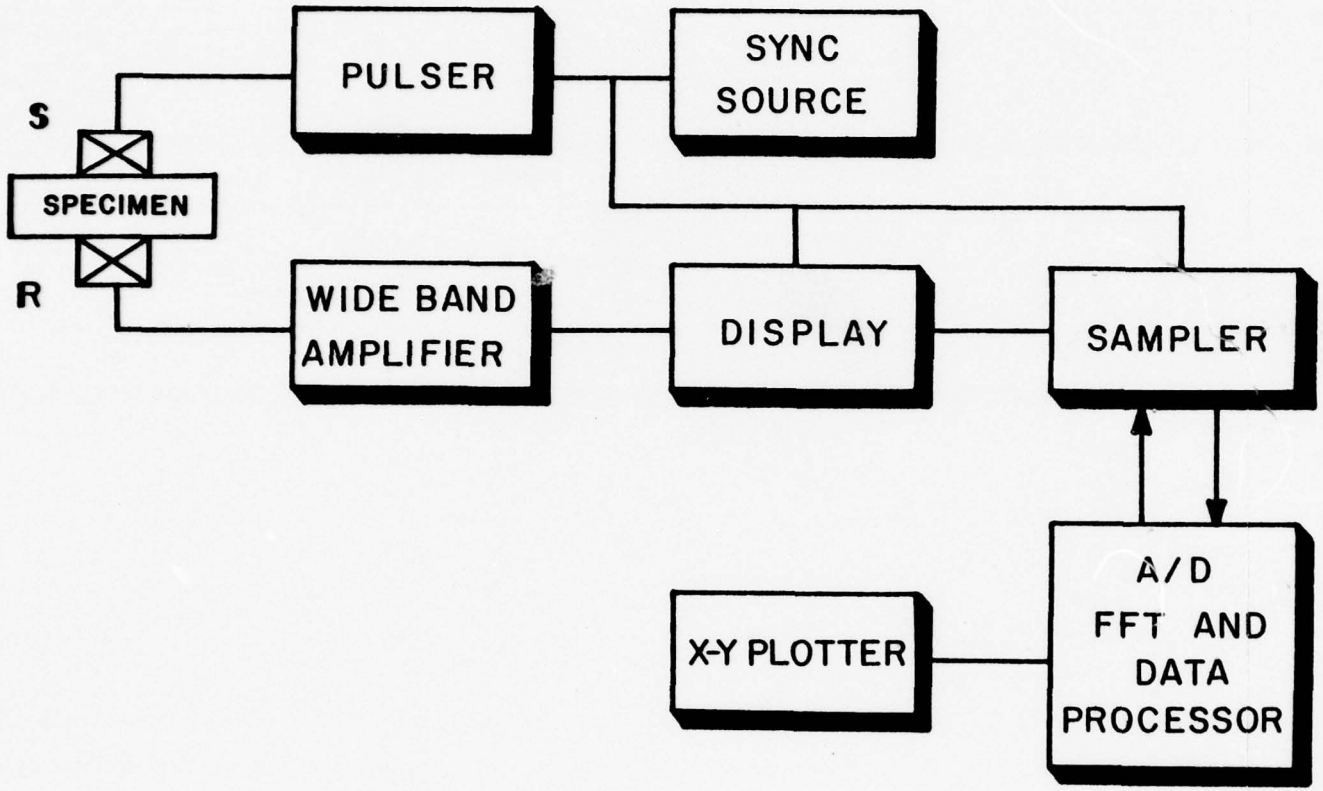
PULSER
SYNC SOURCE
S
SPECIMEN
R
WIDE BAND AMPLIFIER
DISPLAY
SAMPLER
A/D FFT AND DATA PROCESSOR
X-Y PLOTTER

Figure 2

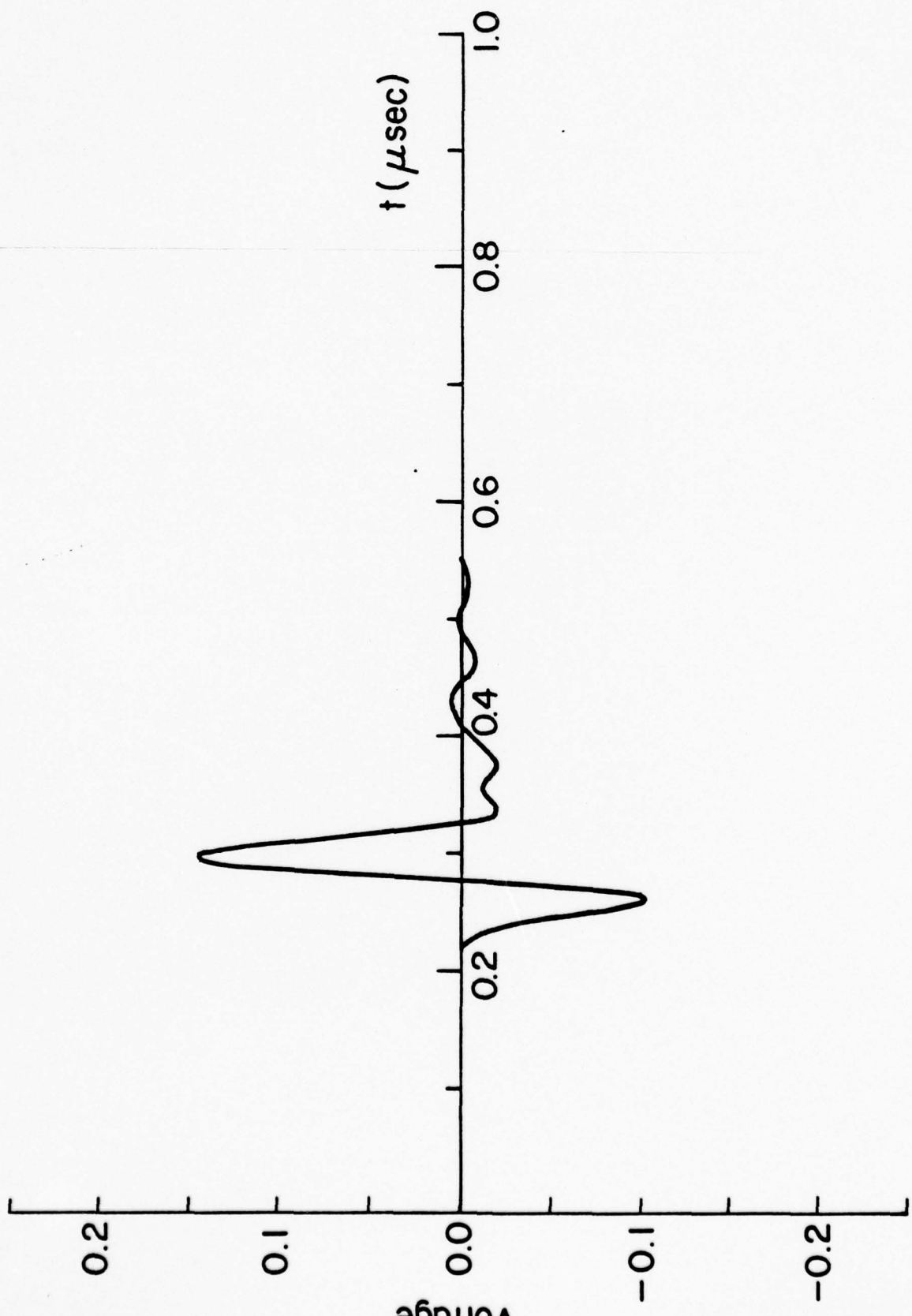

Figure 3a

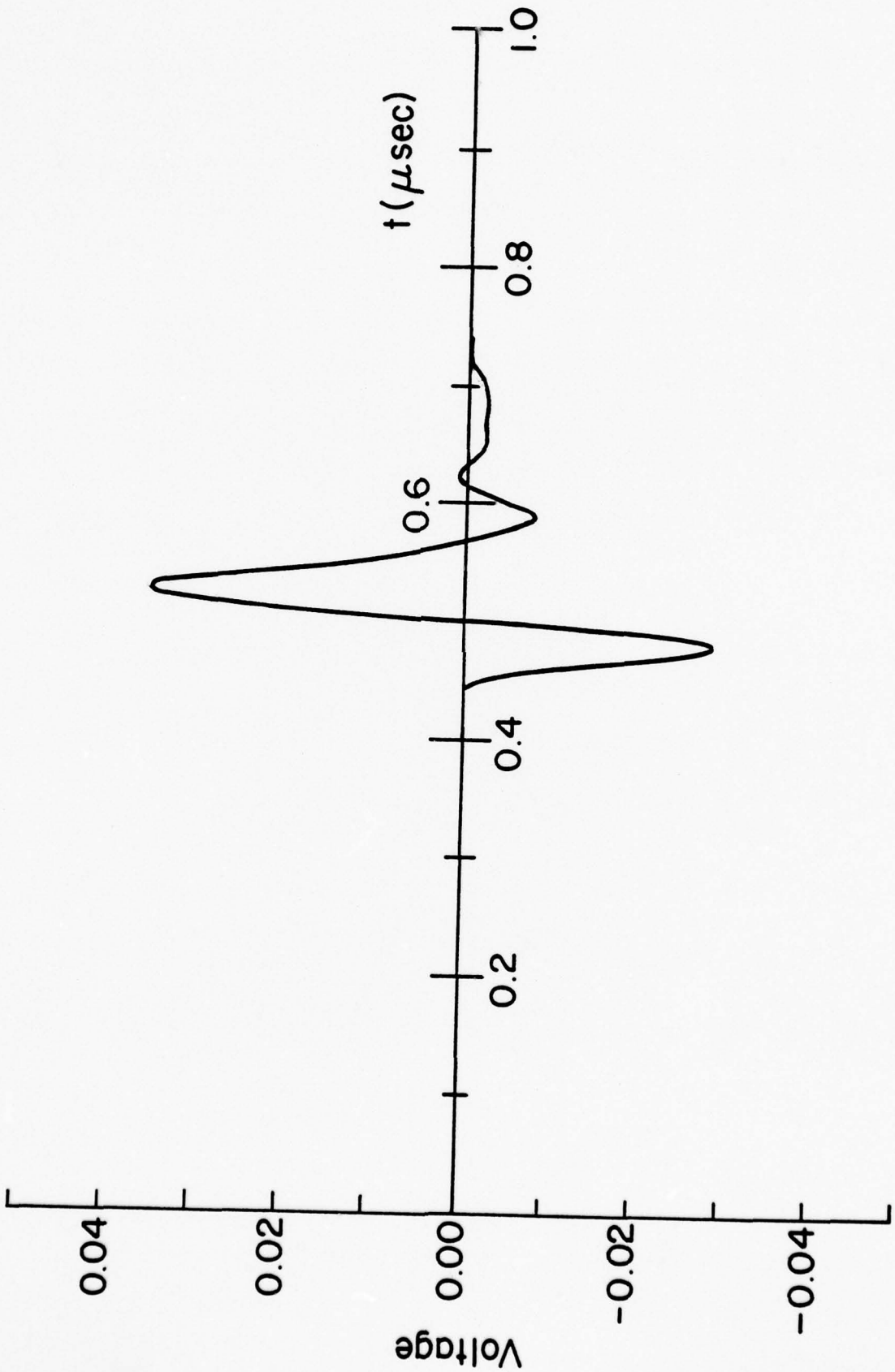

Figure 3b

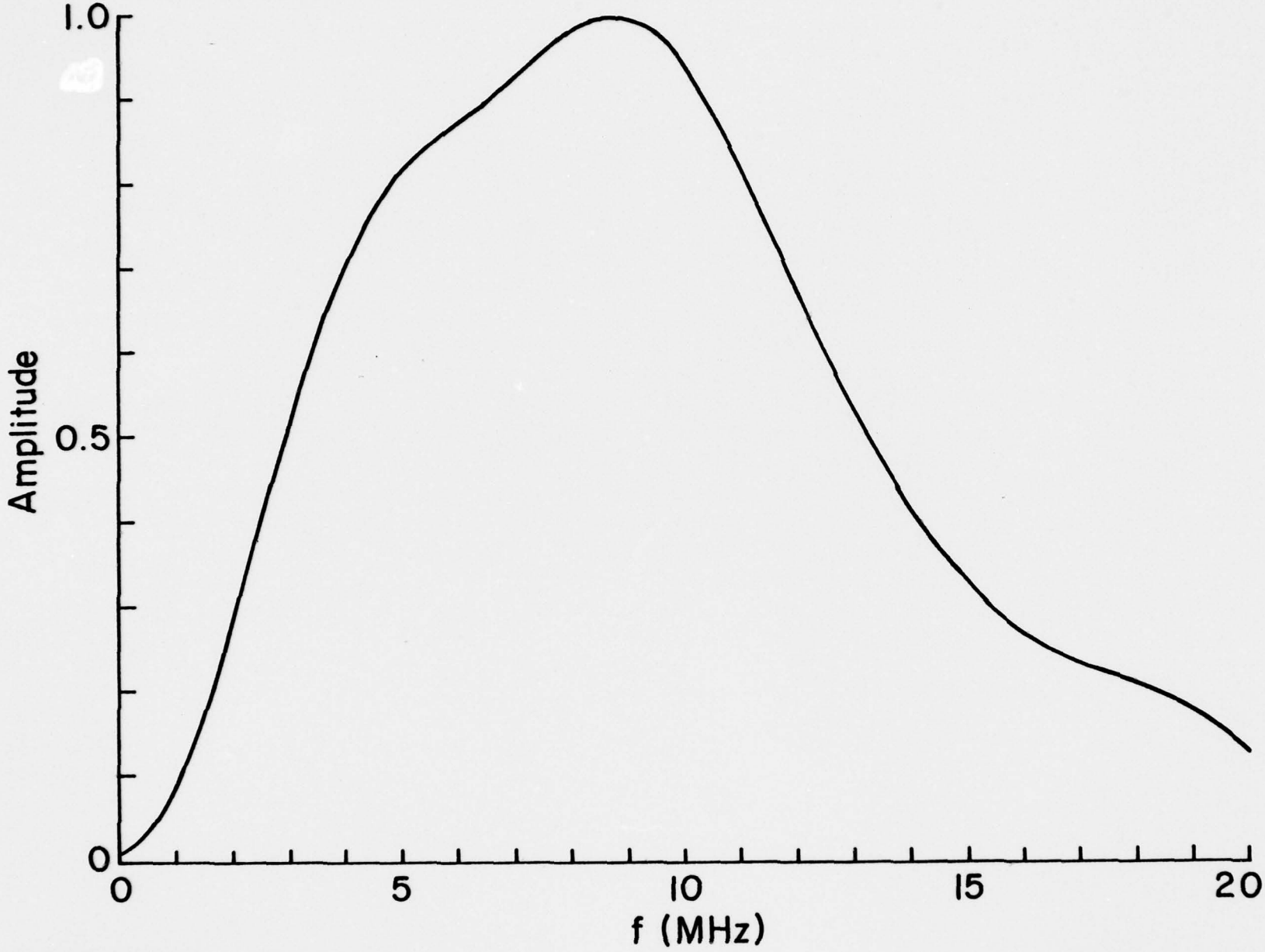

Figure 3c

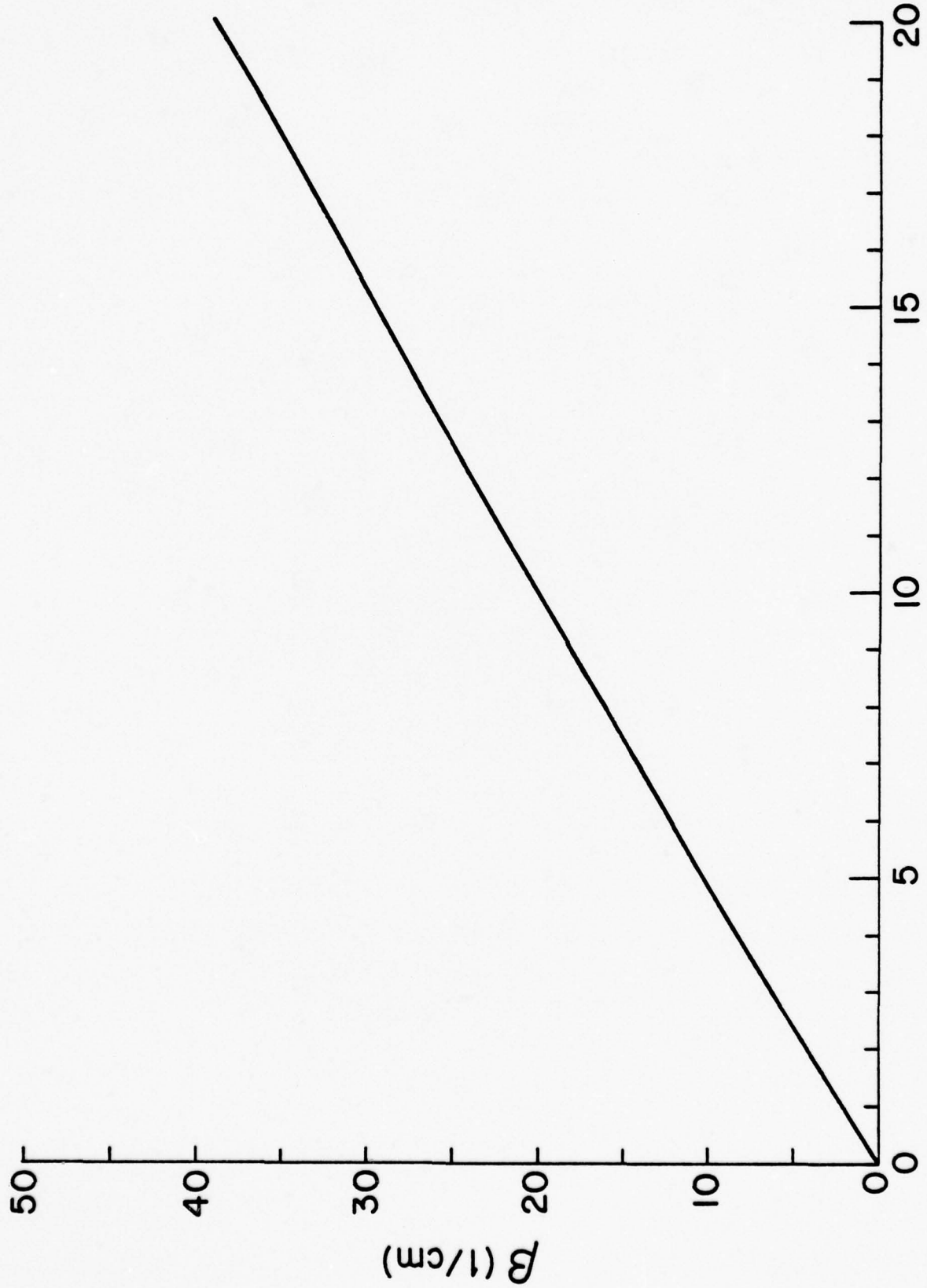

Figure 3d

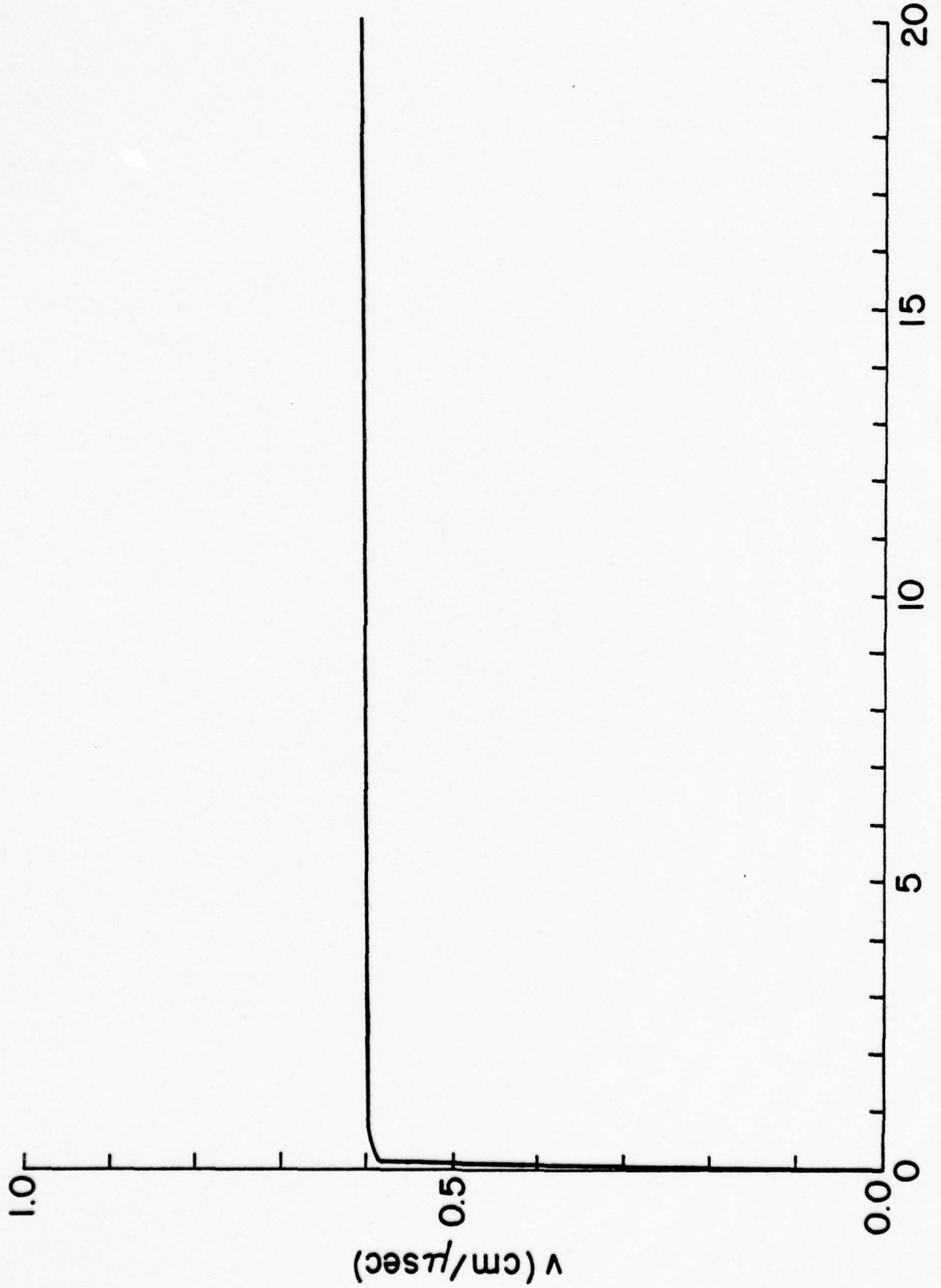

Figure 3e

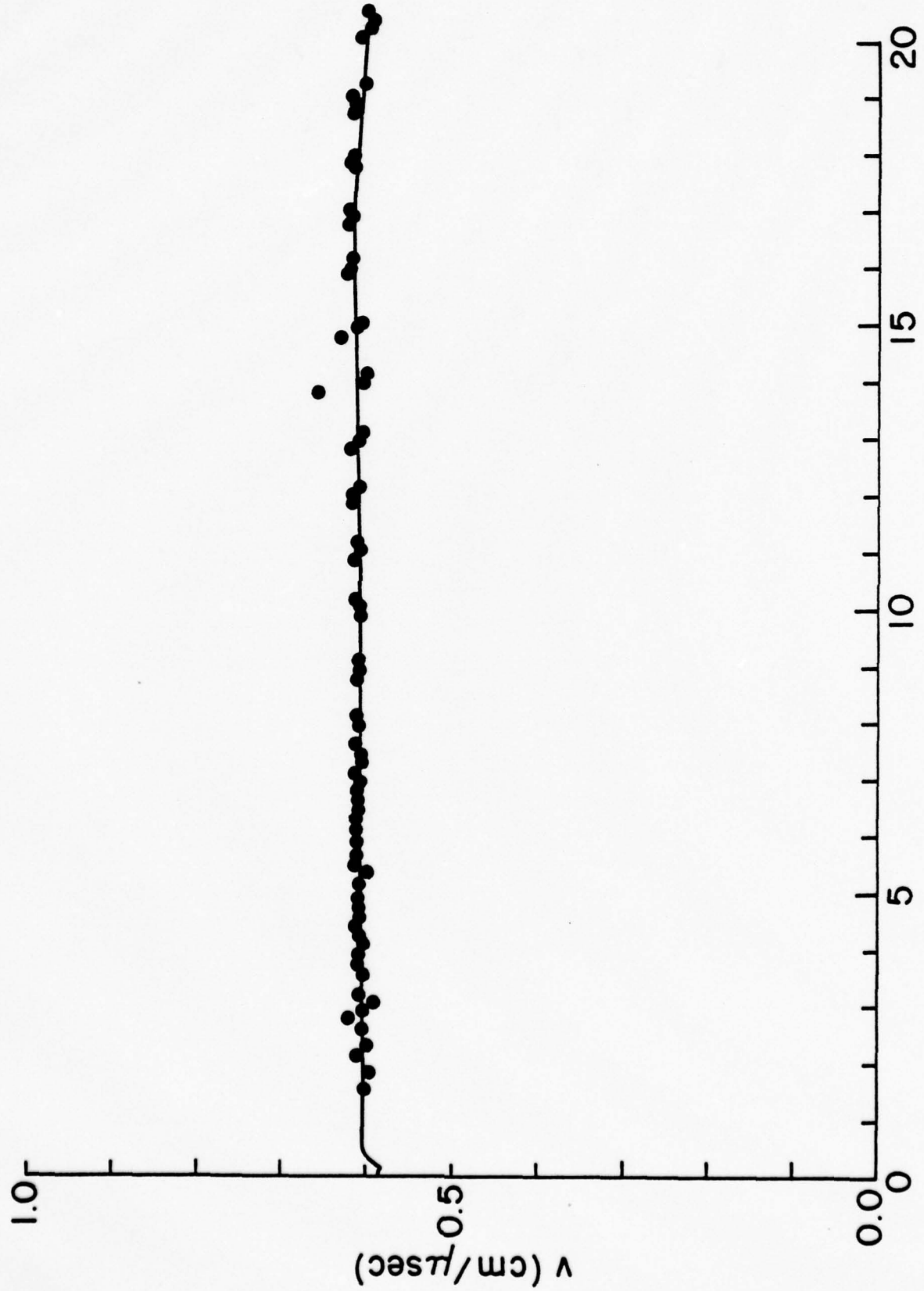

Figure 3f

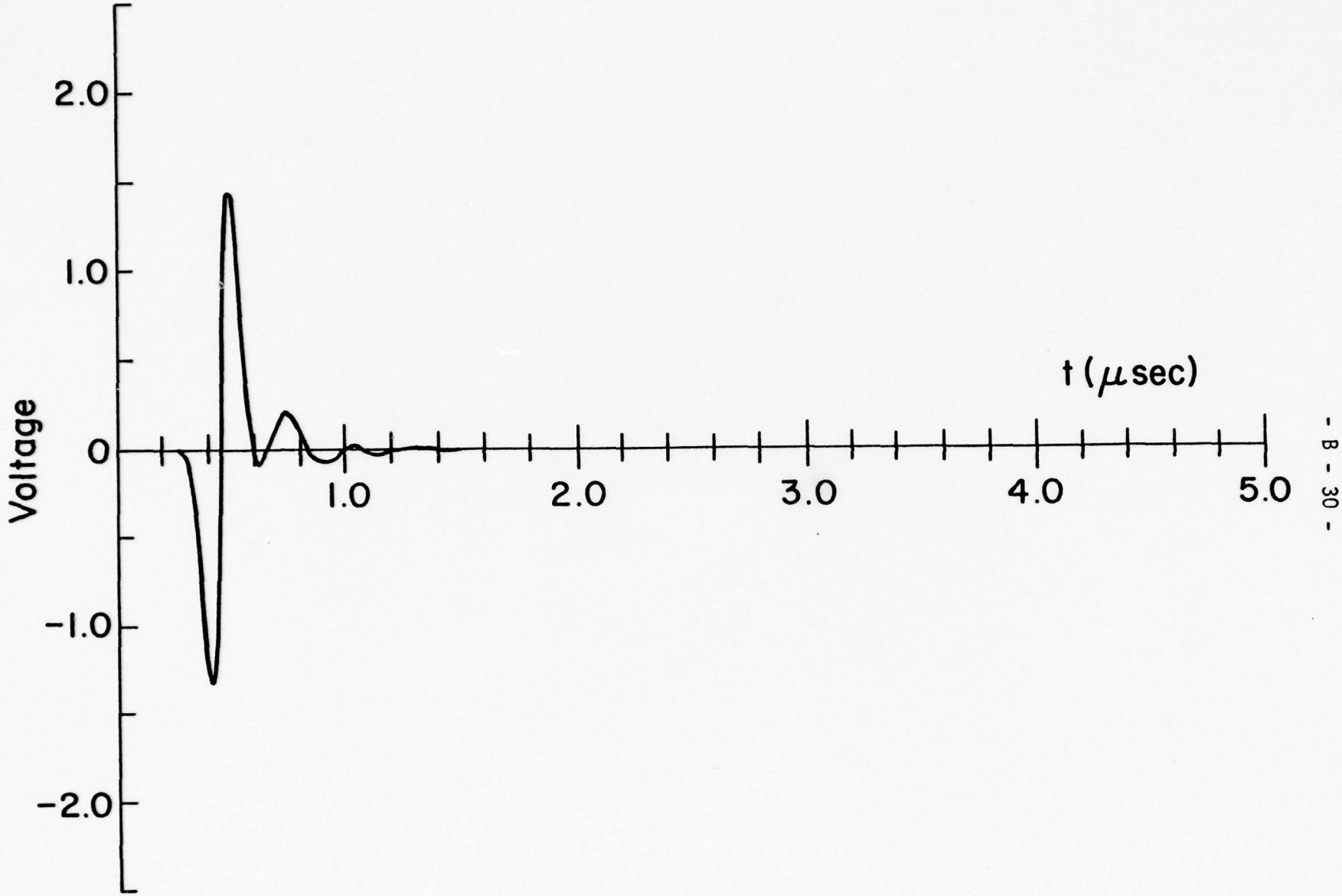

Figure 4a

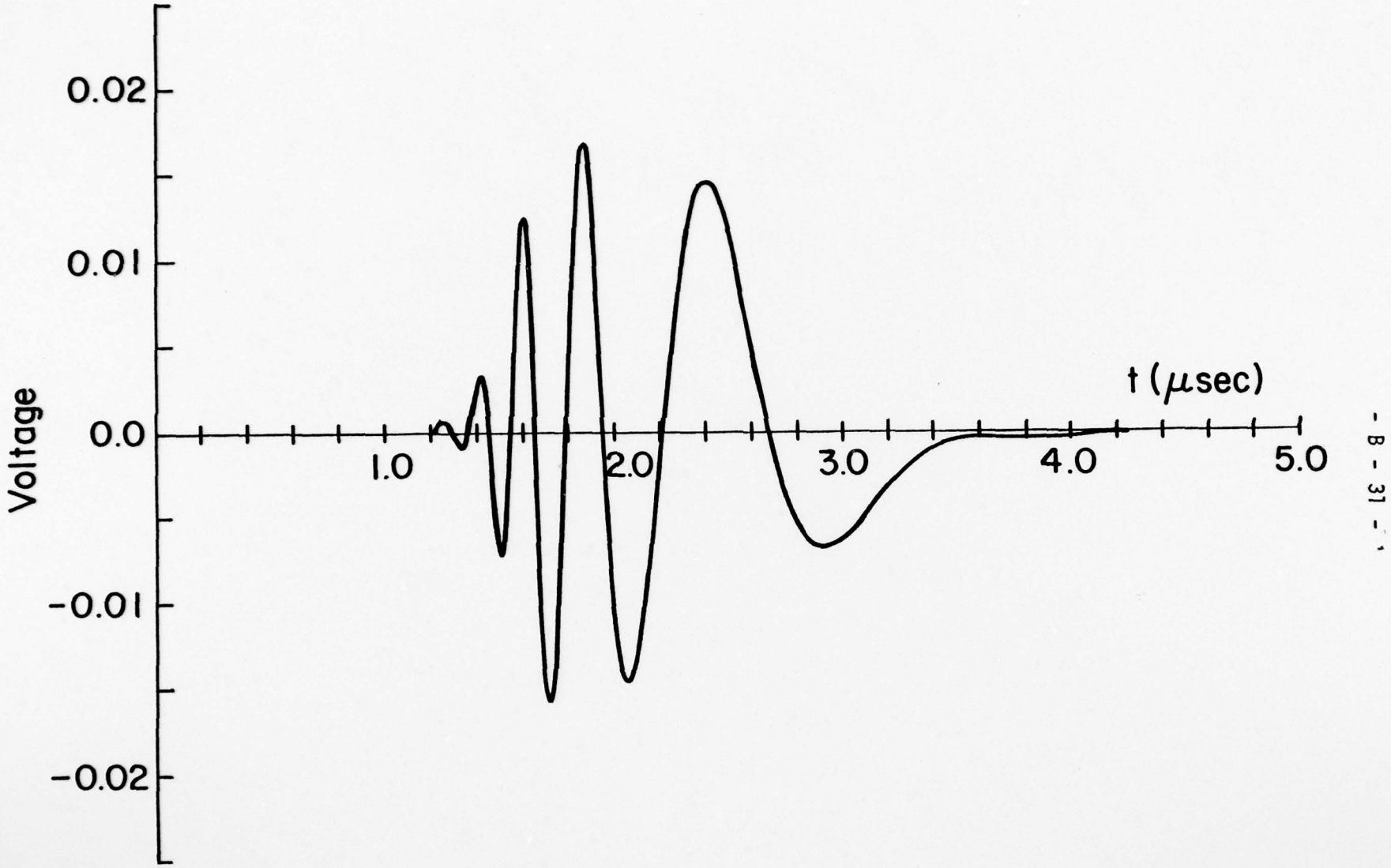

Figure 4b

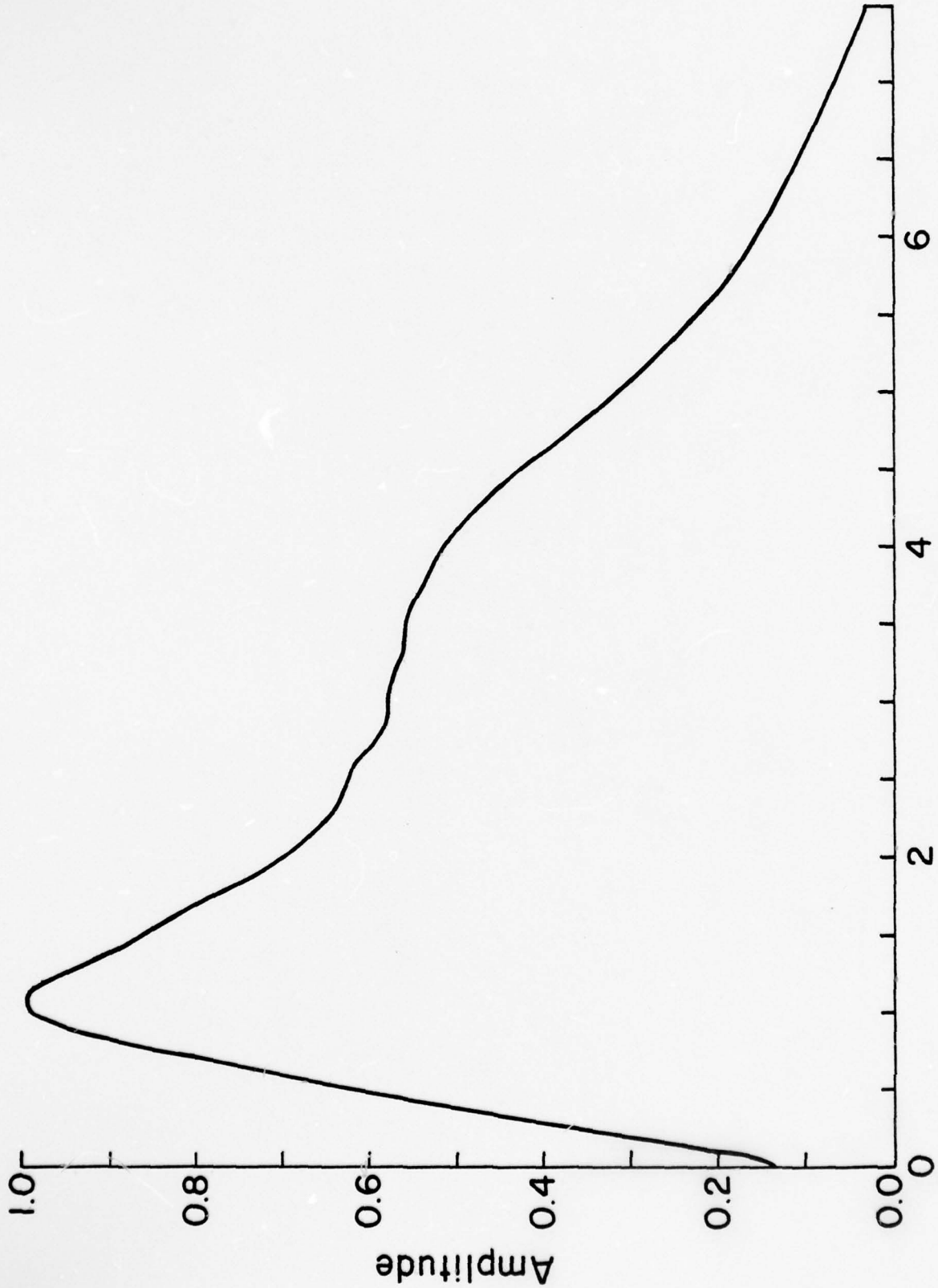

Figure 4c

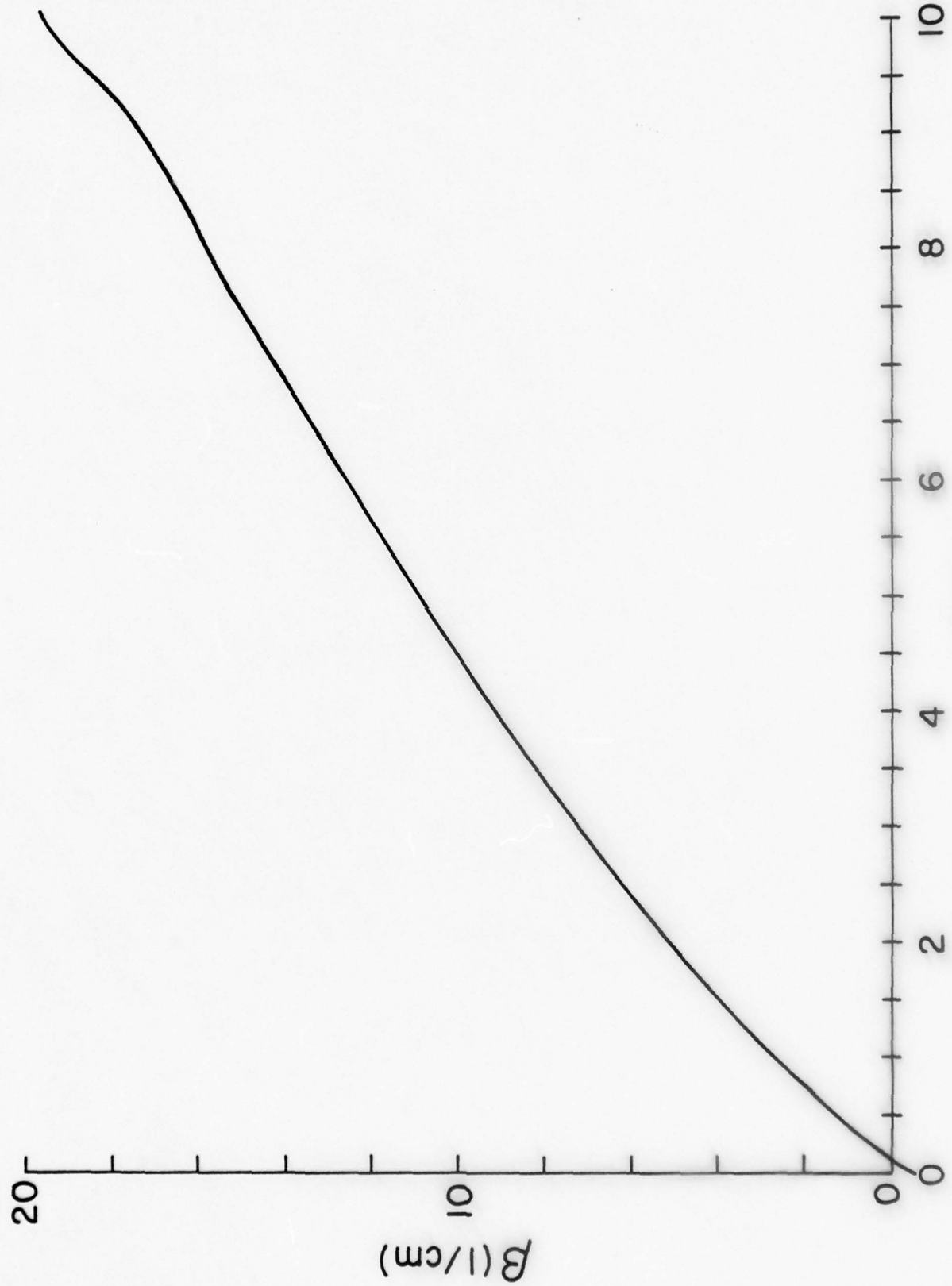

Figure 4d

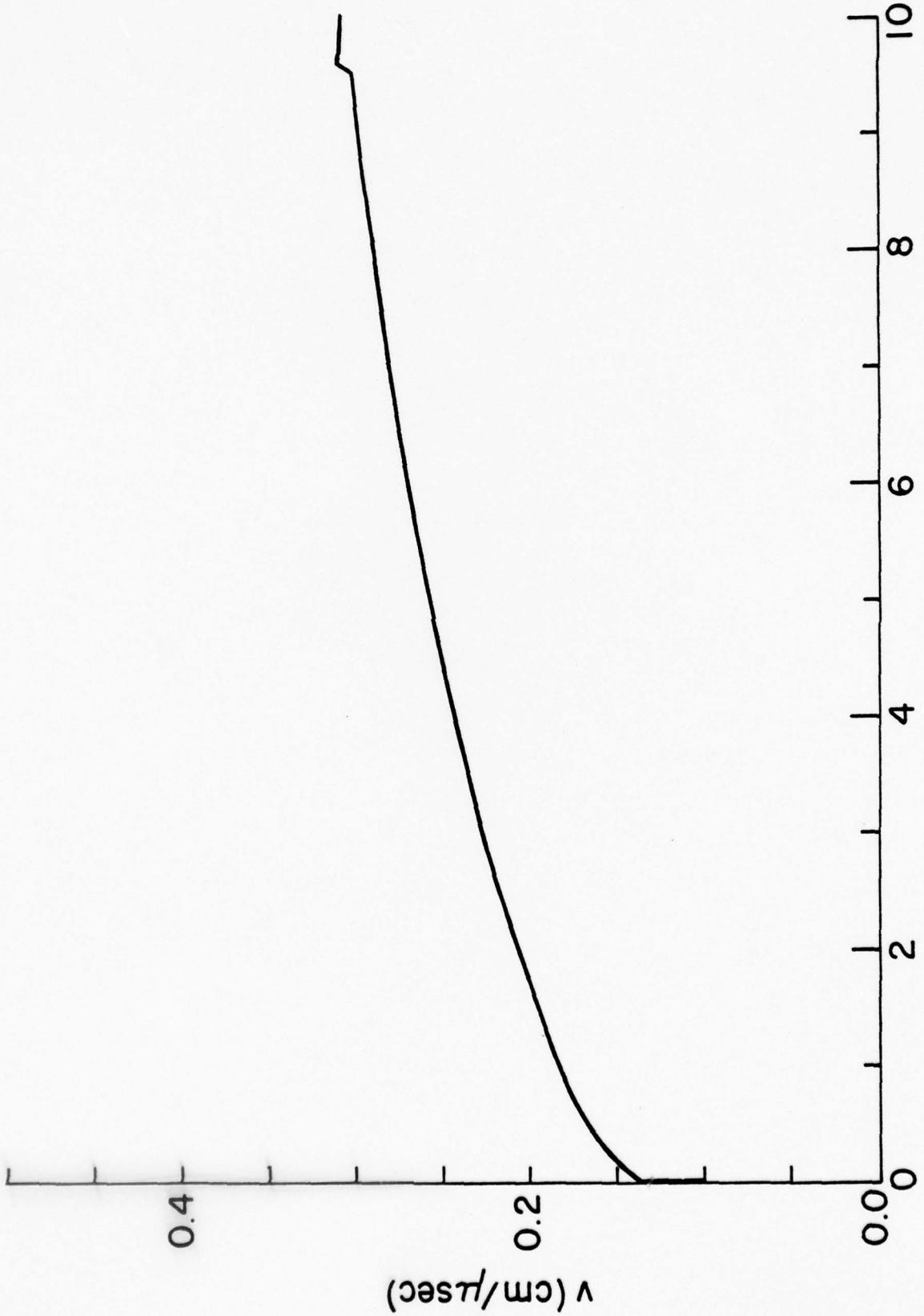

Figure 4e

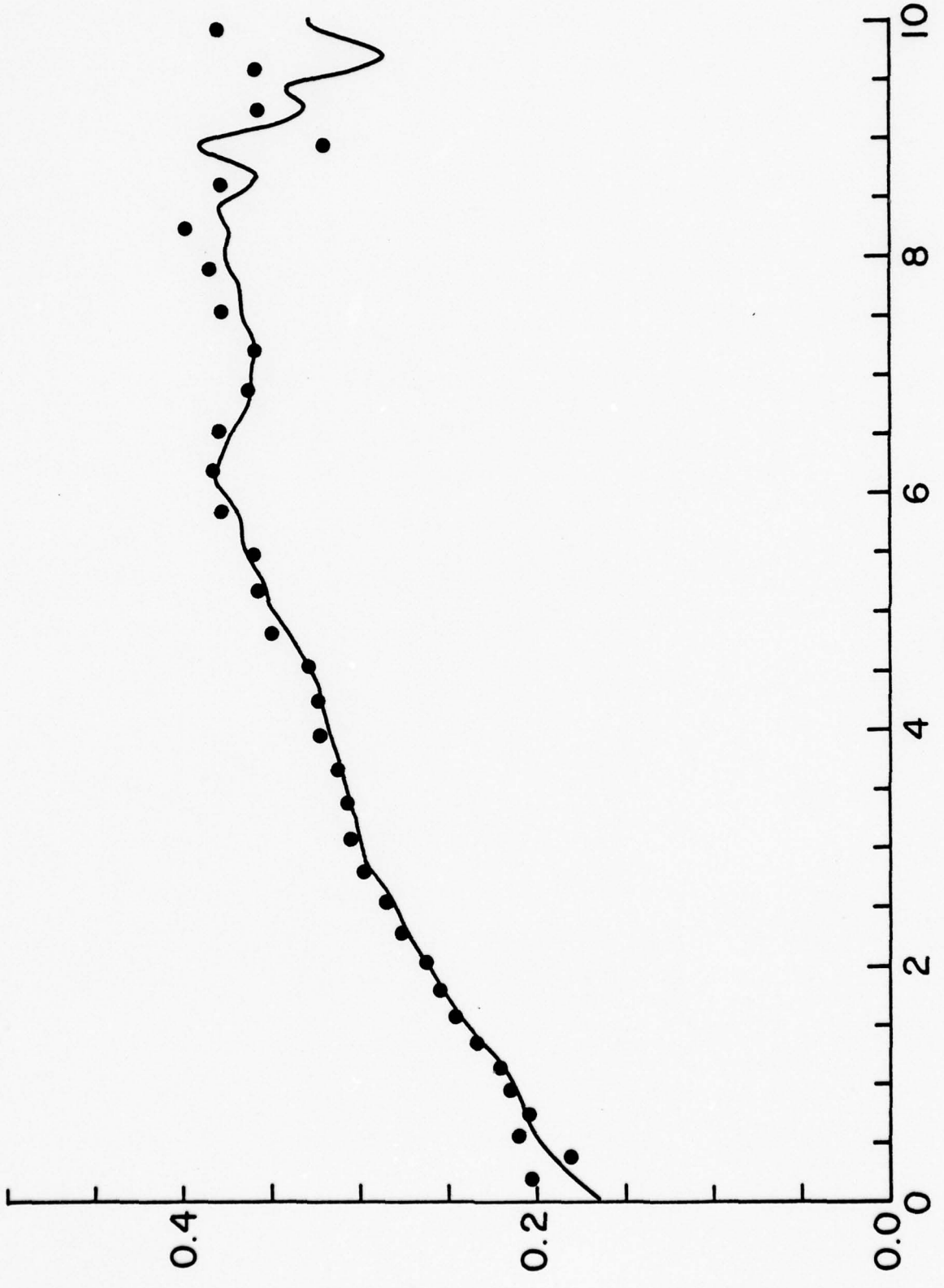

Figure 4f

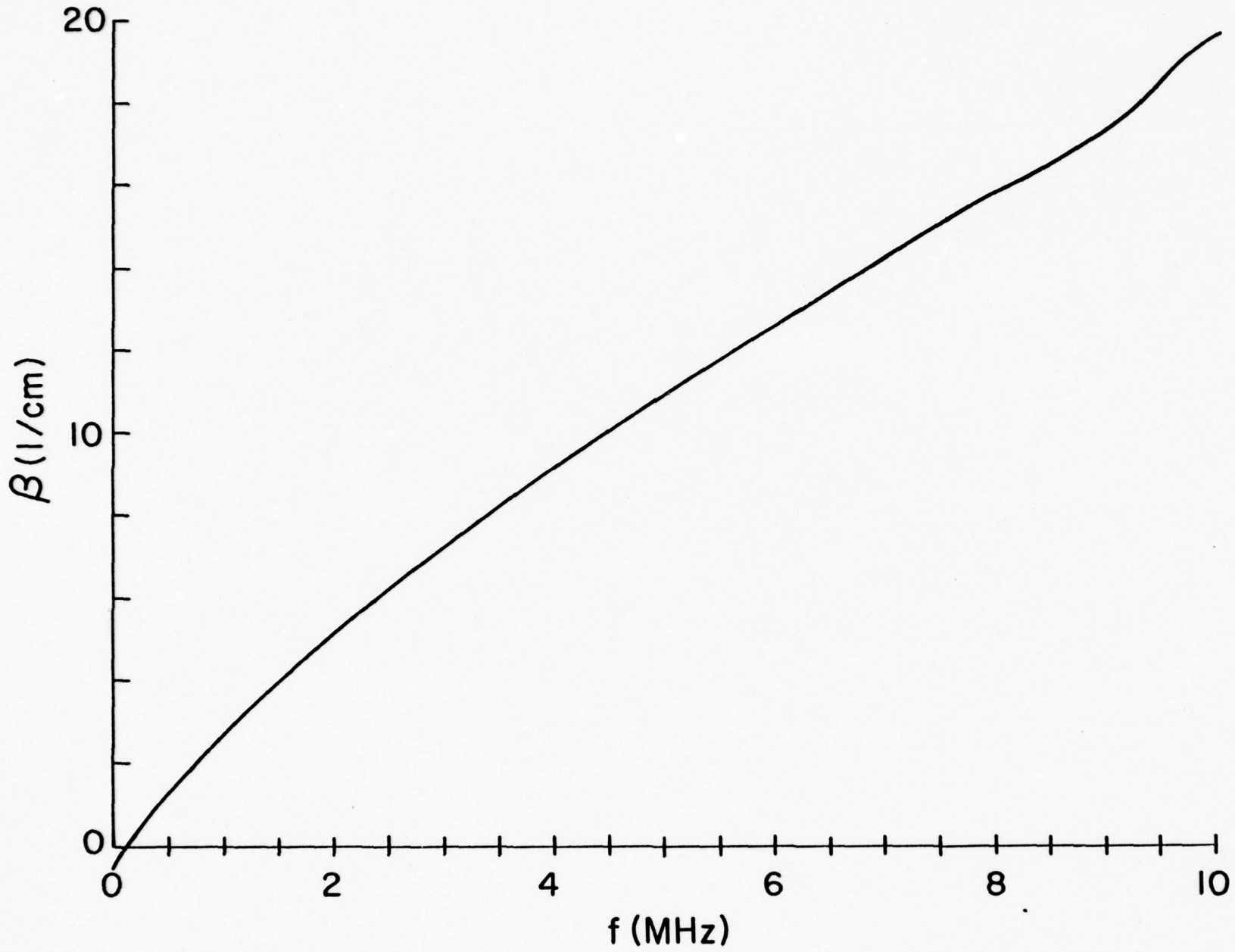

Figure 4d

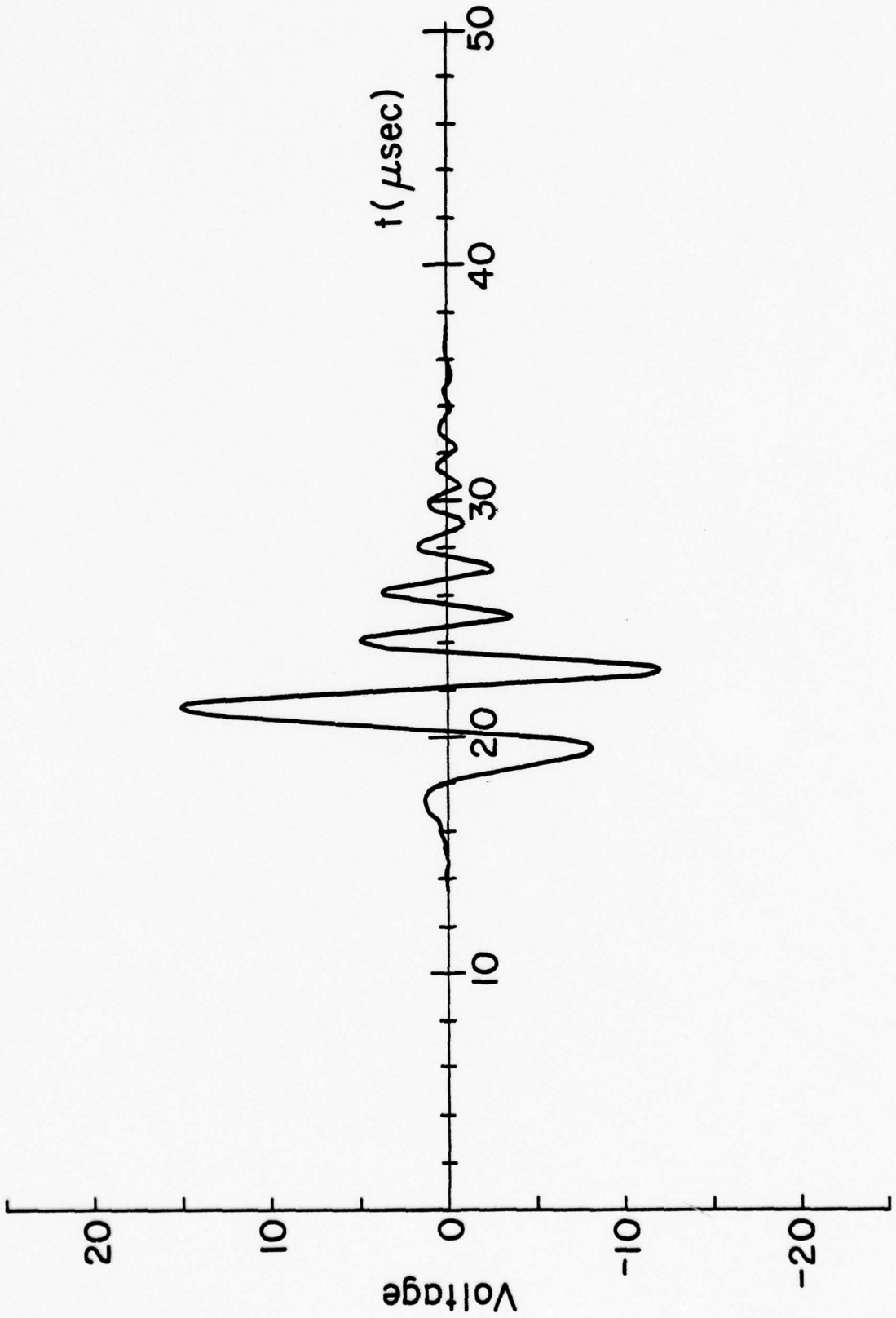

Figure 5a

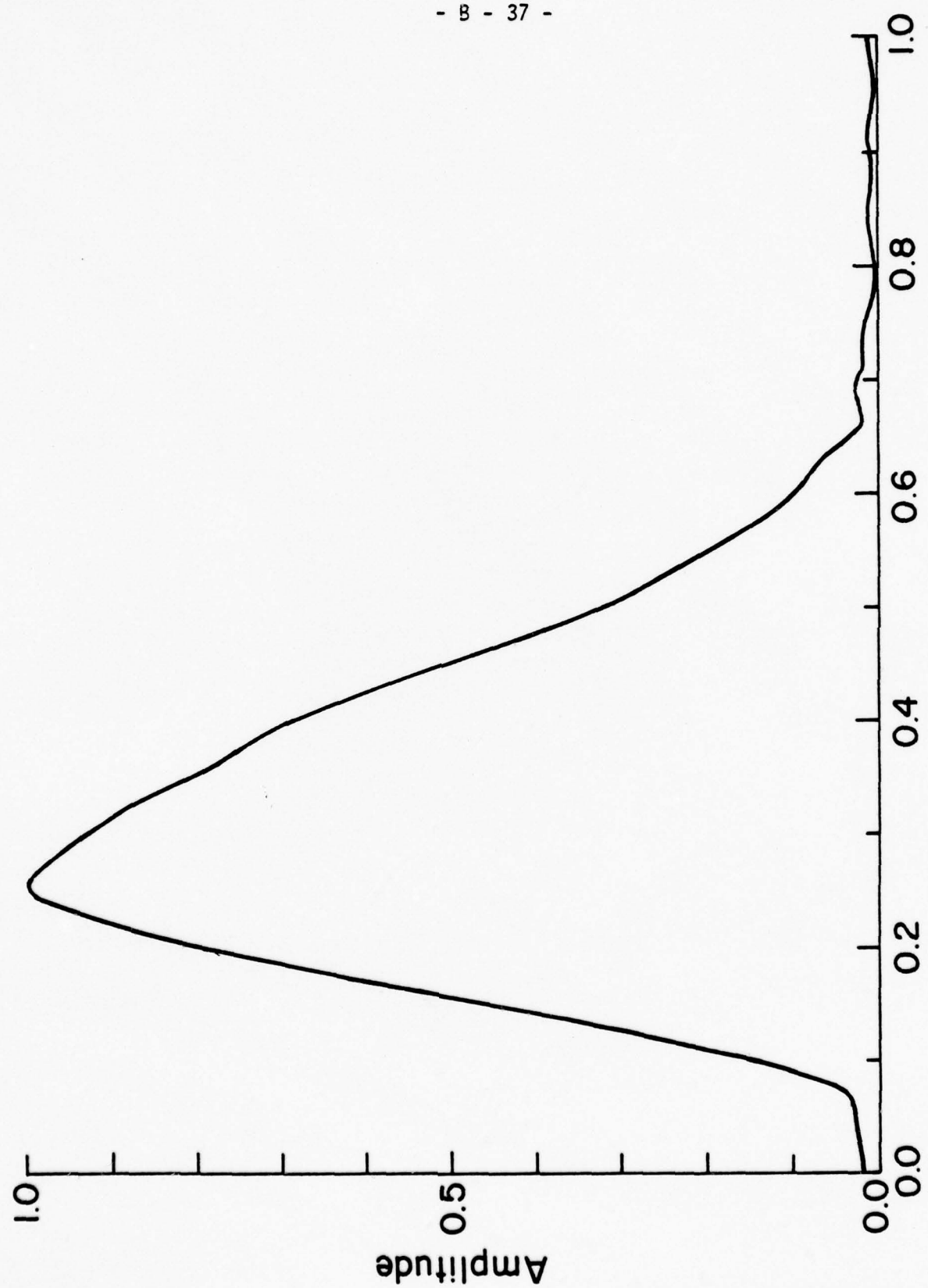

Figure 5b

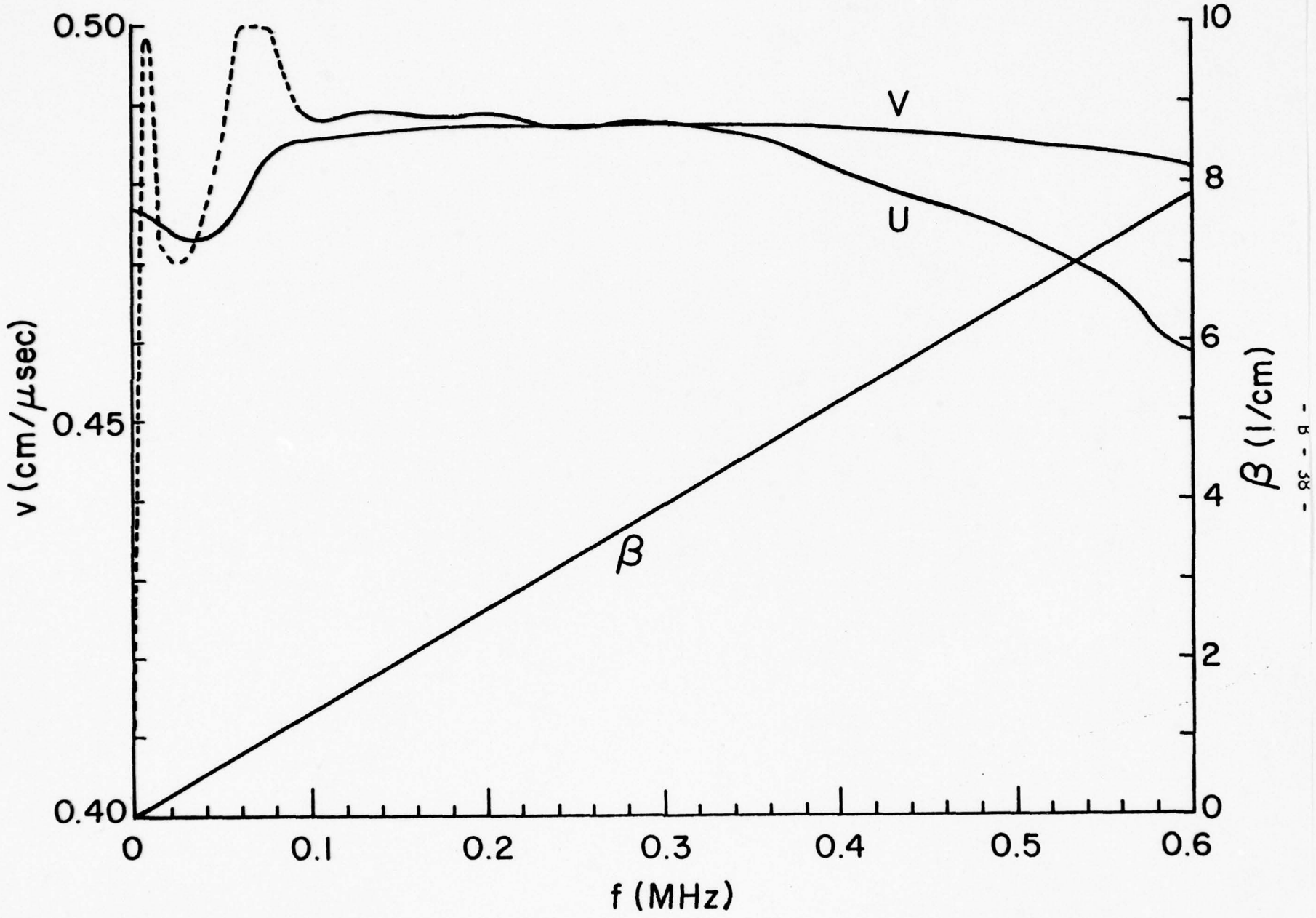

Figure 5c

C.

APPENDIX C

Multiple Scattering of Scalar Waves by Cylinders of Arbitrary Cross Section

by

Vijay K. Varadan*
Vasundara V. Varadan**
Yih-Hsing Pao

Department of Theoretical and Applied Mechanics
Cornell University, Ithaca, New York 14853

Submitted to Journal of Acoustic Society of America, March 1977

---

* The author previously published under the name V.K. Varatharajulu.

** The author previously published under the name V. Varatharajulu.

ABSTRACT

A scattering matrix approach, that involves only the transition matrix of a single obstacle, is proposed for studying the multiple scattering of scalar waves in a medium (matrix) containing identical, long, parallel, randomly distributed cylinders of arbitrary cross section. The elastic properties of the cylinders are assumed to be different from those of the matrix. A statistical approach in conjunction with Lax's "quasicrystalline" approximation is employed to obtain equations for the average amplitudes of the scattered and exciting fields which may then be solved to yield the dispersion relations of the composite medium. Dynamic elastic properties of the composite medium containing circular and elliptical cylinders are found in the Rayleigh or low frequency limit. Numerical results displaying phase velocity and damping effect of the composite medium are presented for a wide range of frequencies.

INTRODUCTION

The subject of multiple scattering of waves is of interest in many fields of engineering and science. In acoustics, it has important practical applications in studies of distribution of flaws in solids, fiber reinforced composites, porous media, fog horn, underwater signal transmissions etc. Ever since Rayleigh's analytical treatment of scattering of waves by randomly distributed particles to study the color of the sky[1], diffraction and scattering of waves have been the subject of extensive research. We cite here papers that are related to our present analysis[2-11], in which additional references may be found. Most of the available results are, however, confined to scatterers of simple geometries like circular cylinder, sphere etc., and often at low frequencies. A detailed analysis of multiple scattering of waves by obstacles of arbitrary shapes and over a wide range of frequencies is still lacking.

In scattering theories, approximations are usually made at a very early stage for: (1) the geometry of the obstacle, (2) size of the obstacle relative to the wavelength of elastic waves and (3) distribution of the obstacles in the medium. The approximations with respect to geometry and size are related. If the obstacle is small compared to the incident wavelength, it is not possible to 'see' exact details of the obstacle and usually one is content to obtain the gross scattering properties of the obstacle. This is the so called Rayleigh limit or low frequency limit, and yields corrections to the solution for point scatterers. As far as the distribution of the obstacles is concerned one either has regular arrays of obstacles, or a random distribution. In the latter case we employ a configurational averaging

procedure. If the concentration of obstacles is small, i.e., they are sparsely distributed we may employ a single scattering or first Born approximation.

Foldy[2], Lax[3,4], Twersky[5,6], Waterman and Truell[7] and Karl and Keller[8] have used a statistical approach to the multiple scattering of scalar waves. Recently, Bose and Mal[9] and Mal and Chatterjee[10] have extended the statistical approach to study the scattering of elastic waves by circular cylinders and obtained solutions in the Rayleigh limit and under static loading, respectively. Datta[11] has studied the scattering of scalar waves by cylinders of elliptical cross section using the method of matched asymptotic expansions in conjunction with first Born approximation in the Rayleigh limit.

The objective of the last mentioned papers (Refs. 9, 10 and 11) is to determine the dynamic characteristics of a medium reinforced by cylindrical fibers. The same objective has also been pursued by many authors using different theories and a review of the subject is given by Achenbach[12], Peck[13] and Moon[14]. Generally, a dispersion relation for plane waves in the composite medium is determined in these papers, but seldom is a discussion of attenuation or damping of the medium. In the Rayleigh limit, this may be due to the fact that the effective wave number in the composite medium is a real quantity, and in the case of periodic layering, the periodic nature of fibers and the boundedness of the body in a direction normal to the wave vector confines all the energy.

On the other hand, Sutherland and Lingle[15] and Tauchert and Guzelsu[16] have observed appreciable damping in these materials and a few experimental values have been given. However, they also stated that

the attenuation measurements are difficult to make for a wide range of frequencies.

In this paper we apply a scattering matrix approach to multiple scattering of horizontally polarized shear waves. Waterman[17] introduced the matrix method to study the response of a single obstacle to acoustic and electromagnetic waves. The matrix method has the advantage of being applicable to obstacles of smooth but arbitrary shape and also at wave-lengths comparable to obstacle size. Peterson and Storm [18] have given formal expressions for the scattering matrix of a distribution of obstacles but they are difficult to compute in practise. We propose an alternate method which combines the scattering matrix of a single obstacle and a suitable statistical averaging technique. This approach can be used conveniently to obtain explicit solutions at the Rayleigh limit, and to obtain the dispersion relation, phase velocity and attenuation constants of inhomogeneous media for a wide range of frequencies.

We consider a homogeneous, isotropic infinitely extended solid containing N number of indentical, long, parallel, randomly distributed cylinders of arbitrary cross section. We assume that time harmonic plane shear waves polarized parallel to the axis of the cylinders are incident normal to the scatterers (SH waves). When N is very large, a statistical analysis is presented using the scattering matrix formulation. The statistically averaged equations are then solved by Lax's "quasi-crystalline" approximation to yield the propagation characteristics of the "average waves" in the medium. Analytical results are obtained for the wave speed, dispersion relation and effective elastic moduli of the composite in the Rayleigh limit, and they are shown to agree with

the existing results. Numerical results are also presented for propagation speeds and attenuations at higher frequencies.

II. TRANSITION MATRIX FORMULATION FOR MULTIPLE SCATTERING

We consider N arbitrary shaped, long and parallel cylindrical scatterers with piecewise smooth boundary surface S embedded in an infinitely extended solid (matrix) which are referred to a coordinate system as shown in figure 1a. 0_i and 0_j denote the centers of the i^{th} and j^{th} inclusions and they can be represented by the polar coordinates r_i, θ_i and z_i and r_j, θ_j and z_j, respectively. Let ρ, μ be the density and rigidity of the matrix and ρ_f, μ_f those of the scatters.

We represent an incident plane SH wave of unit amplitude, frequency ω and wave vector $\underset{\sim}{k}$ by

$$u = 0 \ , \ v = 0 \ , \ w = w^0 = e^{i(\underset{\sim}{k}\cdot\underset{\sim}{r}-\omega t)} \ . \qquad (1)$$

The wave is assumed to move along the positive x-direction, and thus $\underset{\sim}{k}\cdot\underset{\sim}{r} = kx$. In Eq. (1)

$$k = \omega/c_s \ ; \ c_s = (\mu/\rho)^{1/2} \ , \qquad (2)$$

and u, v and w refer to the displacements in the x, y and z directions respectively. We use the superscript (0) to indicate an incident wave, and c_s its wave speed in the matrix.

When the wave impinges on the scatterers, part of the incident wave is scattered back into the matrix and the rest is refracted into the scatterer. The scattered wave will also be of SH-type. The displacement component of the scattered wave is denoted by $w = w^S$ while that corresponding to the refracted wave is denoted by $w = w^F$. Since the incident wave

has time dependence given by $\exp(-i\omega t)$, all field quantities will have the same time factor which will be suppressed henceforth. The displacement field w^S and w^F satisfy the following Helmholtz equations

$$(\nabla^2+k^2)w^S = 0 \quad ; \quad (\nabla^2+k_f^2)w^F = 0 \tag{3a,b}$$

where $\nabla^2 = \partial^2/\partial x^2 + \partial^2/\partial y^2$, and

$$k_f = \omega/c_f \quad ; \quad c_f = (\mu_f/\rho_f)^{1/2} \quad . \tag{4}$$

The index f pertains to the inclusion material. The problem at hand reduces to computing the total displacement field at any point in the matrix satisfying the appropriate boundary conditions on the surface of the inclusions and radiation conditions at infinity.

The total displacement field at any point outside the scatterers is the sum of the incident displacement field and the fields scattered by all the scatterers. This may be written as

$$w(\underset{\sim}{r}) = w^0(\underset{\sim}{r}) + \sum_{i=1}^{N} w_i^S(\underset{\sim}{r}-\underset{\sim}{r}_i) \tag{5}$$

where $w_i^S(\underset{\sim}{r}-\underset{\sim}{r}_i)$ is the field scattered by the i^{th} scatterer to the point of observation $\underset{\sim}{r}$. The field that excites or impinges on the i^{th} scatterer is the incident displacement w^0 plus the field scattered from all the other obstacles. The term exciting field, w^E, is used to distinguish between the field actually incident on a scatterer and the external incident field w^0 produced by sources at infinity. Thus, at a point $\underset{\sim}{r}$ in the vicinity of the i^{th} scatterer, we write

$$w_i^E(\underline{r}) = w^0(\underline{r}) + \sum_{j\neq i}^{N} w_j^S(\underline{r}-\underline{r}_j) \quad ; \quad a \leq |\underline{r}-\underline{r}_i| \leq 2a \tag{6}$$

where 'a' is the radius of the circle circumscribing a scatterer (see Fig. 1b). In the preceding formulation, we have assumed that the intercylindrical spacing is such as to avoid any overlapping (no interpentration).

The matrix formulation of scattering differs from the eigenfunction expansion technique in that the same basis set, for our case the cylindral wave functions, may be used for scatterers of any shape. We expand the exciting field and the scattered field in terms of basis functions ψ_n, and $\mathrm{Re}\ \psi_n$,

$$w_i^E(\underline{r}) = \sum_{n=-\infty}^{\infty} a_n^i \ \mathrm{Re}\ \psi_n(\underline{r}-\underline{r}_i) \tag{7}$$

$$w_j^S(\underline{r}) = \sum_{n=-\infty}^{\infty} b_n^j \ \psi_n(\underline{r}-\underline{r}_j) \tag{8}$$

where

$$\begin{aligned} \psi_n &= H_n[k|\underline{r}-\underline{r}_i|]e^{in\phi_i} \\ \mathrm{Re}\ \psi_n &= J_n[k|r-r_i|]e^{in\phi_i} \end{aligned} \tag{9}$$

are solutions of the Helmholtz equation, and a_n and b_n are undetermined coefficients. In Eq. (9), ϕ_i refers to the angle that $\underline{r}-\underline{r}_i$ makes with the x-axis (see Fig. 1a) and $\mathrm{Re}\ \psi_n$ refers to the regular part of ψ_n i.e., the part that is regular at the origin. For

this choice of the basis set, regular part of ψ_n is different from the real part of ψ_n.

It has been shown that if the total field outside a scatterer is the sum of the incident and scattered fields, the unknown scattered field coefficients can be related to the incident field coefficients through the transition matrix (T-matrix)[17]. We shall extend this definition to the present context. Since $(w_j^E + w_j^S)$ is the total field in the matrix medium, the expansion coefficients of the field scattered by the j^{th} scatterer may be formally related to the coefficients of the field exciting the j^{th} scatterer through the T-matrix:

$$b_n^j = \sum_{m=-\infty}^{\infty} T_{nm}^j \, a_m^j \quad . \tag{10}$$

The elements of the T-matrix involve surface integrals, which can be evaluated in closed form for circular and spherical geometry; for obstacles of arbitrary shape they can only be evaluated numerically. The T-matrix for a single scatterer is of the form

$$T = -\mathrm{Re}\, Q(Q^{-1}) \tag{11}$$

where Re Q and Q are matrices which are functions of the surface S of the scatterer and of the nature of the boundary conditions. A detailed derivation of Eqs. (10) and (11) was given by Waterman[17]. For the sake of completeness, expressions for Q-matrix and the evaluation of the T-matrix are presented in the Appendix A.

Substituting Eqs. (7) and (8) in Eq. (6) and using Eq. (10), we obtain

$$\sum_n a_n^i \, \mathrm{Re}\, \psi_n(\underset{\sim}{r}-\underset{\sim}{r}_i) = w^0(\underset{\sim}{r}) + \sum_{j\neq i}^{N} \sum_{\ell} \sum_{m} T_{\ell m}^j \, a_m^j \, \psi_\ell(\underset{\sim}{r}-\underset{\sim}{r}_j) \quad . \tag{12}$$

It can be seen that the series on the right hand side of Eq. (12) are expressed with respect to the center of the j^{th} scatterer. The addition theorem will be employed later to express these quantities with respect to the center of the i^{th} scatterer. It then remains to expand the incident wave also in the form of a series centered at the i^{th} scatterer. By employing Fourier series expansion in complex form, the incident wave can be expanded as

$$w^0(\underset{\sim}{r}) = \sum_n i^n \, \mathrm{Re}\, \psi_n(\underset{\sim}{r}-\underset{\sim}{r}_i) \, e^{i\underset{\sim}{k}\cdot\underset{\sim}{r}_i} \quad . \tag{13}$$

With Eq. (13), Eq. (12) can be written as

$$\sum_n a_n^i \, \mathrm{Re}\, \psi_n(\underset{\sim}{r}-\underset{\sim}{r}_i) = e^{i\underset{\sim}{k}\cdot\underset{\sim}{r}_i} \sum_p i^p \, \mathrm{Re}\, \psi_p(\underset{\sim}{r}-\underset{\sim}{r}_i) + \sum_{j\neq i}^{N} \sum_{\ell} \sum_{m} T_{\ell m}^j \, \psi_\ell(\underset{\sim}{r}-\underset{\sim}{r}_j). \tag{14}$$

In order to express the basis function $\psi_\ell(\underset{\sim}{r}-\underset{\sim}{r}_j)$ in terms of $\psi_\ell(\underset{\sim}{r}-\underset{\sim}{r}_i)$, we use the following addition theorem (see Fig. 2)

$$H_\ell(k|\underset{\sim}{r}-\underset{\sim}{r}_j|)e^{i\ell\psi} = \sum_m J_m(k|\underset{\sim}{r}-\underset{\sim}{r}_i|) \, H_{\ell+m}(kr_{ij}) \, e^{im(\theta_{ij}-\phi_i)} \quad . \tag{15}$$

After some simple manipulations and using Eq. (9), we can write Eq. (15) as

$$\psi_\ell(\underset{\sim}{r}-\underset{\sim}{r}_j) = (-1)^\ell \sum_m (-1)^m \, \mathrm{Re}\, \psi_m(\underset{\sim}{r}-\underset{\sim}{r}_i) \, \psi_{\ell-m}(\underset{\sim}{r}_i-\underset{\sim}{r}_j) \quad . \tag{16}$$

Substitution of Eq. (16) in Eq. (14) yields

$$\sum_n a_n^i \text{ Re } \psi_n(\underset{\sim}{r}-\underset{\sim}{r}_i) = e^{i\underset{\sim}{k}\cdot\underset{\sim}{r}_i} \sum_p i^p \text{ Re } \psi_p(\underset{\sim}{r}-\underset{\sim}{r}_i)$$

$$+ \sum_{j\neq i}^{N} \sum_{\ell} \sum_{m} \sum_{s} (-1)^{s+\ell} T^j_{\ell m} \, a^j_m \, \psi_{\ell-s}(\underset{\sim}{r}_i-\underset{\sim}{r}_j) \text{ Re } \psi_s(\underset{\sim}{r}-\underset{\sim}{r}_i). \tag{17}$$

Multiplying both sides of Eq. (17) by $\text{Re } \psi_t(\underset{\sim}{r}-\underset{\sim}{r}_i)$ and using the orthogonality condition on the angular part ϕ, Eq. (17) can be reduced to

$$a_n^i = i^n e^{i\underset{\sim}{k}\cdot\underset{\sim}{r}_i} + \sum_{j\neq i}^{N} \sum_{\ell} \sum_{m} (-1)^{n+\ell} \, T^j_{\ell m} \, a^j_m \, \psi_{\ell-n}(\underset{\sim}{r}_i-\underset{\sim}{r}_j). \tag{18}$$

Thus, by employing the T-matrix, we have eliminated the unknown scattering coefficients b_n, resulting in an equation for a_n only. In view of Eq. (10), it can be seen that the scattered field coefficient b_n can be obtained by multiplying Eq. (18) by the transition matrix T. The coefficients a_n, or b_n are functions of the coordinates r_j, θ_j of all the scatterers, although this is not written explicitly.

III. STATISTICALLY AVERAGED WAVE FIELDS

We now wish to average over the positions of all the scatterers. We define a probability density of finding the first scatterer at $\underset{\sim}{r}_1$ and the second scatterer at r_2 and so forth by $p(\underset{\sim}{r}_1, \underset{\sim}{r}_2, \ldots, \underset{\sim}{r}_N)$. The probability density may be written as

$$\begin{aligned} p(\underset{\sim}{r}_1, \underset{\sim}{r}_2, \ldots, \underset{\sim}{r}_N) &= p(\underset{\sim}{r}_i) \, p(\underset{\sim}{r}_1 \, \underset{\sim}{r}_2, \ldots', \ldots, \underset{\sim}{r}_N|\underset{\sim}{r}_i) \\ &= p(\underset{\sim}{r}_i) \, p(\underset{\sim}{r}_j|\underset{\sim}{r}_i) \, p(\underset{\sim}{r}_1, \underset{\sim}{r}_2, \ldots', \ldots', \underset{\sim}{r}_N|\underset{\sim}{r}_j, \underset{\sim}{r}_i) \\ &= \ldots \end{aligned} \tag{19}$$

where $p(\underset{\sim}{r}_i)$ denotes the probability density of finding a scatterer at $\underset{\sim}{r}_i$ while $p(\underset{\sim}{r}_j|\underset{\sim}{r}_i)$ denotes the conditional probability of finding a scatterer at $\underset{\sim}{r}_j$ if a scatterer is known to be at $\underset{\sim}{r}_i$. A prime in the first of Eq. (19) means $\underset{\sim}{r}_i$ is absent while two primes in the second of Eq. (19) means both $\underset{\sim}{r}_i$ and $\underset{\sim}{r}_j$ are absent.

If the scatterers are randomly distributed, the positions of all scatterers are equally probable within volume V, and hence its distribution is uniform with probability density

$$p(\underset{\sim}{r}_i) = \begin{cases} 1/V \ , & \underset{\sim}{r}_i \in V \\ 0 \ , & \underset{\sim}{r}_i \notin V \ . \end{cases} \tag{20}$$

In addition, the assumption that the cylinders are non overlapping suggests that

$$p(r_j|r_i) = \begin{cases} 1/V \ , & |\underset{\sim}{r}_i - \underset{\sim}{r}_j| > 2a \\ 0 \ , & |\underset{\sim}{r}_i - \underset{\sim}{r}_j| < 2a \end{cases} \tag{21}$$

where 'a' is the radius of the circumscribing circle, see Fig. 1. A suitable correlation in the position of cylinders may also be added to (21). The correlation is, however, omitted here for simplicity.

We denote the conditional expectation of a statistical quantity f as

$$\langle f \rangle_i = \int_V \cdots \int_V f \, p(\underset{\sim}{r}_1, \underset{\sim}{r}_2, \cdots', \underset{\sim}{r}_N|\underset{\sim}{r}_i) \, d\underset{\sim}{r}_1 \, d\underset{\sim}{r}_2 \cdots d\underset{\sim}{r}_N$$

$$\langle f \rangle_{ij} = \int_V \cdots \int_V f \, p(\underset{\sim}{r}_1, \underset{\sim}{r}_2, \cdots', \cdots', \underset{\sim}{r}_N|\underset{\sim}{r}_j, \underset{\sim}{r}_i) \, d\underset{\sim}{r}_1 \, d\underset{\sim}{r}_2, \cdots', \cdots', d\underset{\sim}{r}_N \tag{22}$$

In the first of Eqs. (22) we have averaged over all scatterers except the i^{th} and in the second, over all except the i^{th} and j^{th}, and so on.

Multiplying both sides of Eq. (18) by the probability density given by (19) and using Eqs. (20), (21) and (22), we obtain the configurational average of a_n:

$$< a_n^i >_i = i^n e^{i\underset{\sim}{k}\cdot\underset{\sim}{r}_i} + \frac{1}{V} \sum_{j\neq 1}^{N} \sum_{\ell} \sum_{m} (-1)^{n+\ell} T_{\ell m}^j \int_{V'} < a_m^j >_{ij} \psi_{\ell-n}(\underset{\sim}{r}_{ij})\, d\underset{\sim}{r}_j \quad (23)$$

where V' denotes the volume of the medium excluding the volume of the cylinder of radius $2a$. For identical scatterers, $\sum_{j\neq i}^{N}$ can be replaced by $(N-1)$. Equation (21) can be rewritten as

$$< a_n^i >_i = i^n e^{i\underset{\sim}{k}\cdot\underset{\sim}{r}_i} + \frac{N-1}{V} \sum_{\ell} \sum_{m} (-1)^{n+\ell} T_{\ell m} \int_{V'} < a_m^j >_{ij} \psi_{\ell-n}(\underset{\sim}{r}_{ij})\, d\underset{\sim}{r}_j . \quad (24)$$

The above equation indicates that the conditional average with one scatterer fixed is given in terms of the conditional average with two scatterers fixed. This presents a difficulty in solving for the unknown coefficient $< a_n >$. However, Lax[4] has suggested a quasicrystalline approximation, i.e.,

$$< a_m^j >_{ij} = < a_m^j >_j \quad , \quad i \neq j \quad . \quad (25)$$

This approximation implies that there is no correlation between the i^{th} and j^{th} scatterers other than that there should be no interpenetration. With this approximation, Eq. (24) may be written as

$$< a_n^i >_i = i^n e^{i\underset{\sim}{k}\cdot\underset{\sim}{r}_i} + \frac{N-1}{V} \sum_{\ell} \sum_{m} (-1)^{n+\ell} T_{\ell m} \int_{V'} < a_m^j >_j \psi_{\ell-n}(\underset{\sim}{r}_{ij})\, d\underset{\sim}{r}_j . \quad (26)$$

This is a system of integral equations for the unknown coefficients $< a_n^i >_i$. Similar expressions for $< b_n^i >_i$ may be obtained by multiplying (26) by the T-matrix.

IV. PROPAGATION CHARACTERISTICS OF THE AVERAGE WAVES IN THE MEDIUM

We now try a plane wave solution for the average $< a >$ with an effective wave number K characterizing the composite medium:

$$< a_m^i >_i = i^m X_m e^{i\underset{\sim}{K}\cdot\underset{\sim}{r}_i} \quad (27)$$

The averaged wave vector $\underset{\sim}{K}$ is assumed to be parallel to that of the incident wave, which in the present case is along the x-axis. In Eq. (27), X_m is an unknown constant. Substituting Eq. (27) into Eq. (26), we obtain

$$i^n X_n e^{i\underset{\sim}{K}\cdot\underset{\sim}{r}_i} = i^n e^{i\underset{\sim}{k}\cdot\underset{\sim}{r}_i} + \frac{N-1}{V} \sum_{\ell} \sum_{m} (-1)^{n+\ell} T_{\ell m}\, i^m X_m \int_{V'} e^{i\underset{\sim}{K}\cdot\underset{\sim}{r}_{ij}} \psi_{\ell-n}(\underset{\sim}{r}_{ij}) d\underset{\sim}{r}_j . \quad (28)$$

Equation (28) may be rewritten as

$$i^n X_n e^{i\underset{\sim}{K}\cdot\underset{\sim}{r}_i} = i^n e^{i\underset{\sim}{k}\cdot\underset{\sim}{r}_i} + \frac{N-1}{V} \sum_{t} \sum_{m} (-1)^{2n+t} T_{(t+n)m}\, i^m X_m \int_{V'} e^{i\underset{\sim}{K}\cdot\underset{\sim}{r}_{ij}} \psi_t(\underset{\sim}{r}_{ij}) d\underset{\sim}{r}_j . \quad (29)$$

The integral in Eq. (29) is a volume integral and the integrands $e^{i\underset{\sim}{K}\cdot\underset{\sim}{r}_{ij}}$ and $\psi_t(\underset{\sim}{r}_{ij})$ satisfy the wave equation. Thus we can rewrite the integral in the following form

$$\int_{|\underset{\sim}{r}_j - \underset{\sim}{r}_i| > 2a}^{\infty} e^{i\underset{\sim}{K}\cdot\underset{\sim}{r}_{ij}} \psi_t(\underset{\sim}{r}_{ij}) d\underset{\sim}{r}_j$$

$$= \frac{1}{k^2-K^2} \int_{|\underset{\sim}{r}_j - \underset{\sim}{r}_i| > 2a}^{\infty} [\nabla^2(e^{i\underset{\sim}{K}\cdot\underset{\sim}{r}_{ij}}) \psi_t(\underset{\sim}{r}_{ij}) - e^{i\underset{\sim}{K}\cdot\underset{\sim}{r}_{ij}} \nabla^2 \psi_t(\underset{\sim}{r}_{ij})] d\underset{\sim}{r}_j \qquad (30)$$

$$= \frac{1}{k^2-K^2} \int_{S_\infty - S_{2a}} [\psi_t(\underset{\sim}{r}_{ij}) \frac{\partial}{\partial r_j} e^{i\underset{\sim}{K}\cdot\underset{\sim}{r}_{ij}} - e^{i\underset{\sim}{K}\cdot\underset{\sim}{r}_{ij}} \frac{\partial}{\partial r_j} \psi_t(\underset{\sim}{r}_{ij})] dS$$

where Green's theorem has been applied. S_∞ refers to a circle of large radius at infinity while S_{2a} refers to the surface of the circumscribed circle of the scatterer.

Using the following plane wave expansion

$$e^{iK(r_j\cos\theta_j - r_i\cos\theta_i)} = \sum_{n=-\infty}^{\infty} i^n J_n(Kr_{ij}) e^{in\theta_{ij}} \qquad (31)$$

the surface integral on S_{2a} can be evaluated:

$$\frac{1}{k^2-K^2} \int_{S_{2a}} \psi_t(\underset{\sim}{r}_{ij}) \frac{\partial}{\partial r_j} e^{iKr_j\cos\theta_j} - e^{iKr_j\cos\theta_j} \frac{\partial}{\partial r_j} \psi_t(\underset{\sim}{r}_{ij}) \; dS$$

$$= e^{iKr_i\cos\theta_i} \frac{2\pi a\, i^t}{k^2-K^2} [2k\, J_t(2Ka) H_t'(2ka) - 2K\, H_t(2ka) J_t'(2Ka)] \; . \qquad (32)$$

To evaluate the surface integral on S_∞, we replace $\psi_t(\underset{\sim}{r}_{ij})$ by its asymptotic value. We note that when $r_j \to \infty$

$$r_{ij} = |\underset{\sim}{r}_i - \underset{\sim}{r}_j| \to |\underset{\sim}{r}_j| - \frac{\underset{\sim}{r}_j \cdot \underset{\sim}{r}_i}{|\underset{\sim}{r}_j|}$$

$$\frac{1}{r_{ij}} \to \frac{1}{|\underset{\sim}{r}_j|} \quad ; \quad \theta_{ij} \to \theta_j \tag{33}$$

and hence

$$\psi_t(\underset{\sim}{r}_{ij}) \to i^t \; e^{-ik\underset{\sim}{r}_j \cdot \underset{\sim}{r}_i} \frac{2}{i\pi k r_j} e^{ikr_j} e^{it\theta_j} \tag{34}$$

where $\underset{\sim}{r}_j$ is the unit vector. Employing Eqs. (33) and (34), the surface integral on S may be written as

$$\frac{1}{k^2-K^2} \int_{S_\infty} \left[\psi_t(\underset{\sim}{r}_{ij}) \frac{\partial}{\partial r_j} e^{iKr_j \cos\theta_j} - e^{iKr_j \cos\theta_j} \frac{\partial}{\partial r_j} \psi_t(\underset{\sim}{r}_{ij}) \right] dS$$

$$= \frac{i^t}{k^2-K^2} \int_{S_\infty} e^{-ik\underset{\sim}{r}_j \cdot \underset{\sim}{r}_i} \left[\frac{2}{i\pi k r_j} e^{ikr_j} \frac{\partial}{\partial r_j} e^{iKr_j} - e^{iKr_j} \frac{\partial}{\partial r_j} \left(\frac{2}{i\pi k r_j} e^{ikr_j} \right) \right] e^{it\theta_j} r_j \, d\theta_j . \tag{35}$$

In Eq. (29) there are two sets of terms each of which satisfies a different wave equation and hence both can be equated separately to zero. Thus the incident field term and the surface integral at infinity, which satisfy the wave equation with number k cancel each other. This is the so called extinction theorem: the unperturbed incident wave is extinguished within the medium by waves induced at the boundary of the system. The remaining terms in Eq. (29) with Eq. (32) gives the relation for the unknown conditional averaged amplitude:

$$X_n = n_o \frac{2\pi}{k^2-K^2} \sum_{\ell} \sum_{m} i^{m-\ell} X_m \, T_{\ell m} (JH_{\ell-n}) \tag{36}$$

where we have assumed that N and V are infinitely large with $N/V = n_o$ (finite), and

$$JH_{\ell-n} = 2kaJ_{\ell-n}(2Ka)H'_{\ell-n}(2ka) - 2Ka\, H_{\ell-n}(2ka)J'_{\ell-n}(2Ka) \quad . \tag{37}$$

Similar equation can also be obtained from the average scattered field coefficient $< b_n >$, assuming a plane wave solution of the form

$$< b_n^i >_i = i^n Y_n e^{iKr_i\cos\theta_i} \tag{38}$$

where Y_n is an unknown constant.

In Eq. (36), the summation integers ℓ and m varies from $-\infty$ to ∞. For numerical computations, these have to be expressed from 0 to ∞. This can be achieved by formulating certain properties of the T-matrix which are outlined in the Appendix B. Using these properties in Eq. (36), we obtain

$$\begin{aligned} X_n = \frac{2\pi n_o}{k^2-K^2}\Bigg\{ & \sum_{m=1}^{\infty}\Bigg[\sum_{\ell=1}^{\infty}\frac{i^{\ell-m}}{2}T^e_{\ell m}(X_m+X_{-m})(JH_{\ell+m}+JH_{\ell-n}) \\ & + T^o_{\ell m}(X_m-X_{-m})(JH_{\ell-n}-JH_{\ell+n}) + \frac{i^m}{(2)^{1/2}}T^e_{om}(X_m+X_{-m})JH_n\Bigg] \\ & + \sum_{\ell=1}^{\infty}\frac{i^{\ell}}{(2)^{1/2}}T^e_{\ell o}X_o(JH_{\ell-n}+JH_{\ell+n}) + T_{oo}X_oJH_n\Bigg\} \end{aligned} \tag{39}$$

where superscripts ℓ and o refer to even and odd parts of T-matrix elements (see Appendix B).

Equation (39) is a system of simultaneous linear homogeneous equations

for the unknown amplitudes X_n. For a nontrivial solution, we require that the determinant of the coefficients vanishes which yields an equation for the effective wave number K in terms of k and the T-matrix of the scatterer. This is the dispersion relation for the composite medium. It can be shown that the above equation is similar to the one obtained by Bose and Mal[9], for circular fibers, if we substitute the T-matrix of a circular cylinder given in the Appendix A. However, Eq. (39) is a general expression valid for any arbitrary cross section. It may be noted that 2a, the distance of closest approach, coincides with the diameter of the circular cylinders. The T-matrix is the only factor that contains information about the exact shape and nature of the cylinder. If the elements of the T-matrix are known, the dispersion relation of a composite consisting of random distribution of obstacles of arbitrary cross section can be obtained either from Eq. (36) or Eq. (39).

V. RAYLEIGH LIMIT

In the Rayleigh limit or low frequency limit, the size of scatterers is considered to be small when compared to the incident wavelength. It is then sufficient to take only the lowest order coefficients in the expansion of the fields. Neglecting higher order terms in ka and Ka in the expansion of Bessel and Hankel functions, Eq. (37) may be reduced to

$$JH_n \approx \frac{2i}{\pi a}\left[\left(\frac{K}{k}\right)^n - 2a^2(k^2-K^2)\ell nka\right] \tag{39}$$

In this limit, the elements of T-matrix are known in closed form for various simple shapes see Ref. [19], and they are given here for the sake of completeness for circular and elliptical cylinders:

Circular cylinders

$$T_{00}^{e} = \frac{i\pi}{4}(d-1)k^2a^2\left[1-\frac{d-1}{2}k^2a^2 \ell n\, ka\right] + O(k^4a^4)$$

$$T_{11}^{e} = T_{11}^{o} = \frac{i\pi}{4}\frac{(1-m)}{1+m}k^2a^2\left[1-\frac{1-m}{2(1+m)}k^2a^2 \ell n\, ka\right] + O(k^4a^4) \quad (40)$$

$$T_{00}^{o} = 0 \; ; \; T_{\ell n} = 0 \text{ for } \ell, n \geq 2$$

Elliptical cylinders

$$T_{00}^{e} = i\frac{\pi}{4}(d-1)k^2ab\left[1-\frac{d-1}{2}k^2ab \ell n\, ka\right] + O(k^4a^4)$$

$$T_{11}^{e} = \frac{i\pi}{8}\frac{(1-m)(a+b)}{a+mb}k^2ab\left[1-\frac{1}{4}\frac{(1-m)}{a+mb}(a+b)k^2ab \ell n\, ka\right] + O(k^4a^4) \quad (41)$$

$$T_{11}^{o} = \frac{i\pi}{8}\frac{(1-m)(a+b)}{b+ma}k^2ab\left[1-\frac{1}{4}\frac{(1-m)}{b+ma}(a+b)k^2ab \ell n\, ka\right] + O(k^4a^4)$$

$$T_{00}^{o} = 0 \; , \; T_{\ell n} = 0 \text{ for } \ell, n \geq 2$$

where $d = \rho_f/\rho$ and $m = \mu_f/\mu$ and a and b are semi major and minor axes of the elliptic cylinder, respectively.

In view of Eqs. (40) and (41), we obtain the following simultaneous linear homogeneous equations from (39) for the unknown X_0, X_1 and X_{-1} for thin cylindrical fibers

$$X_0 = \frac{2\pi n_o}{k^2-K^2}\left\{X_0 T_{00}^e JH_0 + X_1 T_{11}^e JH_1 + X_{-1} T_{11}^e JH_1\right\}$$

$$X_1 = \frac{2\pi n_o}{k^2-K^2}\left\{X_0 T_{00}^e JH_1 + \frac{X_1}{2}[T_{11}^e (JH_2+JH_0)+T_{11}^o (JH_0-JH_2)]\right.$$

$$\left. + \frac{X_{-1}}{2}[T_{11}^e (JH_2+JH_0)-T_{11}^o (JH_0-JH_2)]\right\} \qquad (42)$$

$$X_{-1} = \frac{2\pi n_o}{k^2-K^2}\left\{X_0 T_{00}^e JH_1 + \frac{X_1}{2}[T_{11}^e (JH_2+JH_0)+T_{11}^o (JH_2-JH_0)]\right.$$

$$\left. + \frac{X_{-1}}{2}[T_{11}^e (JH_2+JH_0)-T_{11}^o (JH_2-JH_0)]\right\} \quad .$$

From the determinant of the coefficients X_0, X_1 and X_{-1} we obtain the following dispersion relations:

Circular cylinders

$$\frac{K^2}{k^2} = \frac{1}{1-\frac{c(1-m)}{1+m}}\left\{[1+\frac{c(1-m)}{1+m}][1+c(d-1)]\right.$$

$$+ k^2a^2 \ell n\, ka \left[\left\{1+c\,\frac{1-m}{1+m}\right\}\left\{1+c(d-1)\right\}\left\{\frac{1-c\,\frac{(1-m)^2}{2(1+m)^2}}{1-c\,\frac{(1-m)}{1+m}} - 1 + c(d-1)\right\}\right. \qquad (43)$$

$$+ \left\{1-c\,\frac{1-m}{1+m}\right\}\left\{1-2c(d-1)\right\} - 1 - \frac{c}{2}\,\frac{(1-m)^2}{(1+m)^2}\left\{1+c(d-1)\right\}$$

$$\left.\left. - \frac{c}{2}(d-1)^2\left\{1+c\,\frac{1-m}{1+m}\right\}\right]\right\} + O(k^4a^4)$$

where $c = \pi a^2 n_0$ is the concentration of circular cylinders per unit area,

AD-A047 487 CORNELL UNIV ITHACA N Y DEPT OF THEORETICAL AND APP--ETC F/G 11/4
ULTRASONIC NONDESTRUCTIVE TESTING OF COMPOSITE MATERIALS.(U)
SEP 77 W SACHSE, Y PAO AFOSR-76-2992

UNCLASSIFIED AFOSR-TR-77-1288 NL

2 OF 2
ADA047 487

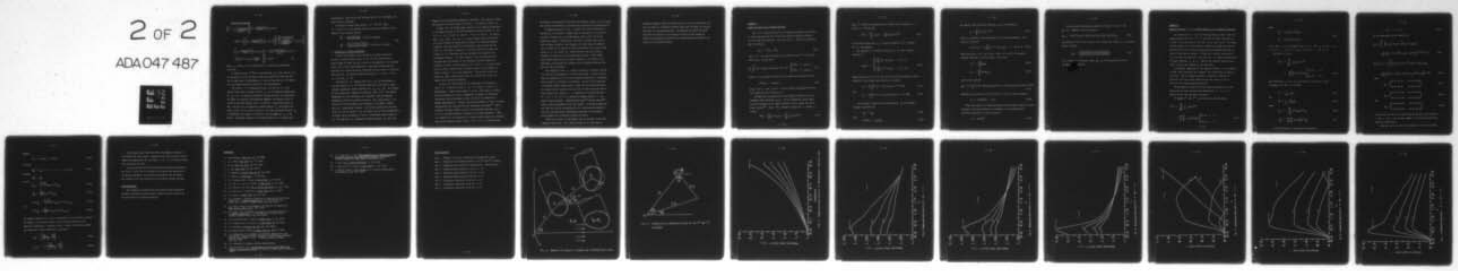

END
DATE FILMED
1 - 78
DDC

Elliptical cylinders

$$\frac{K^2}{k^2} = \frac{1}{1-c_1\frac{(1-m)(a+b)}{2(mb+a)}}\Bigg\{\left[1+c_1\frac{(1-m)(a+b)}{2(mb+a)}\right][1+c_1(d-1)]$$

$$+ k^2a^2 \ln ka\Bigg[\left\{1+c_1\frac{(1-m)(a+b)}{2(mb+a)}\right\}\left\{1+c_1(d-1)\right\}\left\{\frac{1-\frac{bc_1}{8a}\frac{(1-m)^2(a+b)^2}{(mb+a)^2}}{1-c_1\frac{(1-m)(a+b)}{2(mb+a)}}-1+c_1(d-1)\right\}$$

$$+\left\{1-c_1\frac{(1-m)(a+b)}{mb+a}\right\}\left\{1-2c_1(d-1)\right\}-1-\frac{c_1}{8}\frac{b}{a}\frac{(1-m)^2(a+b)^2}{(mb+a)^2}\{1+c_1(d-1)\}$$

$$-\frac{c_1}{4}\frac{b}{a}(d-1)^2\{2+c_1(1-m)\frac{(a+b)}{mb+a}\}\Bigg]\Bigg\} + O(k^4a^4 \ln ka) \qquad (44)$$

where $c_1 = \pi ab\, n_0$ is the concentration of elliptical cylinders per unit area.

If terms of order $k^4a^4 \ln ka$ are neglected, it is seen that Eq. (43) is the same as the one obtained by Hashin and Rosen[24] and Bose and Mal[7]. For the same order of approximation, it can be shown that Eq. (44) agrees with the results obtained by Datta[9] for low concentration.

The value of K as determined by Eqs. (43) and (44) is a real quantity and relates to phase velocity v_p of the composite medium given by $v_p = \omega/K$. To study the dependence of phase velocity on concentration of fibers, we consider boron-aluminium composite with density ratio d = 2.53/2.72 and shear modulus ratio m = 25/3.87. Using these values in Eqs. (43) and (44), we computed the phase velocity v_p and results are shown in Fig. (3) for various values of b/a where the phase velocity v_p is normalized with respect to velocity of wave propagation c_s in the matrix. The general tendency of the phase velocity is to increase with

concentration. The results also indicate that as b/a decreases, the phase velocity increases.

Defining an average shear modulus $\langle\mu\rangle = \omega^2\langle\rho\rangle/K^2$ where $\langle\rho\rangle = c\rho_f+(1-c)\rho$ is the average density, we find the effective shear modulus of the composite medium:

$$\frac{\langle\mu\rangle}{\mu} = \frac{1-c(1-m)/(1+m)}{1+c(1-m)/(1+m)} \quad \text{(circular cylinders)}$$

$$\frac{\langle\mu\rangle}{\mu} = \frac{1-c_1(1-m)(a+b)/2(mb+a)}{1+c_1(1-m)(a+b)/2(mb+a)} \quad \text{(elliptical cylinders)} \tag{45}$$

VI DISPERSION AT HIGHER FREQUENCIES

To study the response of the composite at higher frequencies, one has to consider higher powers of ka and this implies that a larger number of terms (X_n) must be kept in the expansion of the average field. This is best done numerically. Some model calculations are presented for a aluminium matrix reinforced by boron fibers of elliptical cross section. The material properties used are $\rho = 2.72$, $\mu = 3.87$, $\rho_f = 2.53$, and $\mu_f = 25$.

For values of ka ranging from 0.05 to 3.0, the determinant of the coefficients of X_n was computed numerically retaining 13 simultaneous, homogeneous complex equations for $X_{-6}\ldots X_0\ldots X_6$. The elements of the T-matrix were computed as explained in Ref. (17). The complex determinant of the coefficients was calculated using the Gaussian elimination process with partial pivoting. For a given value of ka, the roots of the determinant were searched in the complex K-plane $(K_1+i\,K_2)$ using Muller's method. Good initial guesses were provided by Eq. (44) at low values of ka and these could be used systematically to obtain quick convergence of roots at increasingly higher values of ka. The real part K_1 determines the phase velocity v_p while the

imaginary part K_2 determines damping or attenuation. The results of these calculations for various values of b/a and c are ploted in Figs. 4-9.

In Figs. 4-6, the average phase velocity in the composite narmalized by the phase velocity in the matrix material is plotted versus ka for b/a = 0.4, 0.6, 0.8 and 1.0 and for c = 0.3, 0.5 and 0.7. We observe that $v_p/c_s = k/K_1$. For b/a = 1.0, these results agree qualitatively with those obtained by Sutherland and Lingle[15] for tungsten-aluminum composite, Ting and Sachse[20] for boron-epoxy composites and Yew and Jogi[21] for steel-PLM-4 composites. The phase velocity increases very slightly at low frequencies and then decreases very gradually with increasing frequency. For lower values of b/a, the phase velocity increases much more rapidly at low frequencies and then tapers off gradually to almost the same values as for b/a = 1.0. It may be noted that our results indicate that the phase velocity is much higher for smaller values of b/a at low frequencies. This effect is more pronounced at higher concentrations where the velocity also drops more sharply with increasing frequency.

In Figs. 7-9, we have plotted the coefficient of attenuation α versus ka. We chose to define α as $\alpha = 4\pi K_2/K_1$ so that it is dimensionless. These results appear to be new, since explicit results for the attenuation of waves in composites is lacking in theoretical calculations and as discussed in Refs. 15 and 16, too difficult to measure experimentally. However, the results presented in Figs. 7-9 agree qualitatively with those predicted by Sutherland and Lingle[15]. The attenuation increases rapdily at first with increasing frequency (up to ka $\sim$ 0.5) and then decreases to almost zero at high frequencies. There is a tendency for the attenuation to increase rapidly again with frequency. This can be observed clearly in Fig. 7 for c = 0.3. In these results,

the behavior is qualitatively the same for different values of b/a, although the increase and decrease in α becomes more pronounced with decreasing b/a.

The general behavior of the α versus ka curves indicates the possibility of existance of higher modes of vibration in the composite, or what is referred to in the experimental work in Ref. [15] as the higher pass bands. Although Figs. 4-6 seem to indicate that there is only one phase velocity in the composite for each value of frequency, this is really not so because at higher frequencies, there exists many values of K for a given ka. These multiple roots are, however, difficult to obtain in our root searching algorithm. These higher roots simply indicate that at higher frequencies, the effect of the individual fibers become more apparant and the composite behaves less and less like a continuum.

The frequency at which α begins to decrease is usually referred to as the cut off frequency of the first pass band. It must be noted that the attenuation is due to only geometric dispersion or scattering and no energy is dissipated in the medium. At the cut off frequency, α decreases because energy begins to pass into the second pass band. Our results seem to indicate that the onset of the second pass band is quite rapid at low values of c as indicated by the rapid decrease of α to 0 for b/a = 1.0, whereas for higher values of c the onset is more prolonged. Sutherland and Lingle[15] and Moon and Mow[22] offer a similar explanation from their models. It should be mentioned here that our results are accurate for low concentrations because of the Lax's quasicrystalline approximation employed in the analysis which neglects the correlation between the fibers.

There are a number of improvements that we can make to the model composite chosen here. The random distribution of fibers may be

replaced by regular arrays of fibers since this is true in practice, and also the effect of correlation between fibers must be taken into account especially at high concentrations. As observered by Peck[13] and Sve[23], the effect of porosity or the presence of voids in real composites affects the attenuation properties quite significantly and should be included in our theoretical model.

APPENDIX. A

Transition Matrix for a Single Scatterer

The T- or transition matrix for an obstacle bounded by the surface S can be obtained from the interior and exterior Helmholtz formulae for the scalar wave equation. The total field w outside the scatterer may be written as

$$w(\underset{\sim}{r}) = w^0(\underset{\sim}{r}) + w^S(\underset{\sim}{r}) \tag{A-1}$$

where w^0 is the field incident on the scatterer and w^S is the scattered field. We then have

$$\frac{1}{4\pi}\int_S [w'\underset{\sim}{n}'\cdot\nabla' g(\underset{\sim}{r}|\underset{\sim}{r}') - g(\underset{\sim}{r}|\underset{\sim}{r}')\underset{\sim}{n}'\cdot\nabla' w']\, ds' = \begin{cases} -w^0(\underset{\sim}{r}) \text{ , } \underset{\sim}{r} \text{ inside } S \\ w^S(\underset{\sim}{r}) \text{ , } \underset{\sim}{r} \text{ outside } S \end{cases} \tag{A-2}$$

where g is the Green's function of the scalar wave equation given by

$$(\nabla^2+k^2)g = -4\pi\delta(\underset{\sim}{r}-\underset{\sim}{r}') \quad . \tag{A-3}$$

In Eq. (A-2), w' and $\mu\underset{\sim}{n}'\cdot\nabla' w'$ are the unknown displacement and traction respectively on the surface S.

We expend all the quantities in the integral formula in a set of orthogonal basis functions $\psi_n(\underset{\sim}{r})$. For two dimensional scalar waves, the most convenient set of basis functions is the circular wave functions $H_n(kr)e^{in\phi}$. Since $w^0(\underset{\sim}{r})$ should be regular for $\underset{\sim}{r}$ inside S, we have

$$w^0(\underset{\sim}{r}) = \sum_n a_n \, \mathrm{Re}\, \psi_n(\underset{\sim}{r}) = \sum_n a_n J_n(kr)e^{in\phi} \quad . \tag{A-4}$$

Also, w^S should be outgoing waves at infinity and be regular for $\underset{\sim}{r}$ outside S. We then have

$$w^S(\underset{\sim}{r}) = \sum_n b_n \psi_n(\underset{\sim}{r}) = \sum b_n H_n(kr) e^{in\phi} \quad . \tag{A-5}$$

In the above expressions, a_n are known constants as w^0 is given, but b_n are unknowns.

The expansion of the Green's functions g in terms of basis functions is

$$g(\underset{\sim}{r}|\underset{\sim}{r}') = \begin{cases} i\pi \sum_n \psi_n(\underset{\sim}{r}) \text{ Re } \psi_n(\underset{\sim}{r}') \quad , & |r| > |r'| \\ i\pi \sum_n \psi_n(\underset{\sim}{r}') \text{ Re } \psi_n(\underset{\sim}{r}) \quad , & |\underset{\sim}{r}| < |\underset{\sim}{r}'| \quad . \end{cases} \tag{A-6}$$

Substituting Eqs. (A-4), (A-5) and (A-6) into (A-2) and using the orthogonality of the circular wave functions, we obtain

$$a_n = \frac{-i}{4} \int_S [w'n'\cdot\nabla' \psi_n(\underset{\sim}{r}') - \psi_n(\underset{\sim}{r}') \, n'\cdot\nabla' w'] dS \tag{A-7}$$

and

$$b_n = \frac{i}{4} \int_S [w'n'\cdot\nabla' \text{ Re } \psi_n(\underset{\sim}{r}') - \text{Re } \psi_n(\underset{\sim}{r}') \, n'\cdot\nabla' w'] dS. \tag{A-8}$$

For an elastic inclusion with shear modulus μ_f, the relevant boundary conditions are

$$w|_S = w_f|_S \tag{A-9}$$

and

$$\mu \underset{\sim}{n}\cdot\nabla w|_S = \mu_f \underset{\sim}{n}\cdot\nabla w_f|_S \tag{A-10}$$

The unknown field inside the inclusion, w_f can be expanded as

$$w_f = \sum_n \alpha_n J_n(k_f r)\, e^{in\phi} \tag{A-11}$$

where k_f pertains to the wavenumber for the inclusion material. The traction is given by

$$\mu_f \underset{\sim}{n}' \cdot \nabla' w_f = \mu_f \sum_n \alpha_n \underset{\sim}{n}' \cdot \nabla' \, \mathrm{Re}\, \psi_n(k_f \underset{\sim}{r}) \quad , \quad \underset{\sim}{r} \text{ inside } S. \tag{A-12}$$

Substituting Eqs. (A-11) and (A-12) in Eqs. (A-7) and (A-8) using the boundary conditions (A-9) and (A-10), we can write

$$a_n = -i \sum_m Q_{mn} \alpha_n \tag{A-13}$$

$$b_n = i \sum_m (\mathrm{Re}\, Q_{mn}) \alpha_n \tag{A-14}$$

where we have defined

$$Q_{mn} = (\mu/4) \int_S r(\phi) \underset{\sim}{n}(r) \cdot [\mathrm{Re}\psi_n(k_f r) \nabla \psi_m(kr) - (\mu_f/\mu) \nabla \mathrm{Re}\psi_n(k_f r) \psi_m(kr)] \, |\nabla[r - r(\phi)]| \, d\phi. \tag{A-15}$$

Equations (A-13) and (A-14) can be solved to yield, in matrix notation,

$$\underset{\sim}{b} = -(\mathrm{Re}\, \underset{\sim}{Q}) \underset{\sim}{Q}^{-1} \underset{\sim}{a} = -\underset{\sim}{T}\, \underset{\sim}{a}. \tag{A-16}$$

Thus, the T-matrix of transition matrix for an obstacle relates the coefficients of the field incident on a scatterer to the coefficient of the field scattered by it and is given by

$$\underset{\sim}{T} = -\mathrm{Re}\, \underset{\sim}{Q}\, \underset{\sim}{Q}^{-1} \tag{A-17}$$

For a circular cylinderical scatterer of radius a, $r(\phi) = a$ and $\underline{n}(r) = \underline{r}$. Equation (A-15) then gives

$$Q_{mn} = -(\mu a/4)[J_n(k_f a)k\, H_n'(ka)-(\mu_f/\mu)k_f\, J_n'(k_f a)\, H_n(ka)]\delta_{mn} \quad . \qquad (A\text{-}18)$$

Substitution of Eq. (A-18) into Eq. (A-17) yields the T-matrix for a circular elastic cylinder

$$T_{mn} = \frac{\mu J_n(k_f a)kJ_n'(ka)-\mu_f J_n(ka)k_f J_n'(k_f a)}{\mu_f H_n(ka)k_f J_n'(k_f a)-\mu J_n(k_f a)kH_n'(ka)} \quad . \qquad (A\text{-}19)$$

For a scatterer of arbitrary shape, Q_{mn} can be determined from (A-15) by numerical integration.

APPENDIX B

Relations between T-matrix elements defined in two different basis sets

In formulating the multiple scattering problem, we have chosen the complex angular functions $e^{in\phi}$ to construct the basis functions ψ_n in favor of the real angular functions $\cos n\phi$ and $\sin n\phi$. The reason for this choice is that the addition theorem for cylinder functions in the form of Eq. (15) is more convenient and less awkward than that in terms of the sines and cosines. To make such a choice, we have paid the price that the real part of the basis set ψ_n cannot be constructed by simply replacing H_n by J_n. Had the real angular functions been used, "real ψ_n" and "regular ψ_n" are then equal.

In numerical computation of the T-matrix elements, it is convenient to make "real" synonymous with "regular" for reasons that we cannot go into here. Thus it becomes necessary to compute the T-matrix in a basis set with real angular functions and then convert it into a basis set with complex angular functions.

To distinguish between the Q- and T-matrices defined in the two basis sets, we shall use additional superscripts $\sigma,\nu = e, 0$ to denote the even and odd angular functions.

We expand w^0 and w^S in the two basis sets and obtain

$$w^0(r) = \sum_{n=-\infty}^{\infty} a_n J_n(kr) e^{in\phi}$$

$$= \sum_{\ell} \sum_{\sigma} \sqrt{\varepsilon_\ell}\, a_\ell^\sigma J_\ell(kr) \begin{cases} \cos \ell\phi\ ; & \sigma = e \\ \sin \ell\phi\ ; & \sigma = o \end{cases} \qquad \text{(B-1)}$$

where

$$a_\ell^e = \sqrt{\varepsilon_\ell}[a_\ell+(-1)^\ell a_{-\ell}]/2$$

$$a_\ell^o = i[a_\ell-(-1)^\ell a_{-\ell}]/\sqrt{\varepsilon_\ell} \qquad \text{(B-2)}$$

In Eq. (B-1), ε_ℓ is the Neumann factor $\varepsilon_0 = 1$ and $\varepsilon_\ell = 2$ for $\ell > 0$; $\ell = 0, 1, 2, \ldots$ for $\sigma = e$ and $\ell = 1, 2, 3, \ldots$ for $\sigma = o$.

Similarly, we write

$$w^S(\underline{r}) = \sum_{n=-\infty}^{\infty} b_n H_n(kr)\, e^{in\phi}$$

$$= \sum_\ell \sum_\sigma \sqrt{\varepsilon_\ell}\, b_\ell^\sigma H_\ell(kr) \begin{cases} \cos \ell\phi & ; \quad \sigma = e \\ \sin \ell\phi & ; \quad \sigma = o \end{cases} \qquad \text{(B-3)}$$

The coefficients b_ℓ and b_ℓ^σ are related as given by Eq. (B-2). Proceeding as in Ref. 17, we obtain

$$b_n = \sum_{m=-\infty}^{\infty} T_{nm} a_m \qquad \text{(B-4)}$$

and

$$b_n^\sigma = \sum_m \sum_\nu T_{nm}^{\sigma\nu} a_m^\nu \qquad \text{(B-5)}$$

where

$$T_{nm} = -\sum_{\ell=-\infty}^{\infty} [\mathrm{Re}\ Q]_{n\ell}[Q^{-1}]_{\ell m} \qquad \text{(B-6)}$$

$$T_{nm}^{\sigma\nu} = -\sum_\ell \sum_\delta [\mathrm{Re}\ Q]_{n\ell}^{\sigma\delta}[Q^{-1}]_{\ell m}^{\delta\nu} \ . \qquad \text{(B.7)}$$

Let the surface of a scatterer be expressed by

$$r - r(\phi) = 0 \quad \text{on} \quad S \ . \tag{B-8}$$

The corresponding Q matrix elements are

$$Q_{nm} = \frac{\mu}{4} \int_0^{2\pi} \left\{ [J_m(k_f r)\, H_n'(kr) - \frac{\mu_f}{\mu} H_n(kr)\, J_m'(k_f r)] \right.$$

$$\left. - \frac{i}{r^2(\phi)} \frac{d}{d\phi} r(\phi)(n - m \frac{\mu_f}{\mu})\, J_m(k_f r)\, H_n(kr) \right\} e^{i(m-n)\phi} r(\phi) d\phi \tag{B-9}$$

$$Q_{nm}^{\sigma\nu} = \frac{\pi}{4} \sqrt{\varepsilon_n}\, \sqrt{\varepsilon_m} \int_0^{2\pi} \left\{ [J_m(k_f r)\, H_n'(kr) - \frac{\mu_f}{\mu} H_n(kr)\, J_m'(k_f r)] P_{nm} \right.$$

$$\left. + \frac{1}{r^2(\phi)} \frac{d}{d\phi} r(\phi)\, J_m(k_f r)\, H_n(kr) [n\, R_{nm} - \frac{\mu_f}{\mu} m\, S_{nm}] \right\} r(\phi) d\phi \tag{B-10}$$

where

$$P_{nm} = \begin{pmatrix} \cos n\phi \cos m\phi & \cos n\phi \sin m\phi \\ \sin n\phi \cos m\phi & \sin n\phi \sin m\phi \end{pmatrix} \tag{B-11}$$

$$R_{nm} = \begin{pmatrix} -\sin n\phi \cos m\phi & \sin n\phi \sin m\phi \\ \cos n\phi \cos m\phi & \cos n\phi \sin m\phi \end{pmatrix} \tag{B-12}$$

and

$$S_{nm} = \begin{pmatrix} -\cos n\phi \sin m\phi & \cos n\phi \cos m\phi \\ -\sin n\phi \sin m\phi & \sin n\phi \cos m\phi \end{pmatrix} \tag{B-13}$$

In Eqs. (B-9) and (B-10), the prime denotes derivative with respect to r, and k_f and k are the wave numbers in the inclusion and matrix materials respectively.

From Eqs. (B-9) and (B-10) for boundaries with the following

symmetry

$$r(\theta) = r(2\pi-\theta) = r(\pi\pm\theta) , \tag{B-14}$$

we obtain

$$Q_{nm}^{\sigma\nu} = Q_{nm} = 0 \; ; \; \sigma \neq \nu \; ; \; n+m \text{ odd} \tag{B-51}$$

Defining

$$Q_{nm}^{\sigma\sigma} \equiv Q_{nm}^{\sigma}$$

we have

$$Q_{nm}^{e} = \frac{\sqrt{\varepsilon_n}\sqrt{\varepsilon_m}}{2}[Q_{nm}+(-1)^m Q_{-n,m}] \tag{B-16}$$

$$Q_{nm}^{o} = \frac{\sqrt{\varepsilon_m}}{\sqrt{\varepsilon_n}}(Q_{nm}-(-1)^m Q_{-n,m}) \tag{B-17}$$

$$(Q^{-1})_{nm}^{e} = \frac{\sqrt{\varepsilon_n}\sqrt{\varepsilon_m}}{2}[(Q^{-1})_{nm}+(-1)^n (Q^{-1})_{-n,m}] \tag{B-18}$$

and

$$(Q^{-1})_{nm}^{o} = \frac{\sqrt{\varepsilon_m}}{\sqrt{\varepsilon_n}}[(Q^{-1})_{nm}-(-1)^n (Q^{-1})_{-n,m}] \tag{B-19}$$

The symmetry implied by Eq. (B-14) is applicable to all quadratic surfaces, for example, the fibers of elliptic cross section considered in the numerical calculations. Using Eqs. (B-16) - (B-19), the relation between the T-matrices of the two basis sets is given by

$$T_{nm} = \left[\frac{T_{nm}^{e}}{\sqrt{\varepsilon_n}\sqrt{\varepsilon_m}} + \frac{T_{nm}^{o}}{2}\right] \tag{B-20}$$

$$T_{n,-m} = (-1)^m \left[\frac{T_{nm}^{e}}{\sqrt{\varepsilon_n}\sqrt{\varepsilon_m}} - \frac{T_{nm}^{o}}{2}\right] . \tag{B-21}$$

In arriving at Eqs. (B-20) and (B-21) the symmetry property of the T-matrix has been invoked. Equations (B-20) and (B-21) are used to change the summations in Eq. (36) from $-\infty$ to $+\infty$ to positive values only as given by Eq. (39).

It may be pointed out that the analytical properties presented in Eq. (B-16) - (B-21) are not confined to the scalar wave equation but are equally applicable to the vector wave equation and the elastic wave equation since the definition of the T-matrix remains the same.

ACKNOWLEDGEMENTS

This research was supported by the National Science Foundation through the Materials Science Center, Cornell University, and by the Air Force Office of Scientific Research.

REFERENCES

1. Lord Rayleigh, Phil. Mag. 47, 375 (1899)

2. L.L. Foldy, Phys. Revs. 67, 107 (1945)

3. M. Lax, Rev. Mod. Phys. 23, 287 (1951)

4. M. Lax, Phys. Revs. 85, 621 (1952)

5. V. Twersky, J. Acoust. Soc. Am. 29, 209 (1957)

6. V. Twersky, J. Math. Phys. 3, 700 (1962)

7. P.C. Waterman and R. Truell, J. Math. Phys. 2, 512 (1961)

8. F.C. Karl, Jr. and J.B. Keller, J. Math. Phys. 5, 537 (1964)

9. S.K. Bose and A.K. Mal, Int. J. Solids and Struct. 9, 1075 (1973)

10. A.K. Mal and A.K. Chatterjee, J. Appl. Mech. 44, 61 (1977)

11. S.K. Datta, J. Appl. Mech. 42, 165 (1975)

12. J.D. Achenbach, "Waves and Vibrations in Directionally Reinforced Composites", in Composite Materials (L.J. Broutman and R.H. Krock, eds.) Volume 2, Academic Press, New York (1972)

13. J.C. Peck, "Stress wave propagation and fracture on composites", Symp. Dynam. Compos. Mater. ASME (1972)

14. F.C. Moon, "Wave propagation and impact in composite materials", in Composite Materials (L.J. Broutman and R.H. Krock, eds.) Volume 7, Academic Press, New York (1975)

15. H.J. Sutherland and R. Lingle, J. Comp. Mater. 6, 490 (1972)

16. T.R. Tauchert and A.N. Guzelsu, J. Appl. Mech. 39, 98 (1972)

17. P.C. Waterman, J. Acoust. Soc. Am. 45, 1417 (1969)

18. B. Peterson and S. Strom, J. Acoust. Soc. Am. 56, 771 (1974)

19. V.V. Varadan and V.K. Varadan, Low frequency expansions for the scattering of scalar waves by cylinders of simple shapes, Materials Science Center Report # 2937 , Cornell University, Ithaca, New York (1977)

20. C.S. Ting and W.H. Sachse, private communications.

21. C.H. Yew and P.N. Jogi, Proceedings of the 12th Annual meeting of Society of Engineering Science, University of Texas, Austin, Texas ,497 (1975)

22. F. C. Moon and C. C. Mow, Wave propagation in a composite material containing dispersed rigid spherical inclusions, RM-6139-PR, The Rand Corporation, Santa Monica, California (1970).

23. C. Save, Int. J. Solids and Struct. 9, 937 (1973)

24. Z. Hashin and B. W. Rosen, J. Appl. Mech. 31, 223 (1964)

25. K. Sobczyk, Elastic Wave Propagation in a Discrete Random Medium Acta Mechanics, 25, 13-28 (1976)

FIGURE CAPTIONS

Fig. 1. Geometry of parallel cylinders and circumscribing circle

Fig. 2. Translation of coordinate system of the j^{th} and i^{th} cylinders

Fig. 3. Normalized phase velocity vs concentration - Rayleigh limit

Fig. 4. Normalized phase velocity vs ka for c = 0.3

Fig. 5. Normalized phase velocity vs ka for c = 0.5

Fig. 6. Normalized phase velocity vs ka for c = 0.7

Fig. 7. Attenuation coefficient vs ka for c = 0.3

Fig. 8. Attenuation coefficient vs ka for c = 0.5

Fig. 9. Attenuation coefficient vs ka for c = 0.7

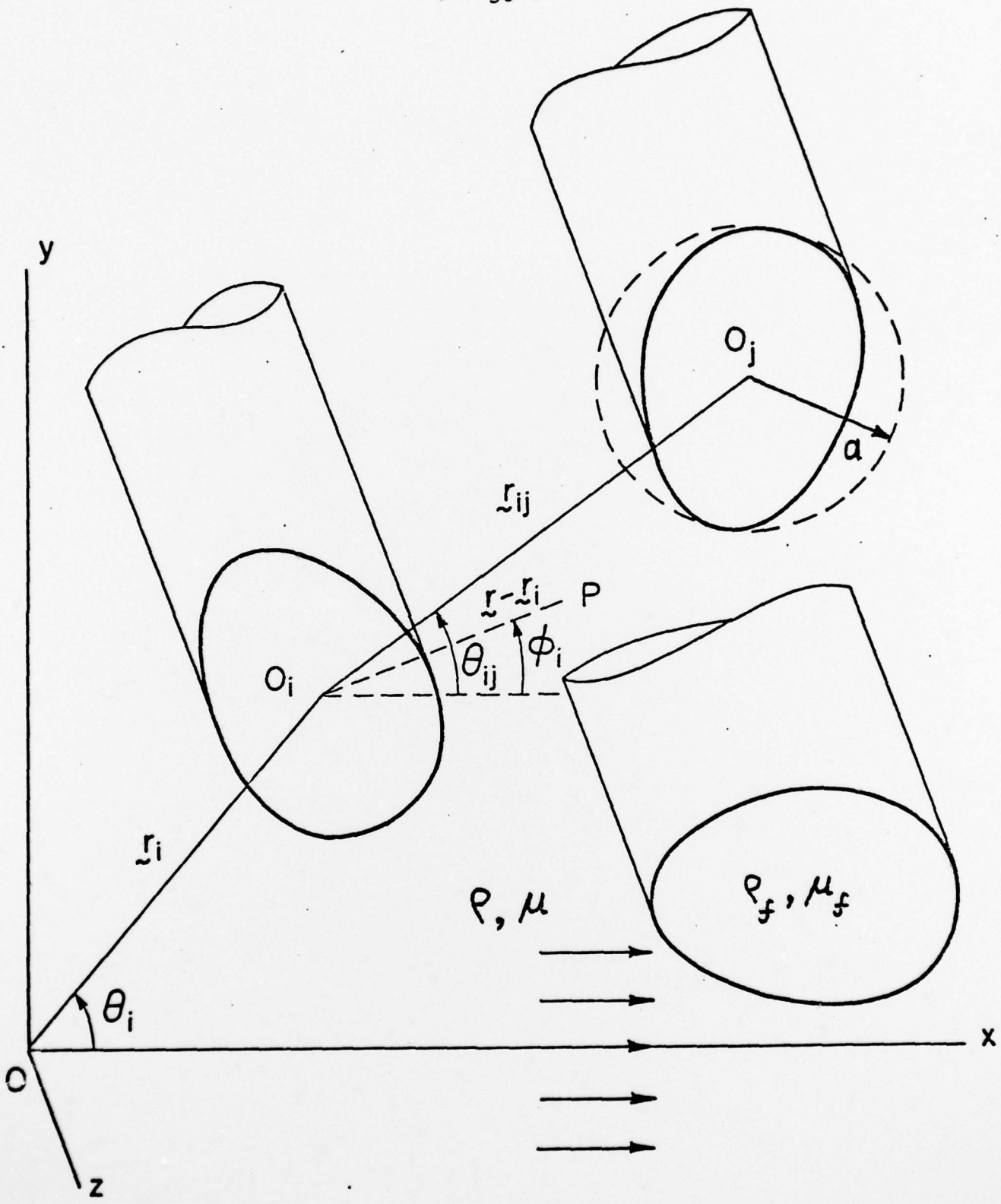

FIG. 1. GEOMETRY OF PARALLEL CYLINDERS AND CIRCUMSCRIBING CIRCLE

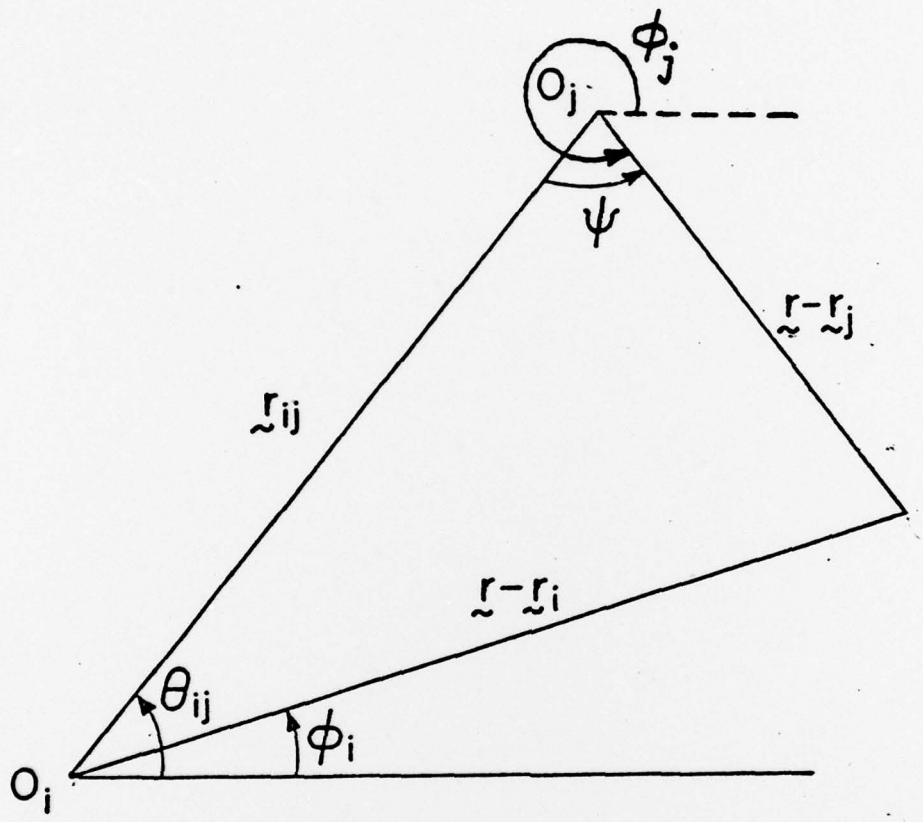

FIG. 2. TRANSLATION OF COORDINATE SYSTEM OF THE J^{TH} AND I^{TH} CYLINDERS

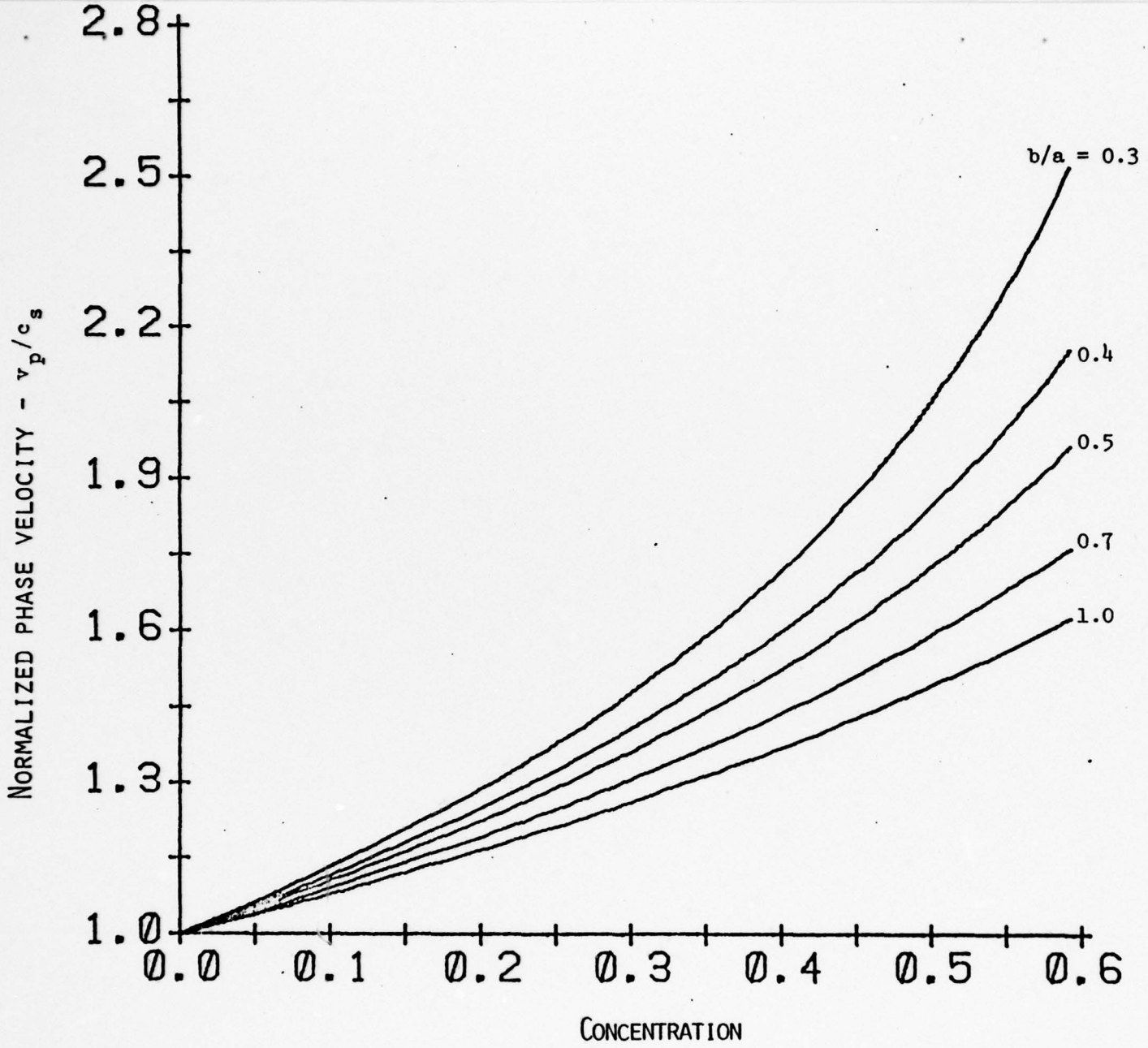

FIG. 3. NORMALIZED PHASE VELOCITY VS CONCENTRATION - RAYLEIGH LIMIT

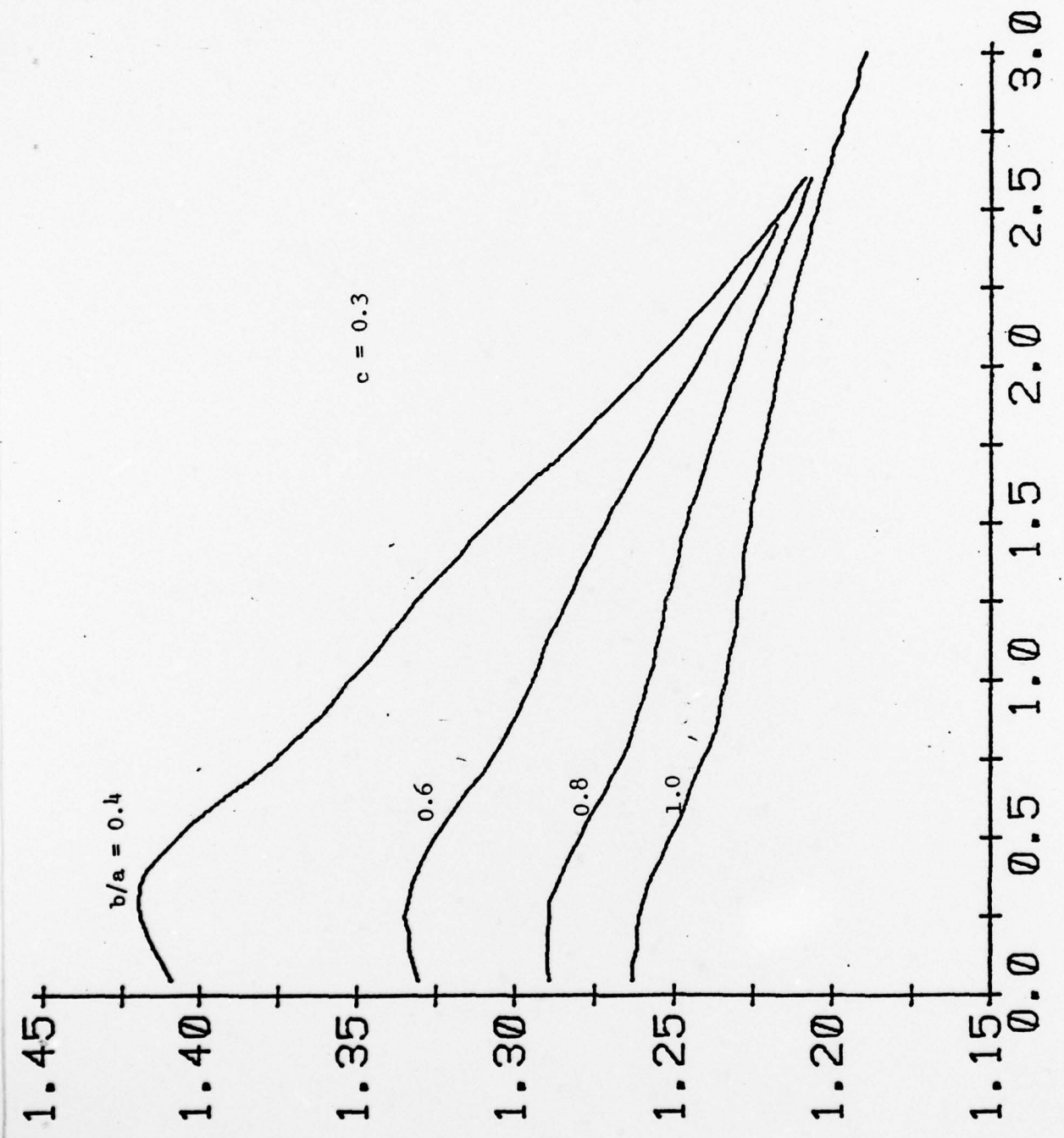

FIG. 4 NORMALIZED PHASE VELOCITY VS ka FOR c = 0.3

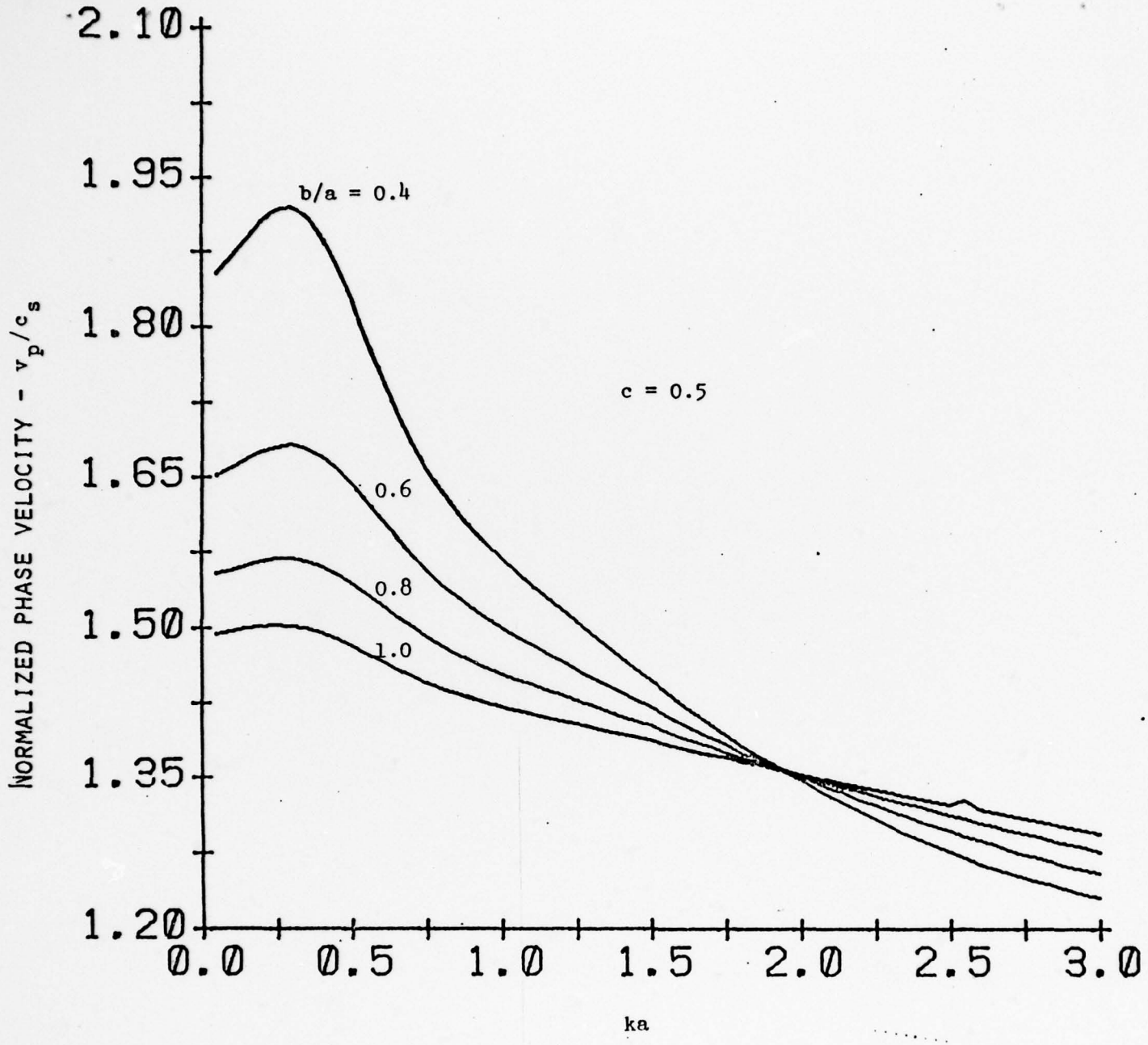

FIG. 5. NORMALIZED PHASE VELOCITY VS ka FOR c = 0.5

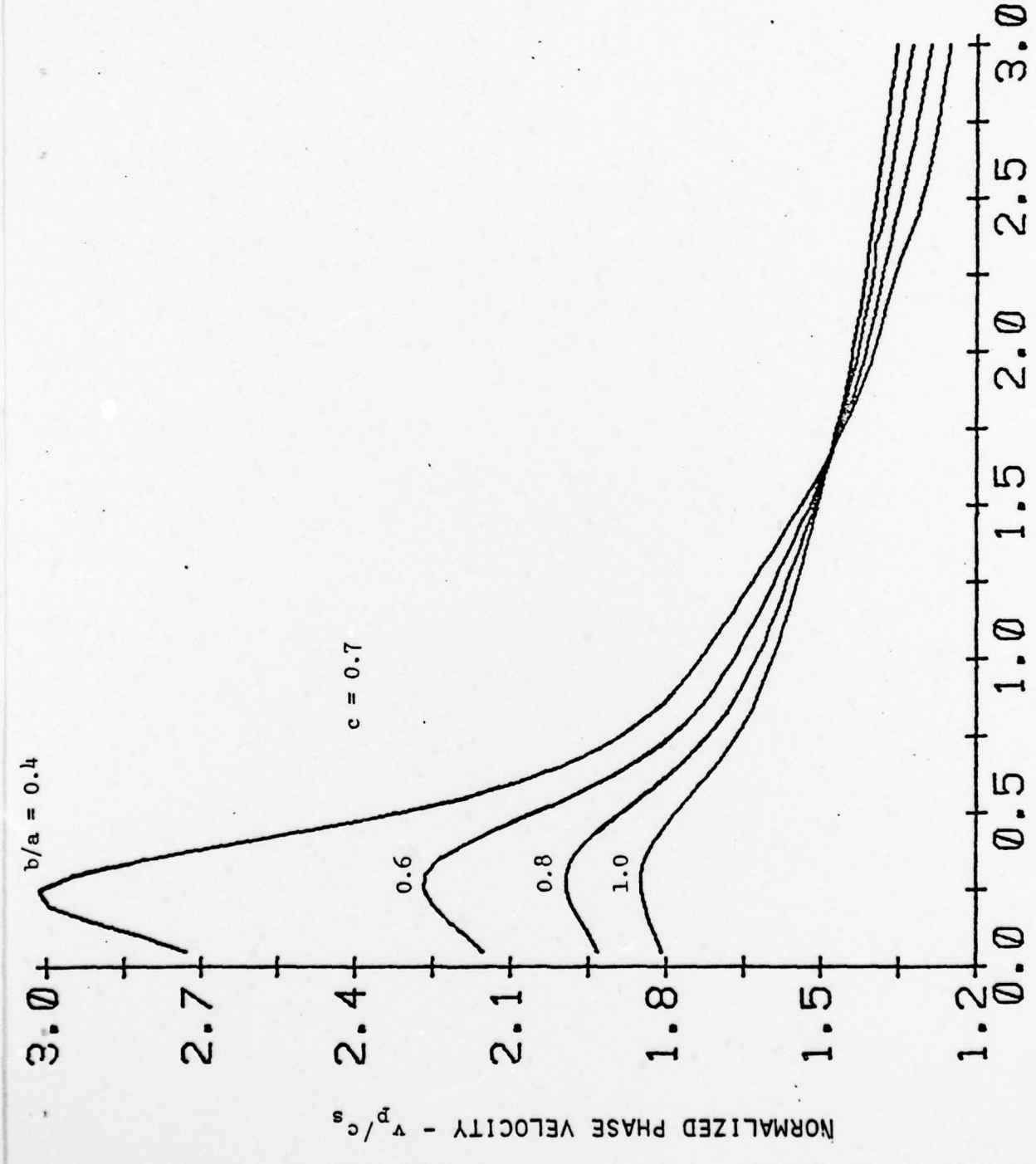

FIG. 6. NORMALIZED PHASE VELOCITY VS ka FOR c = 0.7

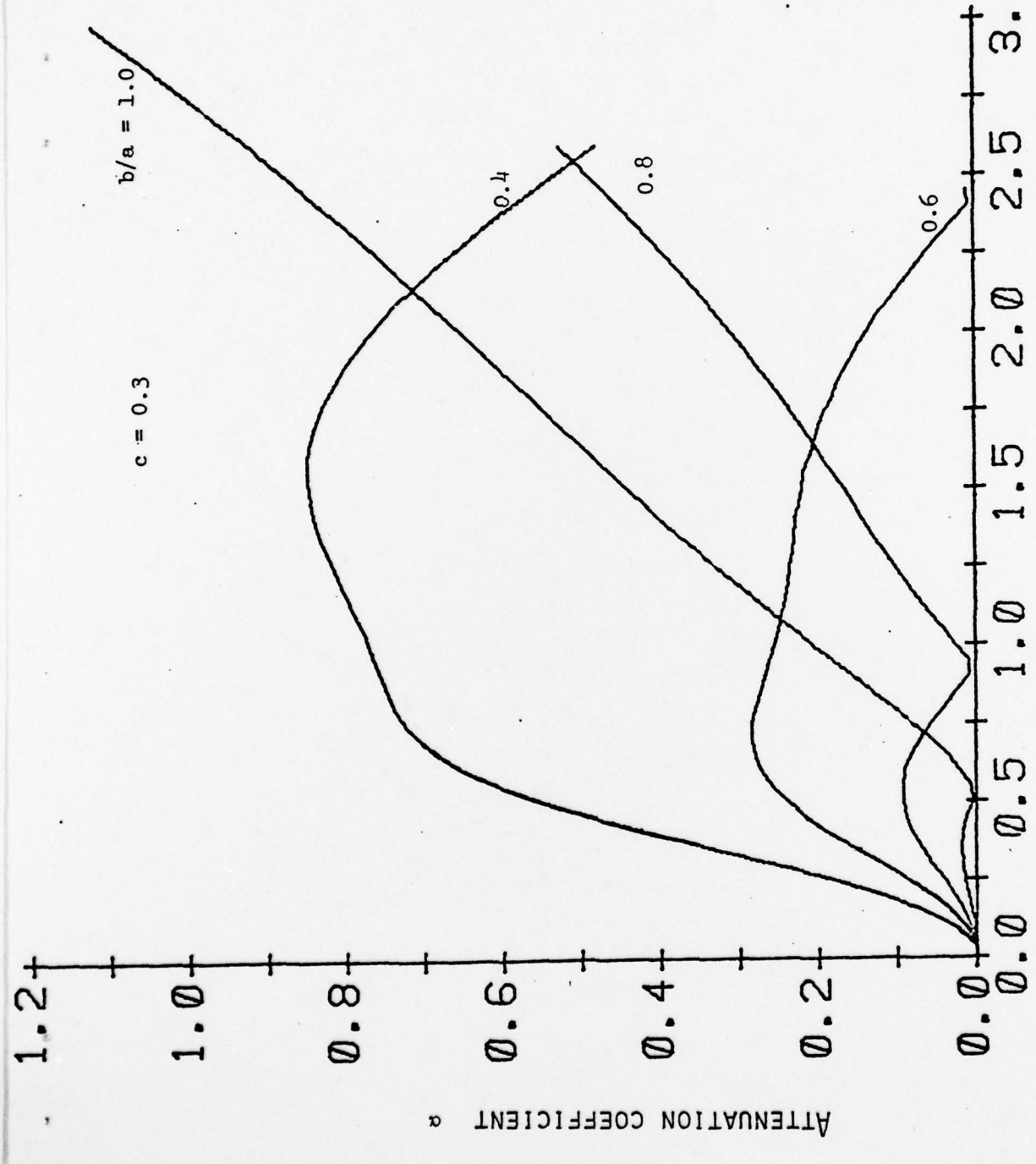

FIG. 7. ATTENUATION COEFFICIENT VS ka FOR c = 0.3

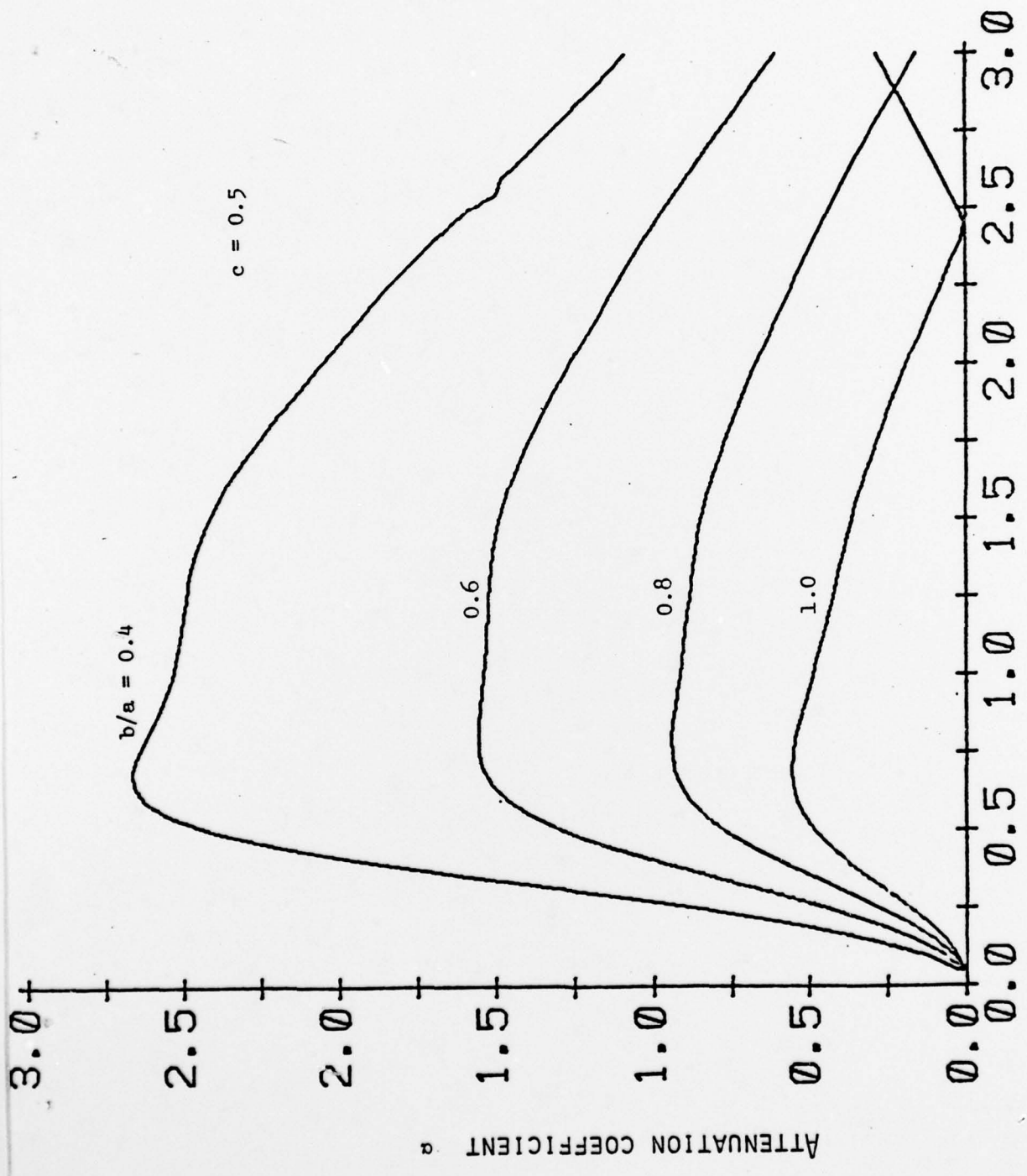

FIG. 8. ATTENUATION COEFFICIENT VS ka FOR c = 0.5

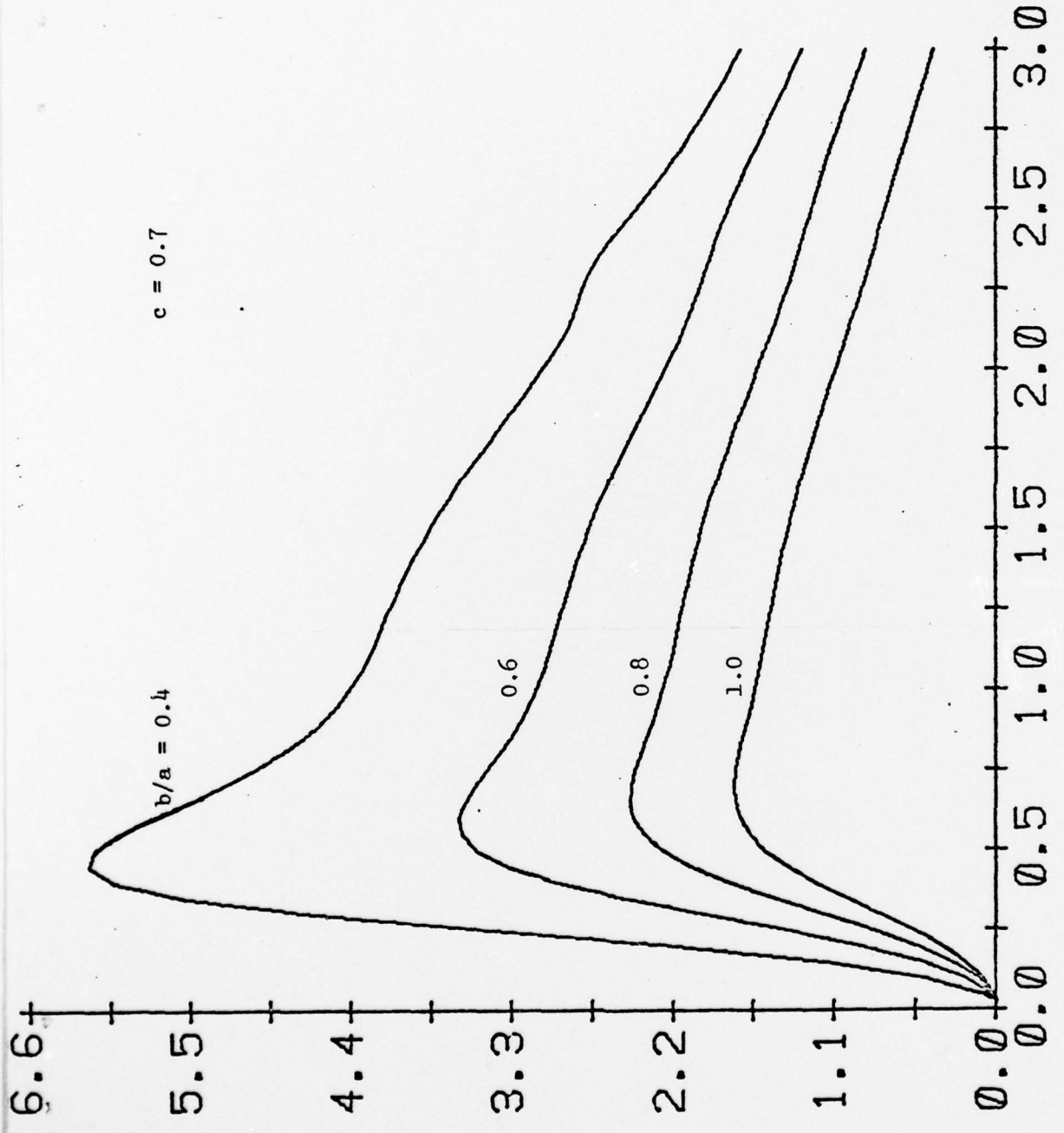

FIG. 5. ATTENUATION COEFFICIENT α VS ka FOR c = 0.7